

Design and Construction Guidelines for Thermally Insulated Concrete Pavements

TPF-5(149)
MnDOT Contract No. 89261

Task 5 Report

Prepared by
Lev Khazanovich
Priyam Saxena
Derek Tompkins

June 2012

Contents

1.	Task Background	1
2.	HMA-PCC Rutting Models	2
2.1	MEPDG Rutting Model	2
2.2	CalME Rutting Model.....	5
2.2.1	Rut Depth.....	6
2.2.2	Fatigue Damage	6
2.3	TPF-5(149) M-E Design to Mitigate Rutting in TICP.....	8
2.3.1	Create and run MEPDG for TICP project file	8
2.3.2	Run TPF-5(149) program to read MEPDG inputs for CalME calibration	8
2.3.3	Run TPF-5(149) program to supplement MEPDG results with predicted rutting depth results from CalME.....	15
2.4	Validation of TPF-5(149) Procedure for Rutting in TICP	15
2.4.1	UCPRC Heavy Vehicle Simulator (HVS) SHRP2 R21 data.....	15
2.4.2	MnROAD TICP Test Section Measured Rutting	23
2.5	Sensitivity Analysis of TPF-5(149) Procedure for Rutting in TICP.....	26
2.5.1	Climate.....	26
2.5.2	Pavement Thickness.....	27
3.	HMA-PCC Reflective Cracking Models	28
3.1	Original MEPDG Reflective Cracking Model.....	29
3.2	NCHRP 1-41 Reflective Cracking Procedure for MEDPG	30
3.2.1	NCHRP 1-41 Reflective Cracking Model	30
3.2.2	NCHRP 1-41 Program to Interface with MEPDG Project Files.....	32
3.2.3	Analysis and Discussion of NCHRP 1-41 Procedure	33
3.3	CalME Reflective Cracking Model.....	38
3.4	TPF-5(149) Procedure for Predicting Reflective Cracking in TICP.....	40
3.4.1	NCHRP 1-41 Suitability for TPF-5(149) Procedure	40
3.4.2	Modified CalME Reflection Cracking Model for TPF-5(149).....	40
3.4.3	Modification of TPF-5(149) Companion Program to the MEPDG	44
3.5	Validation of TPF-5(149) Procedure for Reflection Cracking.....	44
3.6	Sensitivity Analysis of TPF-5(149) Procedure for Reflection Cracking	49
3.6.1	Climate.....	49
3.6.2	Pavement thickness.....	51

3.6.3	Joint load transfer.....	53
4.	JPCP Cracking Models for HMA-PCC	55
4.1	MEPDG Transverse Cracking Model for JPCP.....	55
4.2	Modifications to JPCP Transverse Cracking Model for HMA-PCC Projects and Incorporation into the MEPDG.....	56
4.3	Sensitivity Analysis of Modified MEPDG JPCP Transverse Cracking Model	57
4.4	Confirmation of TPF-5(149) Modifications to MEPDG JPCP Transverse Cracking Model for HMA-PCC Projects	61
5.	JPCP Faulting Models for HMA-PCC.....	64
5.1	MEPDG JPCP Faulting Model	64
5.2	Modifications of MEPDG Faulting Model for HMA-PCC and Incorporation into the MEPDG Procedure	65
5.2.1	Equivalent single-layer pavement.....	65
5.2.2	Load transfer in a HMA-PCC system.....	66
5.3	Validation and Sensitivity Analysis of Modified MEPDG Faulting Model for HMA- PCC	67
6.	Guidelines to TPF-5(149) Procedure for Design and Analysis of TICP	73
6.1	Creating MEPDG Project File.....	73
6.2	Execute MEPDG analysis for TICP project.....	74
6.3	Execute TPF 5(149) analysis for TICP project	74
6.4	Interpret design outputs	75
7.	Task Discussion and Conclusions.....	76
	References.....	78

Table of Figures

Figure 1. Temperature quintiles used by MEPDG to determine HMA sublayer dynamic modulus (from AASHTO 2008).....	3
Figure 2. GUI for extracting MEPDG project input information (at left) and extracting calibration constants (at right)	9
Figure 3. MEPDG file "_space.dat", specifying pavement structure.....	10
Figure 4. MEPDG input file specifying number of months between construction and traffic open	11
Figure 5. MEPDG input file for temperature.....	12
Figure 6. One of three MEPDG files used to obtain traffic inputs	13
Figure 7. MEPDG files used to obtain dynamic modulus of AC layer	14
Figure 8. MEPDG temporary file describing monthly modulus values for all layer and sublayers in the TICP project.....	15
Figure 9. The HVS apparatus at UCPRC.....	16
Figure 10. Section 609HB load history.....	17
Figure 11. Daily average outside air temperatures.	18
Figure 12. Daily average inside air temperatures.	18
Figure 13. Daily average temperatures at surface and various depths of Section 609HB	19
Figure 14. Illustration of maximum rut depth and average deformation of a leveled profile.....	20
Figure 15. Evolution of Section 609HB rutting profile	20
Figure 16. Average deformation for Section 609HB.....	21
Figure 17. Summary of measured rutting (average deformation) observed at the UCPRC facility for HVS testing	22
Figure 18. Summary of predicted rutting (average deformation) from TPF-5(149) procedure described in this report.....	23
Figure 19. Comparison of TPF-5(149) procedure and unmodified MEPDG procedure predictions for rutting (average deformation) and observed rutting at MnROAD Cells 106 and 206.....	24
Figure 20. Comparison of TPF-5(149) procedure and unmodified MEPDG procedure predictions for rutting (average deformation) and observed rutting at MnROAD Cell 70	25
Figure 21. TPF-5(149) procedure for rutting, sensitivity to climate.....	26
Figure 22. TPF-5(149) procedure for rutting, sensitivity to HMA overlay thickness	27
Figure 23. Visual interpretation of NCHRP 1-41 calibration coefficients (from NCHRP 2010)	31
Figure 24. Severity distress curves for NCHRP 1-41 model (from NCHRP 2010)	32
Figure 25. Influence of default coefficients and internal settings for same project for three levels of severity in NCHRP 1-41 procedure.....	33
Figure 26. Influence of HMA overlay thickness on NCHRP 1-41 High (H) severity reflective cracking predictions	34
Figure 27. Influence of HMA overlay thickness on NCHRP 1-41 Low, Medium, and High (L+M+H) severity reflective cracking predictions	35
Figure 28. Influence of JPCP joint load transfer efficiency (LTE) on NCHRP 1-41 Low, Medium, and High (L+M+H) and High (H) severity reflective cracking performance predictions	36
Figure 29. Calibration coefficients for 1-41 self-consistency validation cases	37
Figure 30. Results for 1-41 self-consistency validation.....	38
Figure 31. TPF-5(149) procedure predicted 20-year M+H severity reflective cracking performance for MnROAD Cells 106 and 206.....	45

Figure 32. The first two years of MnROAD Medium and High (M+H) severity reflection cracking data versus TPF-5(149) modeled M+H performance and Original MEPDG modeled performance	46
Figure 33. Predicted 20-year Low, Medium, and High (L+M+H) severity reflective cracking performance for MnROAD Cells 106 and 206 according to TPF-5(149) procedure	47
Figure 34. First two years of MnROAD Low, Medium, and High (L+M+H) severity reflection cracking data versus TPF-5(149) modeled L+M+H performance.....	48
Figure 35. Influence of climate file on TPF-5(149) procedure for M+H reflective cracking	49
Figure 36. Influence of climate file on TPF-5(149) procedure for L+M+H severity reflective cracking.....	50
Figure 37. First 40 months of predicted L+M+H severity reflective cracking by TPF-5(149) procedure for five climate files	51
Figure 38. Influence of HMA overlay thickness on TPF-5(149) procedure for M+H severity reflective cracking.....	52
Figure 39. Influence of HMA overlay thickness on TPF-5(149) procedure for L+M+H severity reflective cracking.....	52
Figure 40. Influence of dowels on TPF-5(149) procedure for M+H severity reflective cracking for project using Seattle, WA, climate file	53
Figure 41. Influence of dowels on TPF-5(149) procedure for L+M+H severity reflective cracking for project using Seattle, WA, climate file	54
Figure 42. Propagation of fatigue cracking in a composite pavement.....	55
Figure 43. Predicted JPCP transverse performance for three JPCP projects (according to original MEPDG) and a HMA-PCC project (according to TPF-5(149) procedure).....	58
Figure 44. Comparison of 9-inch JPCP project and model predictions for PCC transverse cracking according to original MEPDG and TPF-5(149) procedures	59
Figure 45. Influence of HMA overlay thickness on predicted JPCP transverse cracking for a HMA-PCC project	60
Figure 46. Influence of climate on JPCP transverse cracking for a HMA-PCC project	61
Figure 47. Predicted JPCP transverse cracking in HMA-PCC projects for Minneapolis, MN, and Pullman, WA, according to the original and TPF-5(149) modified MEDPG	62
Figure 48. Predicted transverse cracking in MnROAD Cells 106 and 206 according to the original MEPDG and TPF-5(149) procedures.....	63
Figure 49. Comparison of predicted faulting for HMA-PCC and JPCP projects using MEPDG modified according to TPF-5(149)	68
Figure 50. Effect of 1-inch dowels in HMA-PCC projects for Minneapolis, MN, and Pullman, WA.....	69
Figure 51. Influence of climate on predicted faulting in HMA-PCC using TPF-5(149) modified MEPDG for HMA-PCC project with 1-inch dowels.....	70
Figure 52. Influence of climate on predicted faulting in HMA-PCC using TPF-5(149) modified MEPDG for HMA-PCC project without dowels.....	70
Figure 53. Influence of HMA overlay thickness on predicted faulting in HMA-PCC using TPF-5(149) modified MEPDG for HMA-PCC project with 1-inch dowels.....	71
Figure 54. Influence of HMA overlay thickness on predicted faulting in HMA-PCC using TPF-5(149) modified MEPDG for HMA-PCC project without dowels.....	72

Tables

Table 1. Model coefficients for CalME fatigue model	9
Table 2. Model coefficients for CalME rutting model	9
Table 3. HVS loading program for example section	16
Table 4. Section 609HB temperature summary for air and pavement.....	19
Table 5. MnROAD Cell 106/206 design in summary	24
Table 6. Assigned values for H_{eff} , c , and d in original MEPDG reflective cracking model (from AASHTO 2008)	29

1. Task Background

The work of Task 5 represented the most extensive research of the TPF-5(149) project to date. The mechanistic-empirical (M-E) modeling of HMA-PCC pavements for design and analysis is a significant undertaking, and while it is a recent topic of concern, there remain many open questions on this topic. Thus there were many challenges in the process of the Task 5 work.

Other recent efforts in HMA-PCC pavements have examined design and analysis. The most prominent is the SHRP2 R21 project, which developed design guidelines for HMA-PCC. However, the R21 recommendations did not progress beyond MEPDG. That is, R21 identified the MEPDG as a suitable basis for HMA-PCC design but did not modify or extend the HMA-PCC models.

TPF-5(149) viewed the work of R21 as a starting point and made it a project goal to capitalize on the MEPDG framework without accepting the MEPDG models for HMA-PCC as a limitation. Instead, the TPF-5(149) set out to add models and features to the MEPDG for the benefit of HMA-PCC project design and analysis. To this end, the work of Task 5 involved the review of a variety of M-E models for rutting and reflective cracking in HMA-PCC.

Furthermore, Task 5 implemented viable models for rutting and reflective cracking into companion programs to the MEPDG software. This is a notable achievement given that other “companion” programs (including NCHRP 1-41) that involve modifications of MEPDG models are not as compatible as claimed. This work allowed the TPF-5(149) team to evaluate multiple models and determine their suitability for HMA-PCC and TICP.

The following sections detail the Task 5 investigation and implementation of M-E models for important distresses in HMA-PCC pavement sections. Each section is self-contained and also describes the necessary procedure (including software) to reproduce the results presented in this task report.

2. HMA-PCC Rutting Models

One advantage of the timing of the TPF-5(149) project is that it ran concurrently with the SHRP2 R21 project, which examined the suitability of the MEPDG for HMA-PCC design and analysis. One recommendation made by the R21 project was that while the MEPDG was found to adequately predict rutting performance for Level 1 inputs, for Level 3 inputs the MEPDG underestimated the extent of permanent deformation in rutting relative to field data (SHRP2 2012). Hence, a dual objective for Task 5 was to:

- 1) investigate the MEPDG rutting model and the CalME rutting model and
- 2) develop a procedure to incorporate the CalME rutting model into the MEPDG framework that provides reasonable rutting prediction for Level 3 inputs.

The overall goal was to provide a HMA-PCC design and analysis procedure for rutting for pavement engineers that does not require uncommon inputs (most projects do not contain Level 1 detail) and does not force the user outside of the MEPDG framework. The following subsections describe this effort.

2.1 MEPDG Rutting Model

As detailed in previous task reports, the MEPDG divides the layers of the pavement system into sublayers, where the thickness of each sublayer is determined from the layer material properties, overall layer thickness, and the position of the sublayer relative to the thickness of the pavement system (NCHRP 2004). The pavement response in each sublayer is calculated using elastic layer theory (JULEA). Furthermore, the MEPDG uses the Enhanced Integrated Climate Model (EICM) to calculate hourly temperature and moisture conditions through the sublayers of the pavement structure and adjust sublayer modulus values accordingly (Larson and Dempsey 1997).

Before detailing how the MEPDG models rutting, the temperature quintile concept for HMA sublayers should be briefly introduced. HMA sublayer temperatures are combined into five quintiles for each month of the project analysis. A normal distribution is assumed for the frequency distribution of HMA sublayer temperatures (Figure 1).

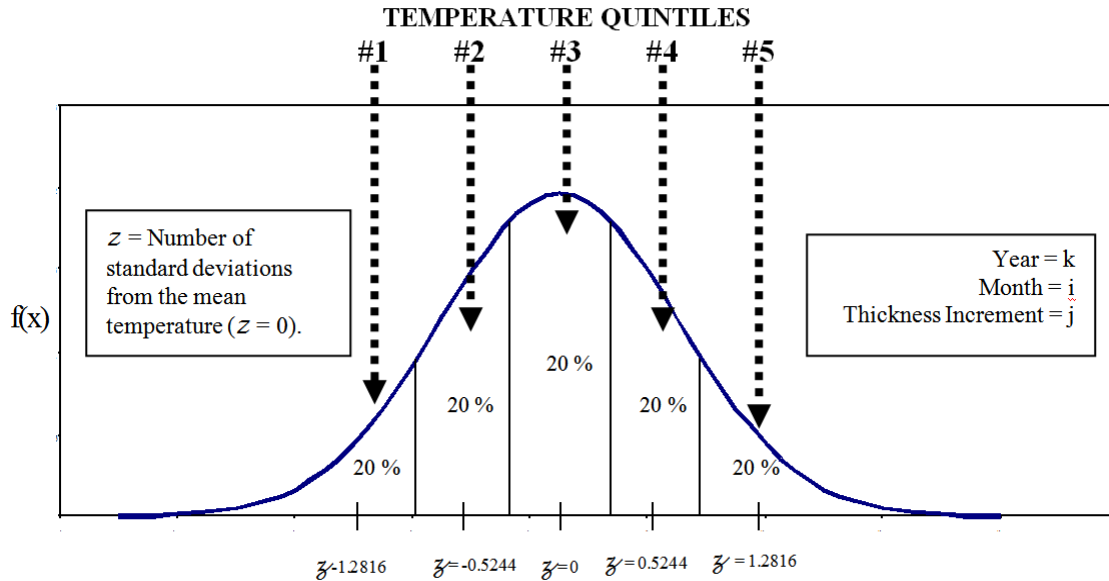


Figure 1. Temperature quintiles used by MEPDG to determine HMA sublayer dynamic modulus (from AASHTO 2008)

The average temperature within each quintile of a sublayer for each month is used to determine the dynamic modulus of that sublayer. It is important to note that traffic is assumed to be equal within each of the five temperature quintiles; hence, for HMA projects, the MEPDG does not relate hourly truck volumes directly to the hourly temperatures (AASHTO 2008).

Furthermore, EICM calculates the temperatures within each unbound sublayer. This calculation is used, for example, to modify the resilient modulus of sublayers that experience freeze-thaw. EICM also calculates the average moisture content in the unbound sublayers for each month of the analysis period; this calculation is used to adjust the resilient modulus of each unbound sublayer for each month throughout the analysis period (Larson and Dempsey 1997; NCHRP 2004).

Permanent deformation in the form of HMA rutting is caused by the plastic or permanent vertical deformation in the layers of the pavement system. Given sublayer properties and associated temperature quintiles, the MEPDG uses sublayer characteristics to determine the maximum permanent deformation within each sublayer from horizontal and vertical strains at critical locations through the sublayer. Hence, according to the MEPDG, rutting for a given season is the sum of the plastic vertical deformations within each layer (AASHTO 2008).

The MEPDG model for rutting uses the plastic vertical strain under specific pavement conditions for the total number of trucks within that condition. As conditions vary on a monthly basis, the MEPDG uses the so-called strain hardening approach to incorporate plastic vertical strains within each month in a cumulative deformation subsystem. The accumulation of plastic deformation is measured in the laboratory using repeated load triaxial tests for both HMA mixtures and unbound materials, and the laboratory-derived relationship is adjusted to match rut depth observed in the field. The expression for permanent vertical deformation in the HMA surface layer, as detailed in AASHTO (2008), is then

$$\Delta_{p(HMA)} = \varepsilon_{p(HMA)} h_{HMA} = \beta_{1r} k_z \varepsilon_{r(HMA)} 10^{k_{1r}} n^{k_{2r} \beta_{2r}} T^{k_{3r} \beta_{3r}} \quad (2.1)$$

where

- $\Delta_{p(HMA)}$ = Accumulated permanent or plastic vertical deformation in the HMA layer/sublayer, in.
 $\varepsilon_{p(HMA)}$ = Accumulated permanent or plastic axial strain in the HMA layer/sublayer, in/in.
 $\varepsilon_{r(HMA)}$ = Resilient or elastic strain calculated by the structural response model at the mid-depth of each HMA sublayer, in/in.
 h_{HMA} = Thickness of the HMA layer/sublayer, in.
 n = Number of axle load repetitions.
 T = Mix or pavement temperature, °F.
 k_z = Depth confinement factor.
 $k_{1r, 2r, 3r}$ = Global field calibration parameters (from the NCHRP 1-40D recalibration; $k_{1r} = -3.35412$, $k_{2r} = 0.4791$, $k_{3r} = 1.5606$).
 $\beta_{1r}, \beta_{2r}, \beta_{3r}$ = Local or mixture field calibration constants; for the global calibration, these constants were all set to 1.0.

and where

$$k_z = (C_1 + C_2 D) 0.328196^D \quad (2.2)$$

$$C_1 = -0.1039(H_{HMA})^2 + 2.4868H_{HMA} - 17.342 \quad (2.3)$$

$$C_2 = 0.0172(H_{HMA})^2 - 1.7331H_{HMA} + 27.428 \quad (2.4)$$

D = Depth below the surface, in.

H_{HMA} = Total HMA thickness, in.

Furthermore, the model adopted by MEPDG for deformation in unbound sublayers (including the foundation), as described in AASHTO (2008), is

$$\Delta_{p(soil)} = \beta_{s1} k_{s1} \varepsilon_v h_{soil} \left(\frac{\varepsilon_o}{\varepsilon_r} \right) e^{-\left(\frac{\rho}{n} \right)^\beta} \quad (2.5)$$

where

$\Delta_{p(Soil)}$ = Permanent or plastic deformation for the layer/sublayer, in.

n = Number of axle load applications.

ε_o = Intercept determined from laboratory repeated load permanent deformation tests, in/in.

ε_r = Resilient strain imposed in laboratory test to obtain material properties ε_o , β , and ρ , in/in.

- ε_v = Average vertical resilient or elastic strain in the layer/sublayer and calculated by the structural response model, in/in.
- h_{Soil} = Thickness of the unbound layer/sublayer, in.
- k_{s1} = Global calibration coefficients; $k_{s1}=1.673$ for granular materials and 1.35 for fine-grained materials.
- β_{s1} = Local calibration constant for the rutting in the unbound layers; the local calibration constant was set to 1.0 for the global calibration effort.

and where

$$\text{Log}\beta = -0.61119 - 0.017638(W_c) \quad (2.6)$$

$$\rho = 10^9 \left(\frac{C_o}{(1 - (10^9)^\beta)} \right)^{\frac{1}{\beta}} \quad (2.7)$$

$$C_o = \text{Ln} \left(\frac{a_1 M_r^{b_1}}{a_9 M_r^{b_9}} \right) = 0.0075 \quad (2.8)$$

- W_c = Water content, percent.
- M_r = Resilient modulus of the unbound layer or sublayer, psi.
- $a_{1,9}$ = Regression constants; $a_1=0.15$ and $a_9=20.0$.
- $b_{1,9}$ = Regression constants; $b_1=0.0$ and $b_9=0.0$.

2.2 CalME Rutting Model

To predict rutting, CalME uses a modified version of the shear-based procedure developed by Deacon et al (2002) to predict accumulated rut depth in HMA layers (Ullidtz et al 2008). This model considers the effects of temperature, material properties, load levels, and speed. Furthermore, it makes use of fundamental physical properties and a theoretical model to predict pavement response caused by a load on the pavement.

CalME follows an increment-recursive (IR) procedure when simulating pavement performance, wherein material properties are updated for each time increment by considering the changes in environmental conditions, traffic characteristics, and HMA stiffness. Calculated damage (permanent deformation for rutting, stiffness change otherwise) for each time increment is recursively accumulated to be able to predict the pavement condition at any point in time. The IR mechanism has been found to be an effective approach for considering damage accumulation (Ullidtz et al 2006).

The CalME model for rutting has been adopted for this work and is described in subsections 2.2.1 and 2.2.2. These subsections also describe the models, at times, in terms of their incorporation into the TPF-5(149) procedure to avoid repeating this information in multiple locations. The CalME procedure has been slightly modified in the sense that MEPDG project inputs are used to develop calibration coefficients, which are detailed in the course of describing the full coupling of the CalME and MEPDG procedures in Section 2.3.

2.2.1 Rut Depth

In order to calculate the permanent deformation in an AC sublayer, the elastic shear strain γ_e for a given increment is calculated as

$$\gamma^e = \frac{\tau_{xz}}{E_{dam}/(1+\nu)} \quad (2.9)$$

where E_{dam} is the damaged modulus; ν is Poisson's ratio; and τ_{xz} is the shear stress calculated using a layered elastic analysis program at 50 mm below the tire edge.

Furthermore, the effective number of load applications N_0 that are required to produce the condition at the beginning of the increment are calculated. The total number of load applications N_{tot} is the sum of effective number of load applications and the number of load applications during the current increment.

$$N_{tot} = N_0 + N \quad (2.10)$$

The inelastic shear strain in the asphalt layer, γ_i , for the total number of load applications during the current increment is

$$\gamma^i = \exp\left(A3 + \alpha3 * \left[1 - \exp\left(-\ln(N_{tot})/\gamma3\right) * \left(1 + \ln(N_{tot})/\gamma3\right)\right]\right) * \exp\left(\beta3 * \tau_{xz}/\tau_{ref}\right) * \gamma^e \quad (2.11)$$

where τ_{ref} is a reference shear stress (0.1 MPa \approx atmospheric pressure) and $A3$, $\alpha3$, $\beta3$, and $\gamma3$ are calibration coefficients, which take values that correspond to the HMA mix design for the upper lift of the TICP. This calibration can be conducted using laboratory-derived values or can be correlated using in-field estimates, as done for the CalME-MEPDG coupling below (Table 2).

The permanent deformation for each AC sublayer, dp , is

$$dp = K * h * \gamma^i \quad (2.12)$$

where h is the thickness of the AC sublayer and K is a calibration constant = 1.4. The total rut depth is calculated by adding the permanent deformation for all AC sublayers.

2.2.2 Fatigue Damage

The damaged modulus, E_{dam} , for a particular month is calculated based on the damage w from the previous month. For the very first month of analysis (traffic open month), the pavement is assumed to be undamaged ($w = 0$).

$$\log(E_{dam}) - \delta = (\log(E_i - \delta)) * (1 - w_{(month-1)}) \quad (2.13)$$

where *month* represents the current month of analysis; E_i is the modulus of intact material; and δ is a material constant.

Using the damaged AC modulus, modulus for other layers, and structural information, strain and shear stress is calculated in the AC layer using layered elastic analysis (LEA). For the combined MEPDG/CALME procedure of TPF-5(149) for TICP design, the program MnLayer is used to calculate the elastic strain either at 100 mm into the AC layer or at the bottom of the AC layer if its thickness is less than 100 mm. This agrees with CalME assumptions that rutting is confined to the upper 100 mm of the asphalt layers (Ullidtz et al 2008). Similarly, the shear stress is calculated either at 50 mm into the AC layer or at half the depth of the AC layer if its thickness is less than 100 mm. Five different positions of traffic wander for each axle weight are considered to obtain the shear stresses and strains.

The next step involves the calculation of allowable number of load repetitions, MN_p , which is defined as

$$MN_p = A_2 * \left(\frac{\mu\epsilon_{xx}}{\mu\epsilon_{ref}} \right)^{\beta_2} * \left(\frac{E_{dam}}{E_{ref}} \right)^{\gamma_2} * \left(\frac{E_i}{E_{ref}} \right)^{\delta_2} \quad (2.14)$$

where E_{ref} is the reference asphalt modulus; $\mu\epsilon_{ref}$ is the reference asphalt strain in microstrains; $\mu\epsilon_{xx}$ is the horizontal strain; and A_2 , β_2 , γ_2 , and δ_2 are calibration coefficients. The CalME procedure was developed for flexible pavements requires the horizontal strain to be computed at the bottom of the HMA layer; for TPF-5(149) adoption of CalME for the MEPDG framework, the horizontal strain is instead computed at the mid-depth of the HMA layer. The calibration coefficients are developed from laboratory tests; in the case of the TPF-5(149) procedure detailed below, these coefficients are correlated to known properties of the pavement system from MEPDG intermediate files (Table 1).

It is now necessary to calculate MN_0 , the effective allowable number of load applications that would reproduce the condition at the beginning of the increment

$$MN_0 = 3 * MN_p * (w)^{1/\alpha_2} \quad (2.15)$$

Note that the damage w used in this calculation is from the previous increment and α_2 is a calibration parameter. The total number of load applications for the current increment, MN_{tot} , is

$$MN_{tot} = MN_0 + \left(\frac{N}{10^6} \right) \quad (2.16)$$

given that

$$N = 30 \cdot N_{IN} \cdot \left(\frac{1}{n_{qt}} \right) \cdot \left(\frac{1}{n_{lp}} \right) \quad (2.17)$$

where N_{IN} is the number of load applications from the traffic file, n_{qt} is the number of quintile temperatures in a single month, and n_{lp} is the number of load positions used.

Finally, the damage w in the current increment corresponding to the total number of load applications, MN_{tot} , is calculated as

$$w = \left(\frac{MN_{tot}}{3 * MN_p} \right)^{\alpha 2} \quad (2.18)$$

where both MN_{tot} and MN_p are in millions (10^6) of load applications.

The damage is then calculated for the next increment of axle weights, axle types, load positions, and quintile temperatures in a single month. Finally, it is calculated for each month in the pavement design life, in a similar manner.

2.3 TPF-5(149) M-E Design to Mitigate Rutting in TICP

The procedure developed under TPF-5(149) to design TICP and better account for rutting 1) employs the input files generated by executing a MEPDG project and 2) calculates the rut depth in an AC overlaid PCC pavement based on the CalME rutting model developed at the University of California-Davis. The rut-depth calculation is a three-step process which involves:

1. Computation of fatigue damage;
2. Calculation of rut depth based on fatigue damage;
3. Extracting information from intermediate MEPDG project files to be used as inputs for the above calculations.

The following subsections describe the specific steps to be employed when incorporating the CalME rutting procedure into an MEPDG project for a TICP.

2.3.1 Create and run MEPDG for TICP project file

The first step in the modified TPF-5(149) procedure is to create a HMA-PCC project file in the MEPDG program that best describes the desired TICP project. Once the project is created, the project file should be run to completion. Doing so creates traffic and climate analysis files that are necessary to augment the MEPDG analysis with the CalME rutting model.

2.3.2 Run TPF-5(149) program to read MEPDG inputs for CalME calibration

The next step is to run the TPF-5(149) program, which will read intermediate MEPDG project files to create calibration coefficients for the CalME fatigue and rutting models, detailed in Sections 2.2.1 and 2.2.2 respectively. Table 1 provides example values for these coefficients for three HMA mix designs for the calculation of fatigue damage. These coefficients were calculated based on laboratory data for the HMA mixes of the HVS (PG 64-28 PM and RHMA-G) and MnROAD (PG 64-34) test sections by using nonlinear regression obtained by the

University of California-Davis under the SHRP2 R21 project. In the combined MEPDG/CalME program for TPF-5(149), these calibration parameters are extracted directly from the MEPDG intermediate files.

Table 1. Model coefficients for CalME fatigue model

HMA Mix	A2	β_2	γ_2	δ_2
PG 64-28 PM	1.9166	2.6490	0	4.2084
RHMA	0.3593	3.9425	0	1.7189
PG 64-34	0.7546	3.3804	0	2.2463

Table 2 describes values for these coefficients for the same HMA mix designs for the rut depth calculation.

Table 2. Model coefficients for CalME rutting model

HMA Mix	A3	α_3	β_3	γ_3	τ_{ref}
PG 64-28 PM	1.9166	2.6490	0	4.2084	0.1
RHMA	0.3593	3.9425	0	1.7189	0.1
PG 64-34	0.7546	3.3804	0	2.2463	0.1

The input files necessary to develop these calibration coefficients are detailed in the following step-by-step procedure. The input files listed below are extracted from the outputs generated by executing a MEPDG project. The extraction process is simplified by executing the program from the compiled and built source code ‘NewCivilGUI.jar’. The program extracts required information from the structural, traffic, and temperature files of a MEPDG project (Figure 2).

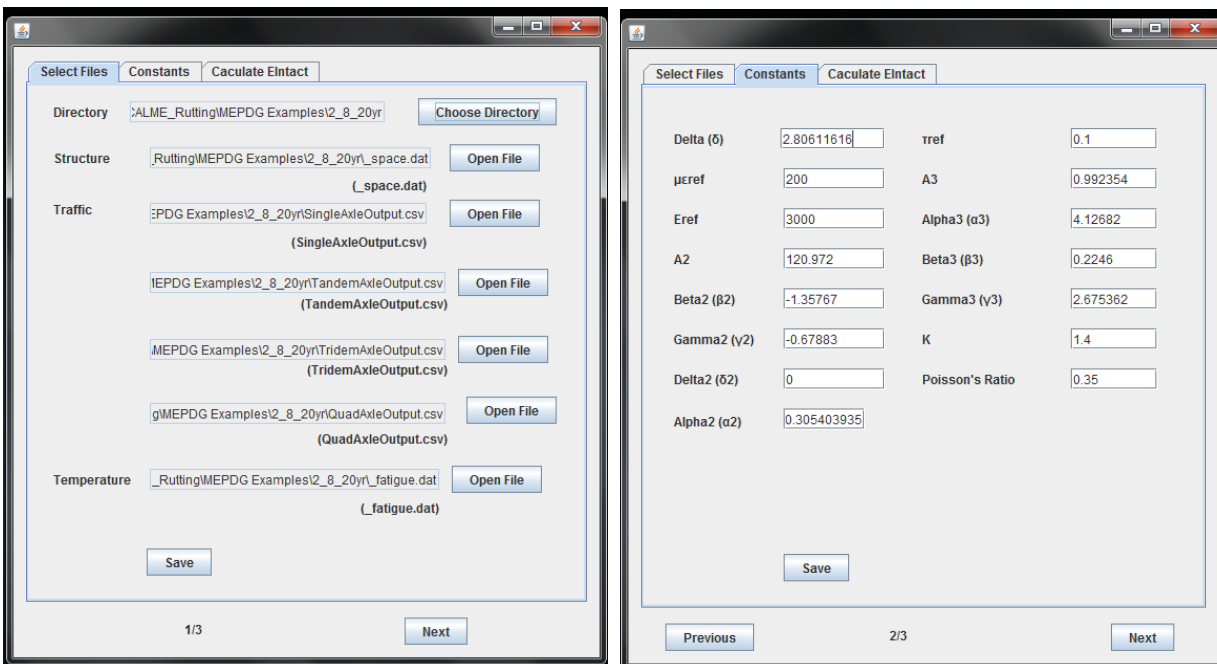


Figure 2. GUI for extracting MEPDG project input information (at left) and extracting calibration constants (at right)

The constants for the calculation of AC dynamic modulus are also extracted from the MEPDG temporary files and saved (Figure 2). The user may overwrite these constants before saving them, if required. The following subsections describe each of the input files containing the required data for the TPF-5(149) pavement design procedure.

Step 1: Structural inputs from `_space.dat`

The MEPDG temporary file “`_space.dat`” is used for reading the number and thicknesses of the AC sublayers. Figure 3 presents the thicknesses of sublayers AC1, AC2, and AC3 as highlighted in rows # 3 to 5. Also, note the total number of months as highlighted in row 10 of the example file.

```

1 8
2 0, 1, 0.00
3 1, 1, 0.50
4 2, 1, 0.50
5 3, 1, 1.00
6 4, 2, 7.00
7 5, 3, 6.00
8 6, 4, 24.07
9 7, 4, 316.92
10 61
11 0,9/ 1/1996, 8
12 0, 1.000, 0.000
13 1, 1.000, 0.000
14 2, 1.000, 0.000
15 3, 1.000, 0.000
16 4, 1.000, 0.000
17 5, 1.264, 0.116
18 6, 0.844, 0.309
19 7, 0.600, 0.346
20 0.637, 0.340, 0.777, 0.318
21 0,10/ 1/1996, 8
22 0, 1.000, 0.000
23 1, 1.000, 0.000
24 2, 1.000, 0.000
25 3, 1.000, 0.000
26 4, 1.000, 0.000

```

Figure 3. MEPDG file “`_space.dat`”, specifying pavement structure

Step 2: Traffic open timing from `MonthlySeasonPattern.txt`

The MEPDG file “`MonthlySeasonPattern.txt`” is used for reading the number of months between construction and traffic open as highlighted in rows # 4. Subtract the number of months between construction and traffic open from the total number of months (highlighted in Figure 4) to obtain the number of months for actual analysis.


```

1 284.2 343.7 254.9 154 163.7 171.2 177.1 180.6 185.8 186 186.5 206.8
2 6.545e+006 5.806e+006 4.759e+006 3.405e+006 2.338e+006 1.803e+006 1.495e+006 1
3 75.6 73.6 68.3 59.8 62.9 66.5 67.8 70.1 68.4 67.7 72.8
4 1, #Number of months between construction and traffic open
5 0 693.1 4.423e+006
6 1 717.6 4.579e+006
7 2 731.1 4.665e+006
8 3 740.2 4.724e+006
9 4 747 4.767e+006
10 5 752.5 4.802e+006
11 6 757 4.831e+006
12 7 760.8 4.855e+006
13 8 764.1 4.876e+006
14 9 767 4.895e+006
15 10 769.6 4.912e+006
16 11 772 4.926e+006
17 12 774.1 4.94e+006
18 24 790.5 5.044e+006
19 36 799.4 5.102e+006
20 48 805.5 5.14e+006
21 60 810 5.169e+006
22 72 813.5 5.192e+006
23 84 816.4 5.21e+006
24 96 818.9 5.226e+006
25 108 820.9 5.239e+006
26 120 822.8 5.251e+006

```

Figure 4. MEPDG input file specifying number of months between construction and traffic open

Step 3: Temperature data from _fatigue.dat

The MEPDG temporary file “_fatigue.dat” is used for reading monthly quintile temperatures corresponding to each sublayer of AC. Skip records corresponding to the number of months between construction and traffic open. Figure 5 presents the five quintile temperatures (T1, T2, T3, T4, and T5) for sublayer AC1 highlighted in row # 8 for the month of October 1996.

Line	Temp	Load Pos	W1	W2	W3	W4	W5	W6	W7	W8
1	0, 9/	1/1996,	10							
2	0,	1,	50.2,	58.1,	65.8,	73.8,	89.7,	67.55,	14.23	
3	1,	1,	50.9,	58.4,	65.9,	73.5,	88.6,	67.46,	13.60	
4	2,	1,	51.9,	58.9,	66.1,	73.0,	86.4,	67.25,	12.50	
5	3,	1,	53.2,	59.5,	66.1,	72.1,	83.8,	66.93,	11.07	
6	0, 10/	1/1996,	10							
7	0,	1,	35.8,	45.1,	52.4,	59.7,	73.8,	53.37,	13.68	
8	1,	1,	36.4,	45.5,	52.6,	59.6,	72.9,	53.41,	13.14	
9	2,	1,	37.6,	46.2,	53.1,	59.5,	71.3,	53.54,	12.17	
10	3,	1,	39.1,	47.2,	53.6,	59.2,	69.3,	53.67,	10.89	
11	1, 11/	1/1996,	10							
12	0,	1,	19.4,	27.1,	32.6,	39.0,	48.2,	33.28,	10.44	
13	1,	1,	20.0,	27.5,	32.8,	38.9,	47.8,	33.41,	10.03	
14	2,	1,	21.0,	28.0,	32.9,	39.0,	47.2,	33.62,	9.44	
15	3,	1,	22.5,	28.8,	33.1,	39.0,	46.4,	33.96,	8.60	
16	1, 11/16/	1996,	10							
17	0,	1,	9.4,	21.3,	25.5,	29.7,	38.3,	24.84,	10.35	
18	1,	1,	10.1,	21.6,	25.7,	29.7,	38.2,	25.04,	10.05	
19	2,	1,	11.5,	22.2,	25.9,	29.8,	37.6,	25.39,	9.40	
20	3,	1,	13.2,	22.9,	26.5,	29.8,	36.9,	25.86,	8.55	
21	1, 12/	1/1996,	10							
22	0,	1,	14.4,	23.5,	26.3,	29.1,	33.6,	25.36,	6.74	
23	1,	1,	15.0,	23.7,	26.3,	28.9,	33.4,	25.46,	6.45	
24	2,	1,	16.0,	24.0,	26.4,	28.8,	32.9,	25.64,	5.93	
25	3,	1,	17.5,	24.6,	26.5,	28.6,	32.3,	25.91,	5.18	
26	1, 12/16/	1996,	10							
27	0,	1,	-4.6,	6.9,	11.8,	16.6,	23.9,	10.98,	9.95	
28	1,	1,	4.0,	7.4,	11.0,	16.7,	22.7,	11.10,	0.66	

Figure 5. MEPDG input file for temperature

Step 4: Traffic data from *.AxleOutput.csv

The MEPDG temporary files “SingleAxleOutput.csv”, “TandemAxleOutput.csv”, “TridemAxleOutput.csv”, and “QuadAxleOutput.csv” are used for reading the number of load applications due to single axle, tandem axle, tridem axle, and quad axle, respectively. The values in the .csv files are listed for an average day in a month. Also, since the monthly temperatures are divided into five quintiles and four load positions are assumed, each cell has to be multiplied with $(30*0.2*0.25)$ to obtain the number of load applications for one month, one quintile temperature, and one load position. The columns of the .csv file denote the weights of an axle. Figure 6 presents the input file for single axle.

The screenshot shows a Microsoft Excel spreadsheet titled 'SingleAxleOutput.csv'. The data is organized in a table with 16 columns (A-P) and 26 rows (1-26). The first column (A) contains years from 2006 to 2008, and the second column (B) contains months from October to November. The remaining 14 columns (C-P) contain numerical values representing traffic inputs for each month-year combination.

Year	Month	C	D	E	F	G	H	I	J	K	L	M	N	O
2006	October	135.743	109.003	150.224	127.212	136.22	167.881	196.658	220.55	200.342	158.581	104.109	69.438	49.8029
2006	November	135.931	109.062	150.184	127.203	136.121	167.768	196.5	220.586	200.338	158.704	104.114	69.4518	49.8029
2006	December	135.916	109.031	150.238	127.11	136.19	167.728	196.514	220.587	200.418	158.645	104.143	69.4409	49.8029
2007	January	135.902	109.017	150.252	127.213	136.117	167.699	196.485	220.633	200.327	158.669	104.171	69.4754	49.8029
2007	February	135.785	109.003	150.194	127.227	136.291	167.699	196.549	220.646	200.413	158.599	104.106	69.4487	49.8035
2007	March	135.83	109.003	150.18	127.096	136.179	167.737	196.604	220.732	200.337	158.674	104.113	69.4478	49.8305
2007	April	135.785	108.887	150.659	127.259	136.163	167.648	196.48	220.605	200.346	158.584	104.097	69.4484	49.8029
2007	May	135.902	109.017	150.297	127.1	136.173	167.685	196.542	220.618	200.374	158.599	104.151	69.4895	49.8167
2007	June	135.93	109.017	150.238	127.119	136.213	167.82	196.571	220.605	200.248	158.607	104.114	69.4522	49.817
2007	July	135.906	109.017	150.242	127.114	136.194	167.722	196.552	220.63	200.377	158.613	104.114	69.466	49.817
2007	August	135.929	109.003	150.224	127.11	136.22	167.727	196.458	220.66	200.363	158.651	104.153	69.4487	49.817
2007	September	135.902	109.017	150.294	127.17	136.211	167.705	196.5	220.573	200.349	158.694	104.1	69.438	49.8063
2007	October	141.173	113.363	156.233	132.3	141.669	174.596	204.524	229.372	208.355	164.924	108.274	72.2155	51.795
2007	November	141.368	113.424	156.191	132.291	141.566	174.478	204.36	229.409	208.352	165.052	108.278	72.2298	51.795
2007	December	141.353	113.392	156.247	132.195	141.637	174.437	204.375	229.411	208.435	164.991	108.308	72.2185	51.795
2008	January	141.338	113.378	156.262	132.301	141.562	174.406	204.344	229.458	208.34	165.015	108.338	72.2543	51.795
2008	February	141.217	113.363	156.201	132.316	141.743	174.407	204.411	229.472	208.43	164.943	108.27	72.2266	51.7956
2008	March	141.263	113.363	156.187	132.18	141.626	174.446	204.468	229.561	208.35	165.021	108.278	72.2256	51.8236
2008	April	141.217	113.242	156.686	132.349	141.61	174.353	204.339	229.429	208.36	164.927	108.26	72.2262	51.795
2008	May	141.338	113.378	156.308	132.184	141.619	174.392	204.404	229.443	208.389	164.942	108.317	72.269	51.8093
2008	June	141.367	113.378	156.248	132.204	141.661	174.533	204.433	229.429	208.258	164.951	108.278	72.2302	51.8097
2008	July	141.342	113.378	156.252	132.198	141.641	174.431	204.414	229.455	208.392	164.958	108.278	72.2445	51.8097
2008	August	141.367	113.363	156.233	132.194	141.669	174.435	204.316	229.487	208.377	164.997	108.319	72.2266	51.8097
2008	September	141.338	113.378	156.306	132.256	141.659	174.413	204.36	229.396	208.363	165.042	108.264	72.2155	51.7986
2008	October	146.819	117.898	162.482	137.592	147.335	181.58	212.705	238.547	216.689	171.521	112.605	75.1041	53.8667
2008	November	147.922	117.951	162.428	137.582	147.328	181.457	212.534	238.586	216.685	171.652	112.609	75.119	53.8667

Figure 6. One of three MEPDG files used to obtain traffic inputs

Step 5: Dynamic modulus parameters from HMA1*.tmp

The constants for the calculation of AC dynamic modulus are read from the MEPDG temporary files “HMA1Input.tmp” and “HMA1Output.tmp”. The file HMA1Input.tmp includes constants MaaT, reference temperature TR, A, and VTS (in this exact order) as shown at left in Figure 7. The location of the constants in the file seems fixed. The file HMA1Output.tmp includes constants i , α , β , γ , and c as shown at right in Figure 7. The location of the constants in the file is at line 21; this has been confirmed for several MEPDG cases and appears to be an MEPDG standard.

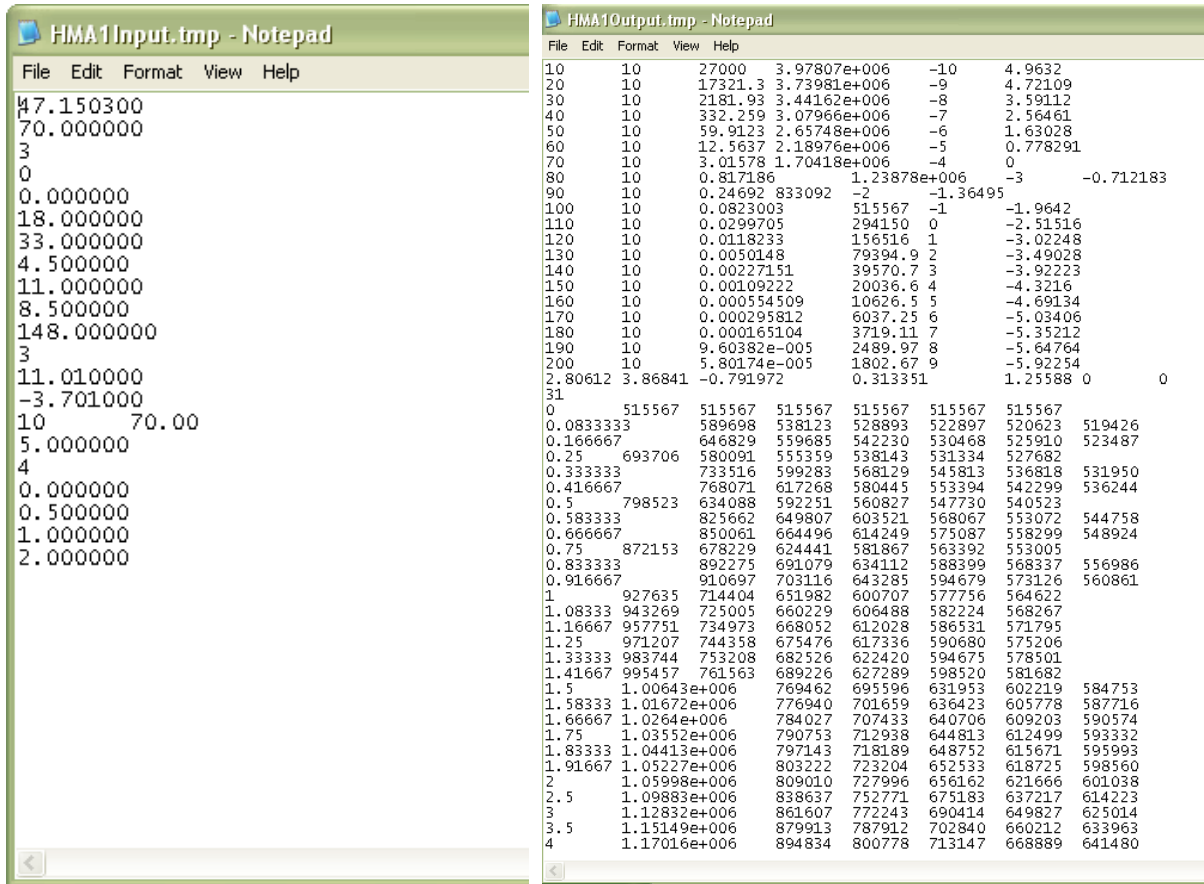


Figure 7. MEPDG files used to obtain dynamic modulus of AC layer

Step 6: Layer moduli from layermodulus.tmp

The MEPDG temporary file “layermodulus.tmp” is used for reading the layer modulus for all layers corresponding to each month of the pavement design life. This file is illustrated in Figure 8.

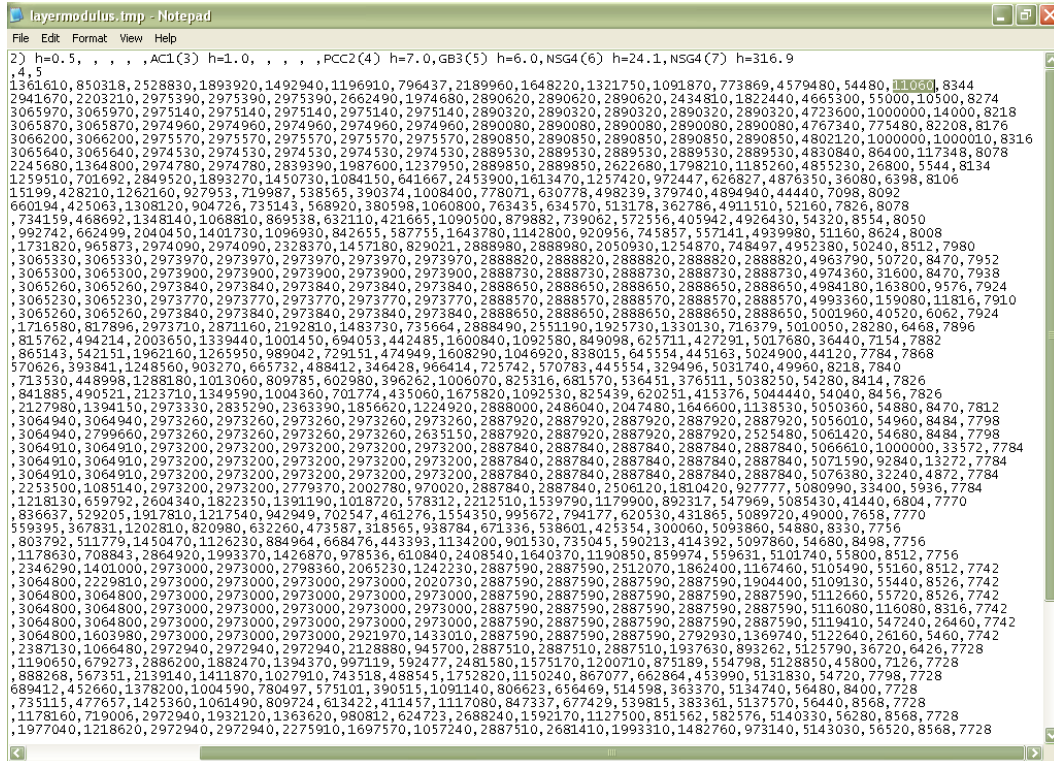


Figure 8. MEPDG temporary file describing monthly modulus values for all layer and sublayers in the TICP project

Step 6 is the final step in the process of intermediate inputs prior to running the TPF-5(149) program for rutting.

2.3.3 Run TPF-5(149) program to supplement MEPDG results with predicted rutting depth results from CalME

After the provision of appropriate calibration coefficients to the CalME models for a given project, the TPF-5(149) program then conducts the CalME rutting analysis and creates modified project output files. These files detail predicted rutting for the HMA-PCC project according to CalME.

2.4 Validation of TPF-5(149) Procedure for Rutting in TICP

The research team used two sources of existing HMA-PCC rutting data to validate the incorporation of the CalME rutting model into the MEPDG framework: full-scale accelerated testing data from the SHRP2 R21 project and HMA-PCC test section data from the MnROAD facility. The following subsections describe validation efforts using those datasets.

2.4.1 UCPRC Heavy Vehicle Simulator (HVS) SHRP2 R21 data

The University of California Pavement Research Center (UCPRC) Heavy Vehicle Simulator (HVS) is a mobile load frame that uses a full-scale wheel (dual or single) to traffic the pavement

test section. This subsection describes an example of HVS testing of a TICP section at UCPRC (Section 609HB) conducted under the SHRP2 R21 project (SHRP/ARA 2012).

2.4.1.1 HVS test procedure

The trafficked test section is 8 m (26.4 ft) long, of which 1 m (3.3 ft) on each end are used for turnaround of the wheel and are generally not included in analysis and reporting of results. This wheelpath length permits the testing of one slab of jointed PCC of up to approximately 6 m (19.8 ft) with the trafficking including both joints and the entire slab. The specifications and a photograph of the HVS are shown in Figure 9.

Overall weight	59,646 kg	
Load weight of the test wheel tire	20-100 kN with truck tire	
	20-200 kN with aircraft tire	
Dimensions of tested area of pavement	1.5 m × 8 m maximum	
Velocity of the test wheel	10 km/hr maximum	
Maximum trafficking rate	1000 repetitions/hr	
Average trafficking rate	750 repetitions/hr	
Average daily repetitions	16,000	
Dimensions:	Length	22.56 m
	Width, overall	3.73 m
	Height	3.7 m
	Wheel base	16.7m
Number of axles	3 (1 in rear, 2 in front)	

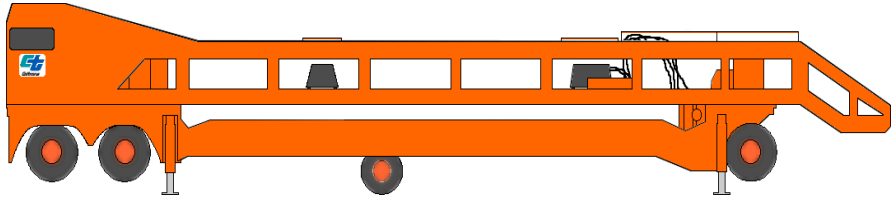


Figure 9. The HVS apparatus at UCPRC

The sections tested to verify the rutting model were assigned a failure criterion of an average maximum rut of 12.5 mm (0.5 in.) over the full monitored section. Testing was continued past a 12.5-mm average rut depth until the rutting accumulation rate stabilized. The HVS loading program for the example is summarized in Table 3. Tire pressure was constant at 690kPa (100 psi) for the test section.

Table 3. HVS loading program for example section

Section	Mix type	As-built Thickness (mm)	Wheel Load (kN)	Temperatures at 50 mm (2 in.)		Total Repetitions
				Average (°C)	SD (°C)	
609HB	PG 64-28 PM	116	40	49.5	1.1	63,750
			60			

The pavement temperature at 50 mm (2.0 in.) depth was maintained at $50^{\circ}\text{C}\pm 4^{\circ}\text{C}$ ($122^{\circ}\text{F}\pm 7^{\circ}\text{F}$) to assess rutting potential under typical pavement conditions. Heaters were operated inside the temperature control box to maintain the pavement temperature. The pavement surface received no direct rainfall as it was protected by the temperature control unit. The sections were tested predominantly during the wet season, however, measures were taken to keep water from entering the pavement structure inside the temperature control box, and there was an extensive drainage system placed around the entire set of pavement test sections. In addition, plastic sheets were placed on the surface to keep water out of the pavement.

2.4.1.2 HVS test temperature and loading conditions

All HVS sections were monitored closely. The following examples for Section 609HB detail the monitoring of load history and temperature at UCPRC. Figure 10 illustrates the HVS loading history for the example section.

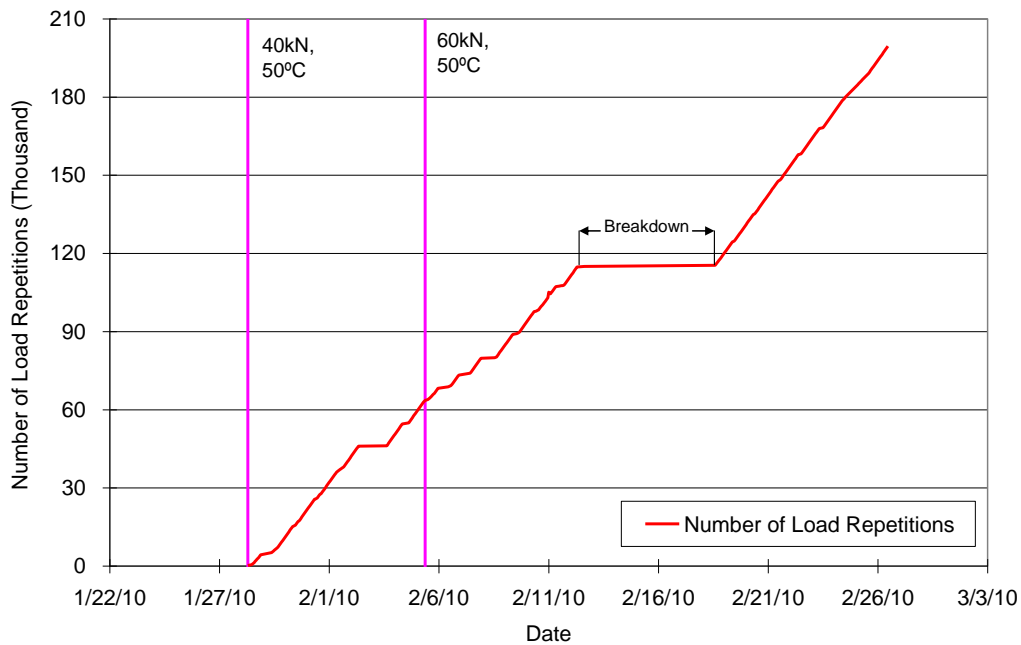


Figure 10. Section 609HB load history

Outside air temperatures for the example section are summarized in Figure 11. Vertical error bars on each point on the graph show daily temperature range. Hence, for Section 609HB, temperatures ranged from 1.4°C to 20.9°C (34.5°F to 69.6°F) during the course of HVS testing, with a daily average of 10.6°C (51.1°F), an average minimum of 6.7°C (44.1°F), and an average maximum of 15.5°C (59.9°F).

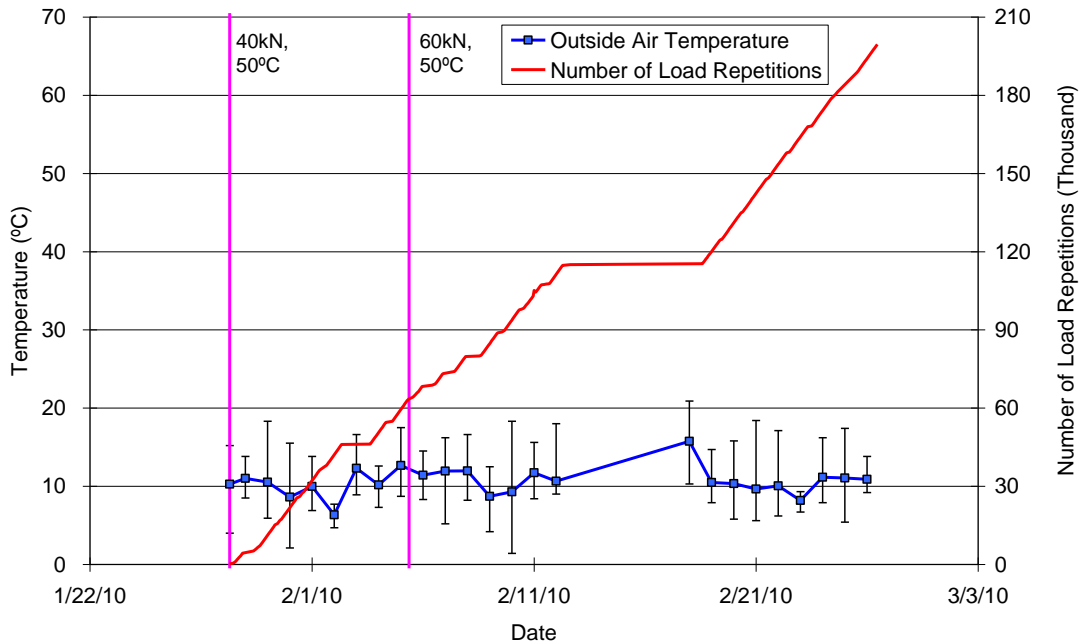


Figure 11. Daily average outside air temperatures.

During the test, air temperatures inside the temperature control unit at Section 609HB ranged from 15.6°C to 52.9°C (60.1°F to 127.2°F) with an average of 41.1°C (106°F) and standard deviation of 2.6°C (4.7°F). The daily average air temperatures recorded in the temperature control unit, calculated from the hourly temperatures recorded during HVS operation, are shown in Figure 12. Vertical errors bars on each point on the graph show daily temperature range.

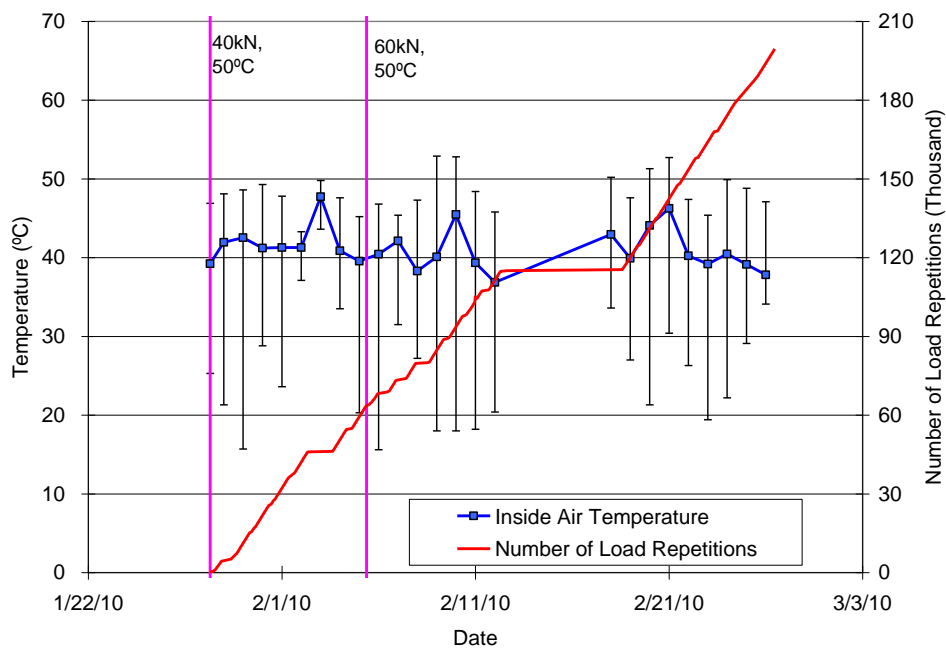


Figure 12. Daily average inside air temperatures.

Daily averages of the surface and in-depth temperatures of the asphalt concrete layers of Section 609HB are listed in Table 4 and shown in Figure 13. Similar tables were constructed for other sections involved in the SHRP2 R21 tests at UCPRC. Pavement temperatures decreased slightly with increasing depth in the pavement, which was expected as there is usually a thermal gradient between the top and bottom of the asphalt concrete pavement layers.

Table 4. Section 609HB temperature summary for air and pavement.

Temperature	Average (°C)	Std Dev (°C)	Average (°F)	Std Dev (°F)
Outside air	10.6	1.8	51.1	3.2
Inside air	41.1	2.6	106.0	4.7
Pavement surface	47.8	2.0	118.0	3.6
- 25 mm below surface	49.7	1.3	121.4	2.4
- 50 mm below surface	49.5	1.1	121.1	2.0
- 90 mm below surface	48.6	0.9	119.5	1.7
- 120 mm below surface	47.5	0.9	117.4	1.7

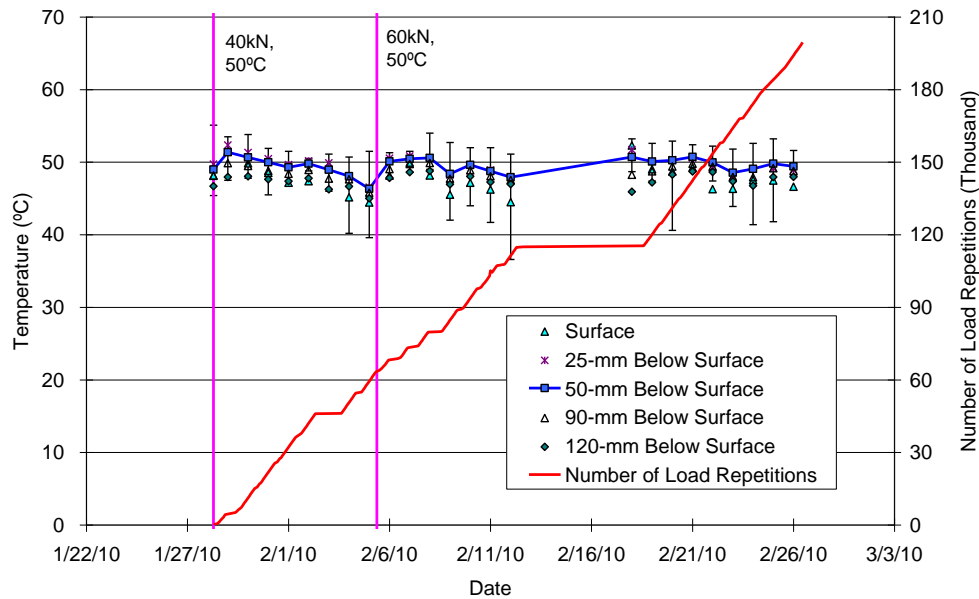


Figure 13. Daily average temperatures at surface and various depths of Section 609HB

2.4.1.3 HVS rutting measurements

The section was monitored closely through its load history to determine strain and deformation of the section at regular intervals. Plastic strain was computed using temperature at 50 mm depth of the asphalt concrete and the temperature gradient. Permanent deformation at the pavement surface (rutting) was monitored with a surface profilometer and strain gauges at 50 mm depth in the asphalt in the sections with thicker HMA layers (strain gauges placed between the two lifts of HMA used to construct the surface layer). The profilometer is a stand-alone moveable device with a traveling downward-shooting vertical laser, which is used to take surface profiles transverse to the direction of the HVS wheel track. Transverse profiles are taken at 0.5-m (1.15-ft) intervals along the test section.

The profilometer, as illustrated in Figure 14, was used to determine average maximum rut depth, average deformation, location and magnitude of the maximum rut depth, and rate of rut development. This discussion for this example will focus on average deformation.

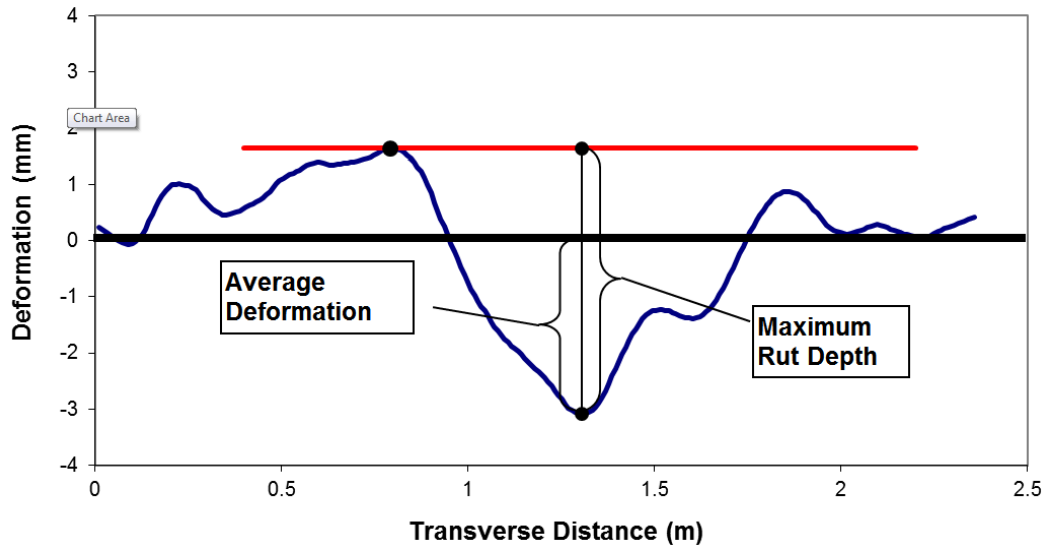


Figure 14. Illustration of maximum rut depth and average deformation of a leveled profile.

The average transverse cross-section for the example section discussed here is illustrated in Figure 15. Note the evolution of rut depth of the course of repeated loading.

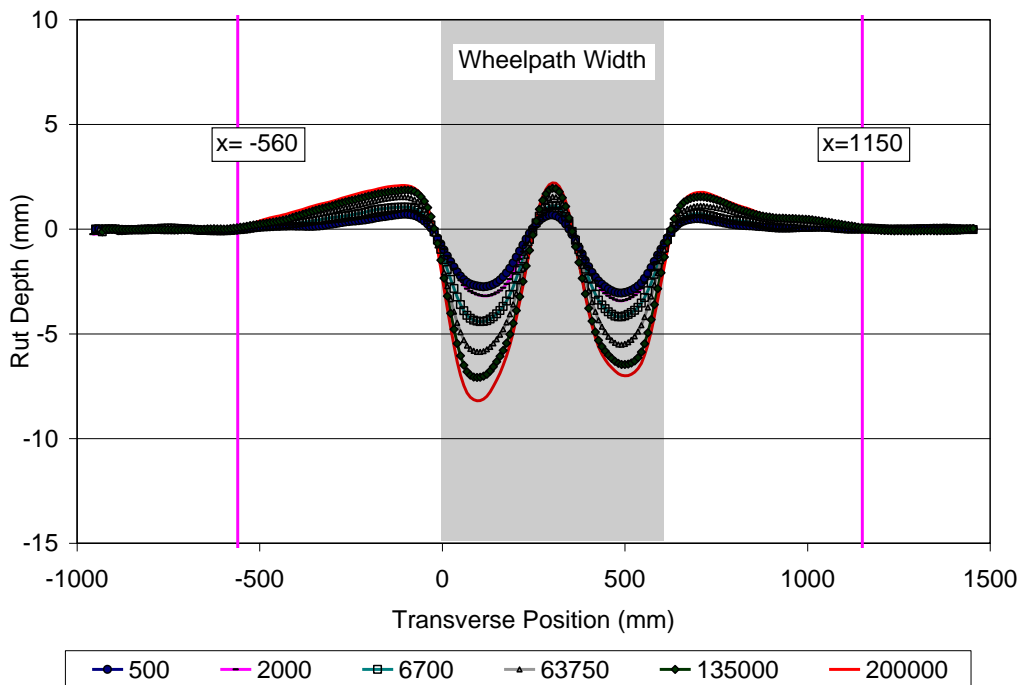


Figure 15. Evolution of Section 609HB rutting profile

During HVS testing, rutting usually accumulates at a faster rate initially due to fast reduction of air voids (densification). Thereafter, it diminishes as trafficking progresses until reaching a steady state. This initial phase is referred to as the “embedment” phase. Figure 16 describes the development of average deformation with load repetitions, with an embedment phase only apparent at the beginning of the experiment (i.e. the first 15000 repetitions). Error bars on the average reading indicate that there was high variation along the length of the section which was a result of the HMA blocks removed for CT image evaluation.

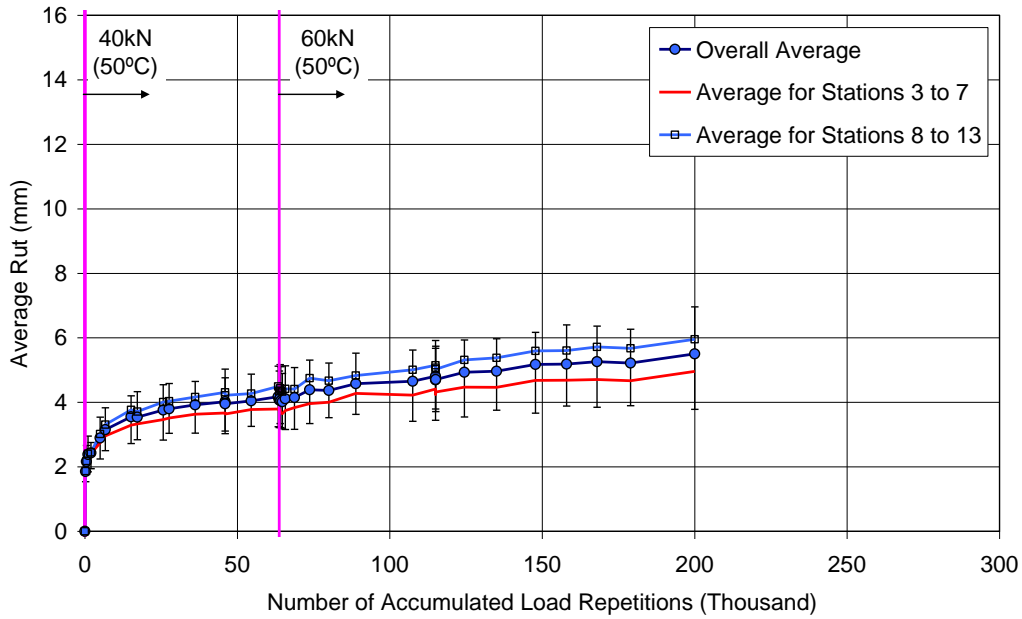


Figure 16. Average deformation for Section 609HB

Apart from rutting, no other distresses were observed on the section. A summary of results from all four HVS sections at UCPRC for the SHRP2 R21 project are illustrated in Figure 17. These results are provided for later validation of the TPF-5(149) procedure.

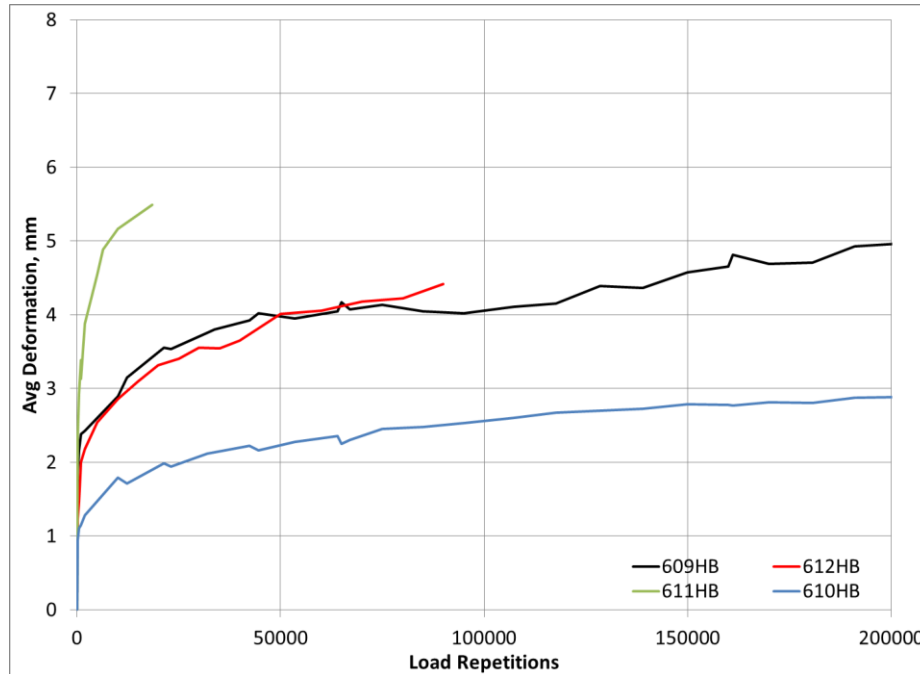


Figure 17. Summary of measured rutting (average deformation) observed at the UCPRC facility for HVS testing

2.4.1.4 TPF-5(149) predicted rutting for HVS test sections

The research team developed MEPDG project files for each of the four SHRP2 R21 test sections at UCPRC, and using the method described in Section 2.3, these project files were used as project inputs for the TPF-5(149) procedure. The measured rutting (in average deformation) for each of these projects relative to HVS load repetitions is illustrated in Figure 18.

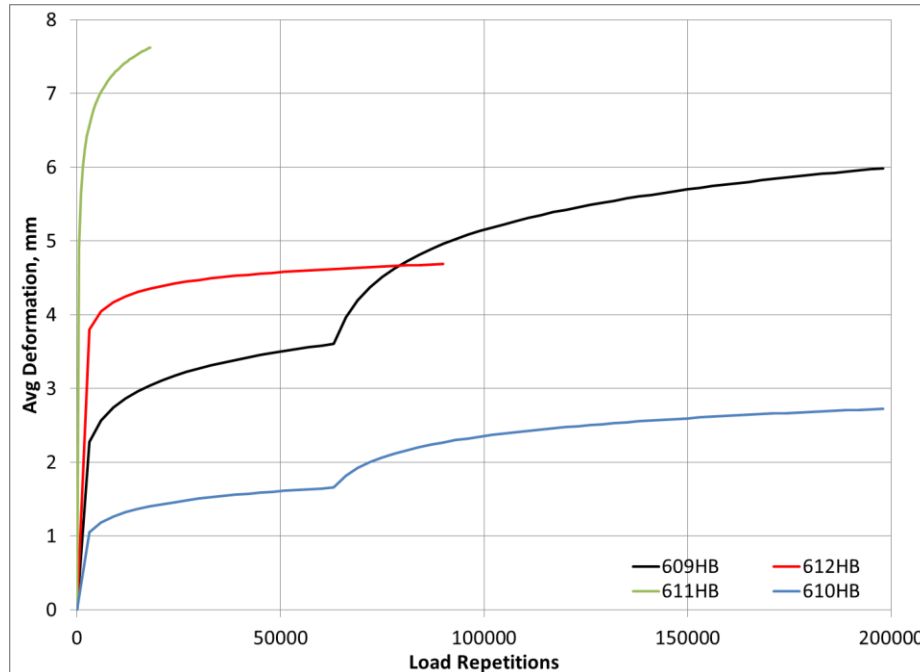


Figure 18. Summary of predicted rutting (average deformation) from TPF-5(149) procedure described in this report

In validating the TPF-5(149) using measured rutting (Figure 17), the research team used MEPDG project files developed by ARA, Inc, that assumed basic Level 3 inputs for all MEPDG material parameters (H. Von Quintus, personal communication, 2012). In this light, the predicted rutting (Figure 18) is reasonable. The goal of the TPF-5(149) procedure is to operate within the MEPDG framework and provide a better model for rutting. By producing reasonable curves for the HVS sections, the TPF-5(149) procedure is validated.

The SHRP2 R21 project used CalME only to evaluate rutting in HMA-PCC, and R21 illustrated that with further calibration, the CalME rutting predictions for HMA-PCC improved. As the CalME rutting model was incorporated into the MEPDG framework without modification to the model itself, tuning the TPF-5(149) procedure is simply a case of modifying the MEPDG project files. Hence, further calibration of the MEPDG project files – including tuning the material properties of the HMA to, in turn, modify the CalME calibration coefficients – would bring the permanent deformation in rutting curves of Figure 18 closer to the HVS measured results of Figure 17.

2.4.2 MnROAD TICP Test Section Measured Rutting

As part of TPF-5(149), TICP full-scale test sections were constructed at MnROAD. This includes Cells 106 and 206 at MnROAD, which have been extensively detailed in earlier task reporting. These cells feature a 2-inch HMA overlay over a 5-inch JPCP slab. The cells are identical in cross-section and materials other than 106 using 1-inch dowels, while 206 is undoweled; Table 5 summarizes the design of Cells 106 and 206.

Table 5. MnROAD Cell 106/206 design in summary

Section	HMA overlay	PCC slab	Base	Subbase	Subgrade	JPCP panel size	Doweling	Construction date
106	2" PG 64-34	5" (Mesabi 4.75 mm Super P)	6" Class 1 Stabilized Aggregate	6" Class 5	Clay	15' x 12'	1" dia dowels	Oct 08
206	2" PG 64-34	5" (Mesabi 4.75 mm Super P)	6" Class 1 Stabilized Aggregate	6" Class 5	Clay	15' x 12'	None	Oct 08

Since construction, Cells 106 and 206 have been included in the varied tests conducted on all pavement test sections at MnROAD. Among these measurements are rutting profiles in average deformation. These profiles are created using an ALPS laser profilometer in a manner similar to that of UCPRC detailed in Section 2.4.1.

The research team developed MEPDG project files for Cells 106 and 206. Default (Level 3) values for the MEPDG were assumed for project files; HMA material properties were adopted from testing by UCPRC for CalME. Using the method described in Section 2.3, these project files were used as a project input for the TPF-5(149) procedure. The measured rutting (in average deformation) for Cells 106 and 206 over time (months since construction) is illustrated in Figure 19.

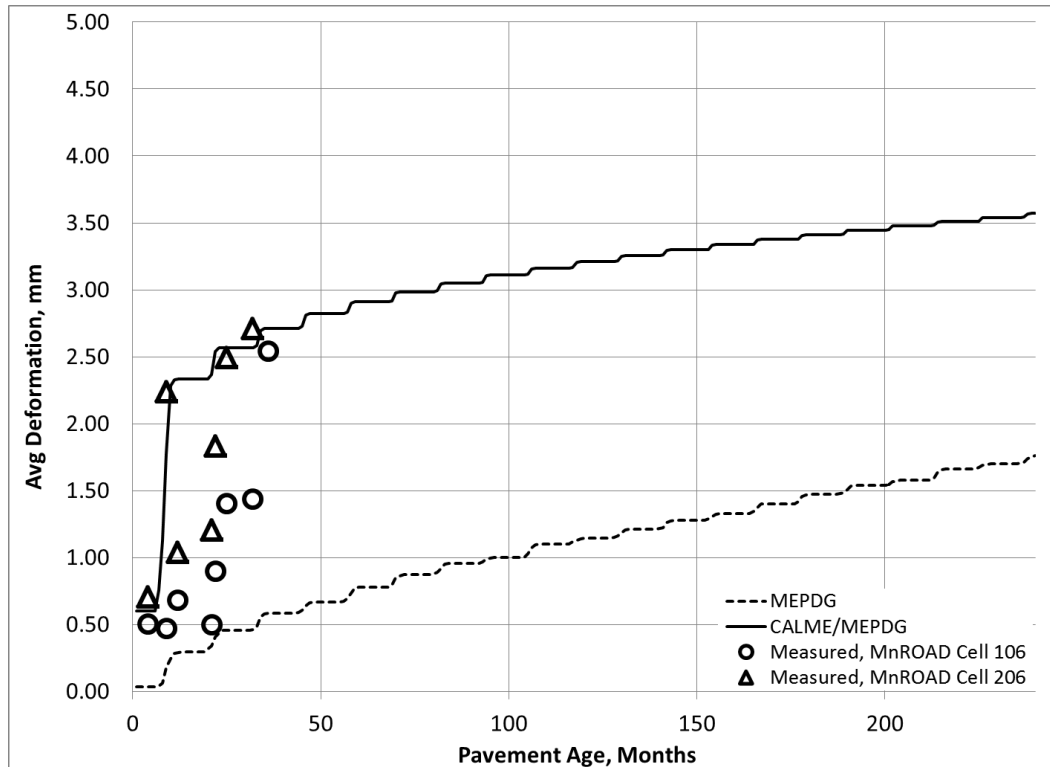


Figure 19. Comparison of TPF-5(149) procedure and unmodified MEPDG procedure predictions for rutting (average deformation) and observed rutting at MnROAD Cells 106 and 206

One of the first observations to be made from Figure 19 is the underprediction for rutting in HMA-PCC by the MEPDG in this case. However, a difficulty of Figure 19 is the measured rutting data itself, which is muddled by natural variability in measurements. In general, a trend in rutting for either test section is difficult to determine from the data, and as a result a comparison with rutting predictions is not informative.

MnROAD contains other HMA-PCC pavements with rutting data that may be of assistance. Figure 20 illustrates average deformation in rutting measured on Cell 70 at MnROAD, which was constructed for the SHRP2 R21 project.

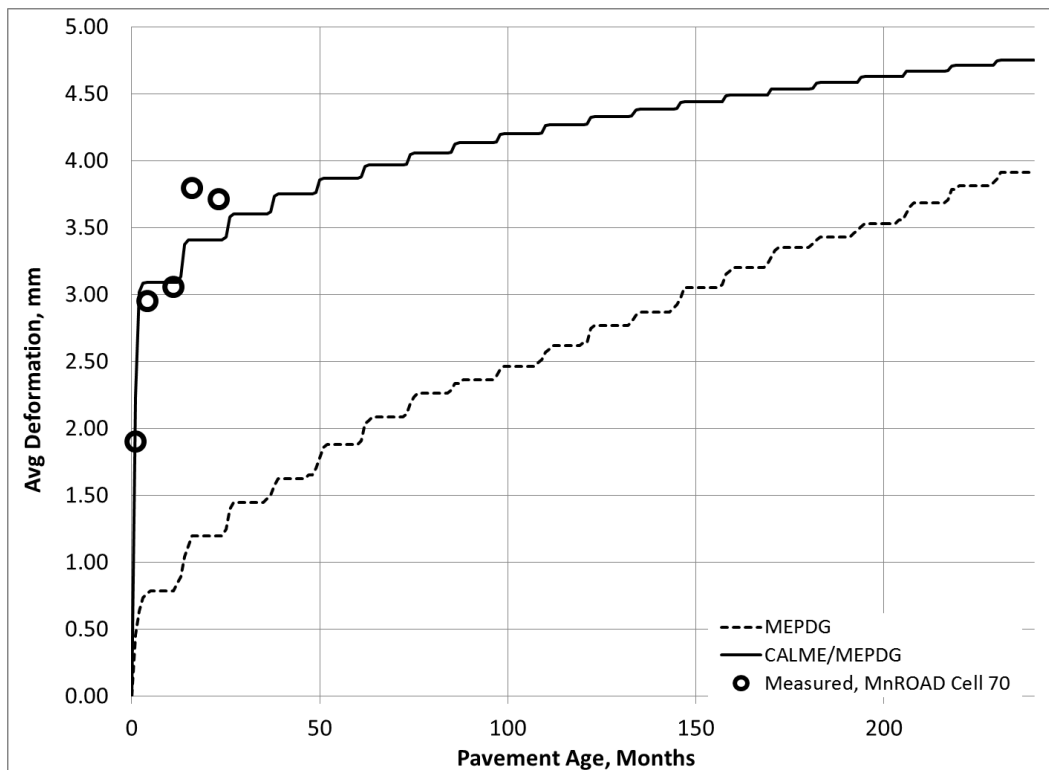


Figure 20. Comparison of TPF-5(149) procedure and unmodified MEPDG procedure predictions for rutting (average deformation) and observed rutting at MnROAD Cell 70

Again, while there is some variability in the data set illustrated in Figure 20, a trend is much easier to spot in this data set. For Cell 70, the TPF-5(149) procedure appears to capture rutting behavior for its early life. In the cases of Cells 106/206 and Cell 70, continued monitoring at MnROAD will help evaluate the effectiveness of the TPF-5(149) procedure.

Overall, the validation of Figure 19 and Figure 20 indicates that the TPF-5(149) procedure is attractive alternative to the exclusive use of MEPDG. It should also be noted that the analysis using TPF-5(149) above assumed Level 3 inputs, and thus it could be further calibrated and modified to resemble MnROAD Cell 106/206 and Cell 70 conditions.

2.5 Sensitivity Analysis of TPF-5(149) Procedure for Rutting in TICP

Given that both the MEPDG and CalME rutting model have been subjected to extensive review and sensitivity analysis, the need for an in-depth sensitivity analysis of the TPF-5(149) procedure was not a critical concern for the work of Task 5. However, the research team undertook a brief analysis of rutting performance sensitivity to two important parameters: HMA thickness and climate. Other than these two parameters, the sensitivity study assumed structural properties of an HMA-PCC pavement with 2 inches (50 mm) HMA over 7 inches (175 mm) JPCP. Furthermore, the analysis assumed MEPDG defaults for material properties (Level 3 inputs) for all projects. Assumed traffic was 2000 AADTT.

2.5.1 Climate

Figure 21 illustrates the sensitivity of rutting predictions to climate for 5 locations. Each of these locations corresponds to EICM climate files (*.icm) for Seattle, WA; Pullman, WA; Sacramento, CA; San Francisco, CA; and Minneapolis-Saint Paul, MN.

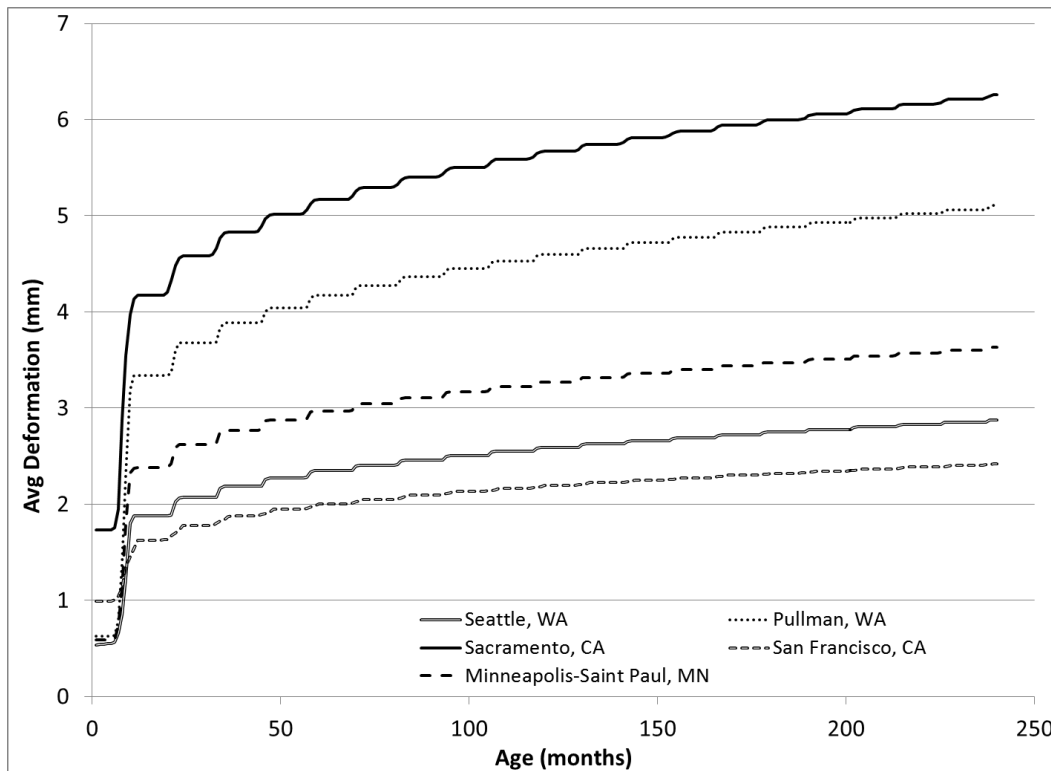


Figure 21. TPF-5(149) procedure for rutting, sensitivity to climate

Climate is an influential parameter on rutting performance. This behavior is in keeping with other M-E models for rutting, and thus the TPF-5(149) procedure performs acceptably in this regard. Furthermore, it should be noted that in this analysis, the asphalt mix properties are kept constant, which obviously does not mirror in-field conditions, wherein the properties would change along with climate conditions.

2.5.2 Pavement Thickness

Figure 22 illustrates the sensitivity of TPF-5(149) procedure predictions for rutting to 4 levels of HMA thickness. The projects in Figure 22 were developed for an EICM climate file developed from weather data for Sacramento International Airport (SMF) in Sacramento, CA. For projects examining sensitivity to HMA thickness, PCC thickness was held at a constant 7 inches (175 mm).

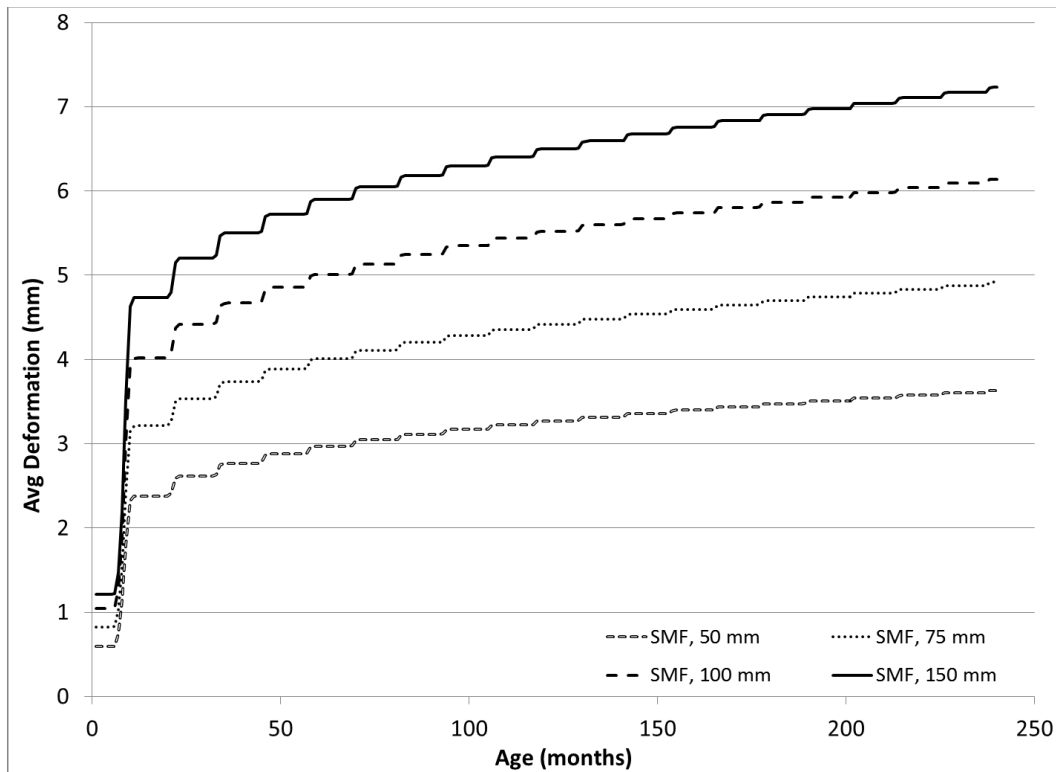


Figure 22. TPF-5(149) procedure for rutting, sensitivity to HMA overlay thickness

As with climate, the objective of the HMA thickness sensitivity study is merely to validate the TPF-5(149) procedure against M-E expectations. Here as overlay thickness increases, so does the extent of rutting. This agrees with HVS testing experience observed under the SHRP2 R21 project (SHRP 2012).

3. HMA-PCC Reflective Cracking Models

In HMA-PCC composites such as TICPs, localized high stresses at the base of the HMA overlay above joints/cracks can result in cracks that propagate through the overlay thickness. These cracks can be caused by various phenomena, most notably the displacement of cracks or joints in the underlying PCC pavement (due to traffic loading or temperature) and the deformation of the overlay due to thermal effects. The initiation and propagation of cracking in the overlay due to preexisting cracks/joints in the rigid pavement is known as reflective (or reflection) cracking.

As state, local, and federal interest in composite pavements increases, so does research in the mechanistic-empirical (M-E) modeling of reflective cracking. Some of these models include:

- CRACKTIP, a two-dimensional finite element model developed for HMA overlays by Jayawickrama and Lytton (1987), is capable of modeling reflective cracking for HMA-PCC in the presence of traffic loads (not thermal effects).
- The Computer Aided Pavement Analysis (CAPA) program developed by Scarpas et al (1993) included the ability to investigate the response of the HMA overlay to both thermal and traffic loads and the propagation of fracture through the overlay.
- Kohale and Lytton (2000) developed an M-E model for overlay design involving interlayer techniques.
- Ullidtz et al (2006) developed a reflection cracking model for the California Mechanistic-Empirical Design (CalME).
- NCHRP (2010) recently released a reflective cracking model developed under NCHRP Project 1-41 specifically to update the MEPDG procedure for HMA-PCC design and analysis (NCHRP 2010).

Additional M-E models for reflective cracking are detailed in Bennert (2011).

Given the modification of the MEPDG using the CalME rutting model for TPF-5(149), the research team considered an investigation of the CalME reflective cracking model and possible modification of the MEPDG similar to the TPF-5(149) procedure for rutting. After discussions with the technical panel, the NCHRP 1-41 model was also considered a focus of TPF-5(149) for modeling reflective cracking in TICP. As a part of Task 5, the research team:

- Reviewed the original MEPDG reflective cracking model;
- Reviewed the NCHRP 1-41 model and the NCHRP 1-41 program to be used alongside the MEPDG;
- Reviewed the CalME reflection cracking model;
- Evaluated the suitability of NCHRP 1-41 for HMA-PCC design using the MEPDG, including the development of MEPDG project companion tools; and
- Developed reflection cracking procedure for TPF-5(149) using MEPDG framework and CalME reflective cracking model.

These efforts are detailed in the following subsections, which also include a brief overview of the original MEPDG reflective cracking model.

3.1 Original MEPDG Reflective Cracking Model

The MEPDG predicts reflection cracks in HMA overlays of HMA-PCC projects using a regression model derived from empirical data. The MEPDG does not specify a severity level to be associated with predicted reflection cracking. This regression equation estimates the percentage of area of cracks that propagate through the overlay, RC , as a function of time, t , using a sigmoid function

$$RC = \frac{100}{1 + e^{a(c)+bt(d)}} \quad (3.1)$$

where a and b are regression fitting parameters defined through a calibration process and parameters c and d are defined by the user to describe cracking progression. The parameters a and b are a function of the effective HMA overlay thickness, H_{eff} , which is a function of the overlay thickness and a rating of the load-transfer efficiency.

$$a = 3.5 + 0.75(H_{eff}) \quad (3.2)$$

$$b = -0.688684 - 3.37302(H_{eff})^{-0.915469} \quad (3.3)$$

Values assigned for H_{eff} can be found in AASHTO (2008).

Table 6. Assigned values for H_{eff} , c , and d in original MEPDG reflective cracking model (from AASHTO 2008)

Pavement Type	H_{eff}	c	d	
			(to delay cracking by 2 years)	(to accelerate cracking by 2 years)
Rigid-Good Load Transfer	$H_{eff} = H_{HMA} - 1$	---	---	---
Rigid-Poor Load Transfer	$H_{eff} = H_{HMA} - 3$	---	---	---
Effective Overlay Thickness, H_{eff}, inches	---	---	---	---
<4	---	1.0	0.6	3.0
4 to 6	---	1.0	0.7	1.7
>6	---	1.0	0.8	1.4

The user-defined cracking progression parameters c and d can be used to accelerate or delay the amount of reflection cracks. The model is very sensitive to these parameters, and as a result of their being arbitrarily assigned for the release of MEPDG and left to the user to refine, the original MEPDG reflective cracking model is essentially uncalibrated and to be implemented with caution. Thus reflective cracking was incorporated into the MEPDG as a placeholder, assuming that either the model would be calibrated or revised entirely (which was the result of NCHRP 1-41).

3.2 NCHRP 1-41 Reflective Cracking Procedure for MEPDG

As detailed in the section introduction, the NCHRP 1-41 project was recently completed. This project provides MEPDG uses with an updated model for reflective cracking and a program that interfaces with the MEPDG to use project file inputs to predict reflective cracking. The following subsections discuss these components individually and describe the TPF-5(149) research team experiences in running self-consistency checks and sensitivity analyses on the NCHRP 1-41 procedure.

3.2.1 NCHRP 1-41 Reflective Cracking Model

The NCHRP 1-41 model for reflective cracking is the most sophisticated reflective cracking currently available for HMA-PCC design and analysis (NCHRP 2010). It utilizes many inputs that are similar to those in MEPDG project files, and it also uses EICM for climate response (as does the MEPDG). This is no accident, as the NCHRP 1-41 project specifically targeted improving the MEPDG reflection cracking model in a manner that produced a model that is consistent with the MEPDG framework.

Targeting the MEPDG does not limit the 1-41 model, however, and in fact it is very complex and is built on a finite element model to approximate strains in the HMA overlay. The 1-41 model accounts for a wide variety of user inputs. This includes climate, HMA overlay thickness and material properties, PCC layer thickness and material properties, joint load transfer characteristics, and subgrade properties. Thus the 1-41 model considers load transfer at the joint, which has been shown to be a key factor in delaying the onset of reflective cracking in HMA-PCC (Bennert 2011). Furthermore, the 1-41 model considers three levels of cracking severity (low, medium, and high), and thus provides flexibility in examining the effects of reflective cracking on a given project/design.

For each group of severity levels, the 1-41 model has the form

$$D(N_i)(\%) = e^{-\left(\frac{\rho}{N_i}\right)^\beta} \quad (3.4)$$

where $D(N_i)$ is the percent of reflection crack length of maximum crack length associated with maximum allowable load repetitions N ; i is the i^{th} crack observed; and N_i is the number of days after overlay construction. For the NCHRP 1-41 model, the calibration coefficients ρ and β are associated with properties of the sigmoidal curve for reflection cracking. The parameter ρ “describes the spread of the rising portion of the curve,” and furthermore for a given project ρ is equivalent to the total number of days to reach 36.8 percent ($1/e$) of the total amount of expected reflection cracking (NCHRP 2010). In terms of the curve for reflection cracking, the parameter β describes “how steep the rising portion of the curve is” (NCHRP 2010). The curves of Figure 23, excerpted from NCHRP 2010, are associated by its authors with this interpretation of the calibration coefficients.

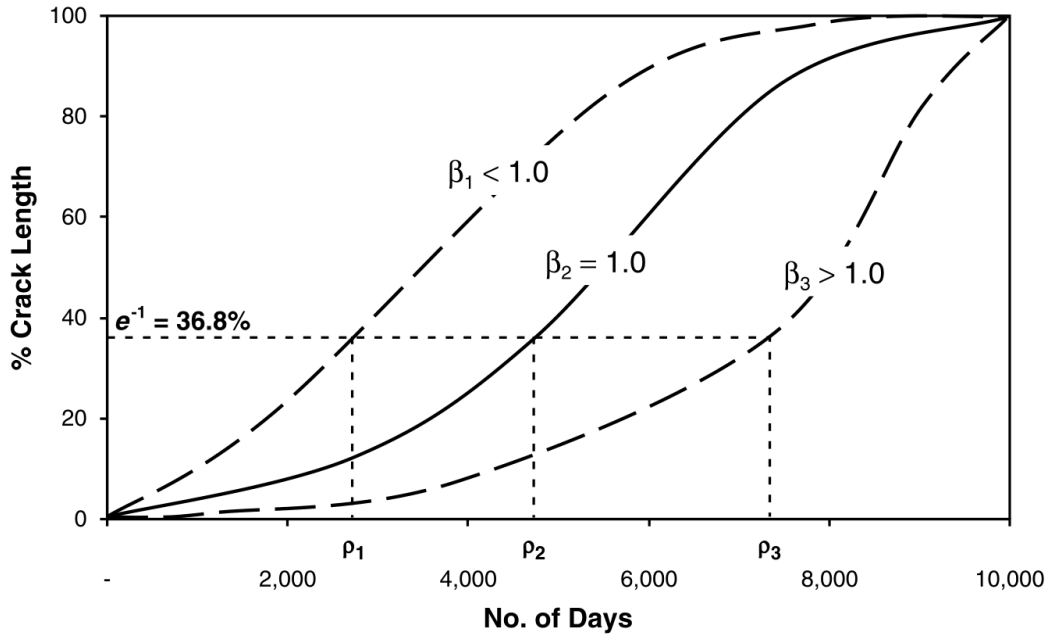


Figure 23. Visual interpretation of NCHRP 1-41 calibration coefficients (from NCHRP 2010)

NCHRP 1-41 provides predictive equations to determine the coefficients ρ and β . These equations are based on the linear regression model for each parameter (corresponding to a given severity level) and a consideration of thermal, bending, and shearing stresses. Hence, the NCHRP 1-41 model considers both thermal effects and traffic loads. Accounting for both forms of loading is critical for the analysis of reflective cracking, as each of these loads affects cracking depending on the severity of cracks under consideration.

An example calibration for ρ for L+M+H severity would result in

$$\rho_{LMH} = N_{fB1} \left(\alpha_0 - \alpha_1 \frac{N_{fB1}}{N_{fT1}} - \alpha_2 \frac{N_{fB1}}{N_{fS1}} \right) + N_{fT2} \left(\alpha_3 - \alpha_4 \frac{N_{fT2}}{N_{fS2}} \right) \quad (3.5)$$

where $\alpha_0, \alpha_1, \alpha_2, \alpha_3, \alpha_4$, and β_{LMH} are calibration coefficients, which are discussed in more detail in Section 3.2.3. Calibrations for each severity level for a given project are necessary to develop the final ρ and β for the reflective cracking model. The model results in predicted levels of reflective cracking for a given project in a form that resembles Figure 24.

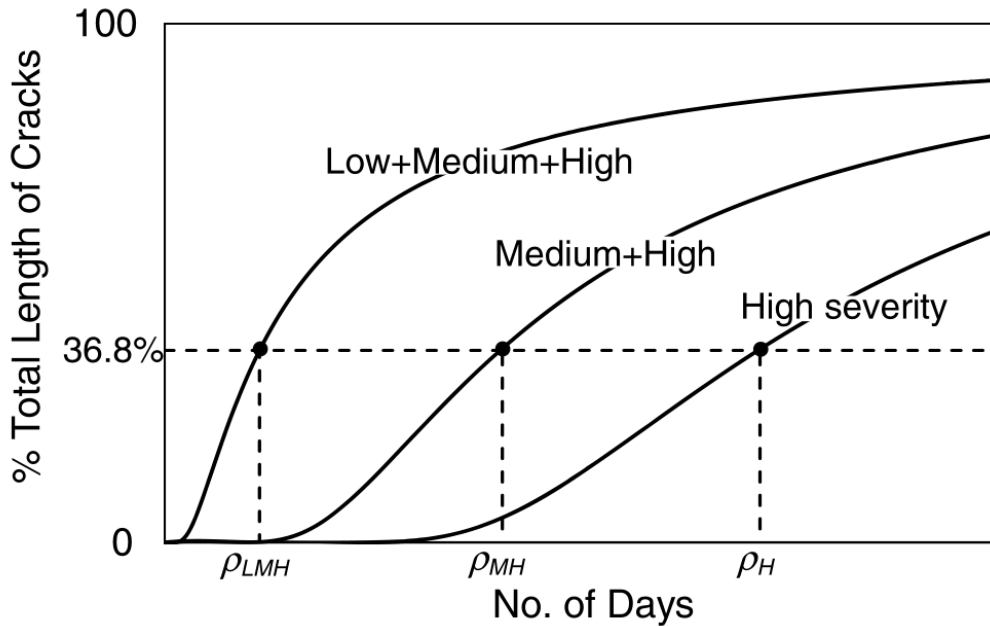


Figure 24. Severity distress curves for NCHRP 1-41 model (from NCHRP 2010)

However, the 1-41 model sophistication does not come without complications. To begin, its neural networks were tested for goodness of fit, but not in terms sensitivity to respective parameters. A succinct way of summarizing this issue is that high R-squared values do not necessary imply that the model provides robust predictions for a wide range of input parameters. A comprehensive sensitivity study must be conducted to eliminate concerns.

Although the NCHRP 1-41 model appears to be theoretically sound and the most sophisticated model currently available to pavement engineers, its immediate implementation depends on the robustness of the NCHRP 1-41 software. Therefore, a comprehensive evaluation of the software was an important part of Task 5. The research team conducted this evaluation and encountered a number of issues – including apparent software bugs – that produce unrealistic reflection cracking predictions for basic HMA-PCC projects. These are discussed in Section 3.2.2.

3.2.2 NCHRP 1-41 Program to Interface with MEPDG Project Files

Although the NCHRP 1-41 model has many inputs similar to MEPDG inputs, those inputs cannot be directly imported from the MEPDG into the 1-41 procedure. While the 1-41 program can be used with the MEPDG, it does not interface in a manner that is easy to reproduce. This would likely be especially true for a typical pavement engineer who has little understanding of MEPDG folder locations and files and is unable to manually move data from MEPDG to the required location for the NCHRP 1-41 program. (Note that this observation is made in light of the TPF-5(149) procedure for rutting, which automatically finds necessary files and moves and utilizes them for the user, who merely has to run an MEPDG project file and then run the TPF-5(149) executable to receive modified rutting results.)

To overcome the issue of moving files for NCHRP 1-41, during Task 5 the research team developed a driver program that allows user to create NCHRP 1-41 project files directly from the

MEPDG project files. This driver converts MEPDG intermediate files into an EICM climate file for 1-41 analysis. The TPF-5(149) research team will apply the developed driver to all future work with NCHRP 1-41, and the research team recommends a similar tool to others who wish to investigate 1-41 and the MEPDG.

3.2.3 Analysis and Discussion of NCHRP 1-41 Procedure

The research team conducted many project runs using the MEPDG and the NCHRP 1-41 software and uncovered a number of issues with the NCHRP 1-41 procedure. Given the complexity of the NCHRP 1-41 model, it is not feasible to use it without the accompanying software. Thus any bugs in the software would create significant impedance to the implementation of the 1-41 procedure. To evaluate the robustness of the NCHRP 1-41 procedure (including the software), a basic sensitivity analysis was conducted for key structural design parameters.

Figure 25 presents an example of predicted reflective cracking for all three severity levels for a single HMA-PCC project located in Minnesota. All calibration coefficients assumed for this project are the NCHRP 1-41 defaults.

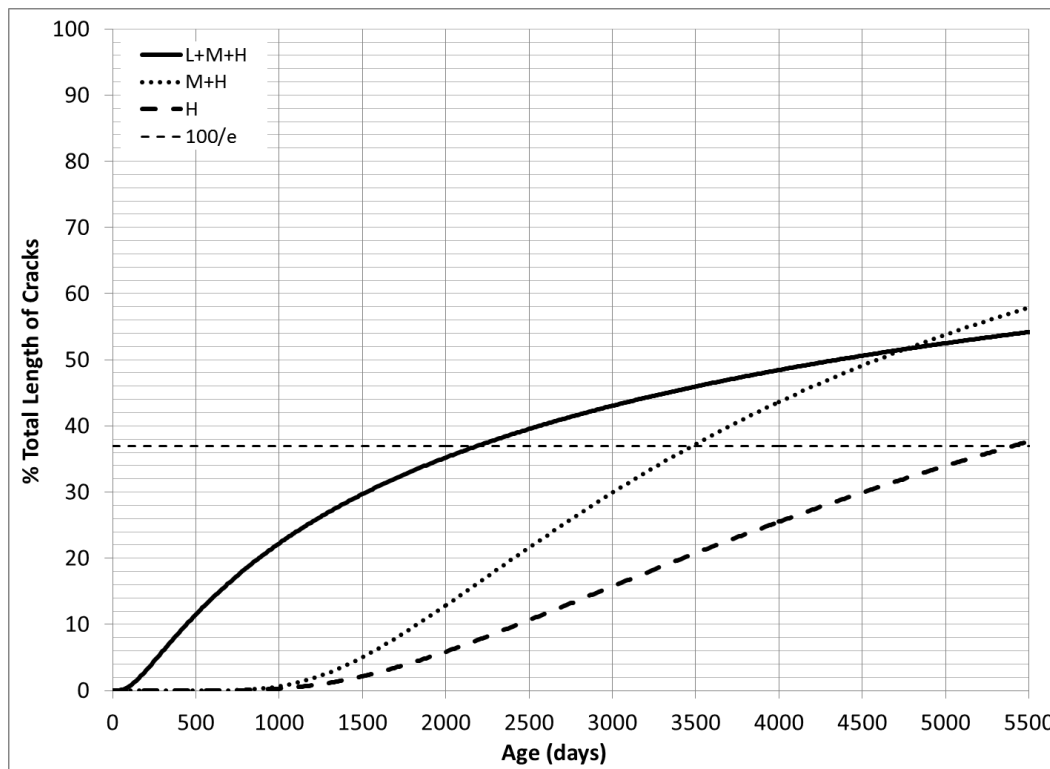


Figure 25. Influence of default coefficients and internal settings for same project for three levels of severity in NCHRP 1-41 procedure

Figure 25 presents a recurring issue for project analyses with NCHRP 1-41, which is in the project cases that were run for the work of Task 5, many times L+M+H cracking length would be exceeded by M+H or H cracking length. This result defies the rationale behind the definitions

of the severity levels, and the frequency with which similar irrational results occurred was noted by the research team.

The contradiction identified above is not the only unrealistic prediction identified in Task 5. Figure 26 and Figure 27 illustrate the effect of HMA overlay thickness on predicted H and L+M+H reflective cracking. Again, only NCHRP 1-41 default values have been selected for the calibration coefficients.

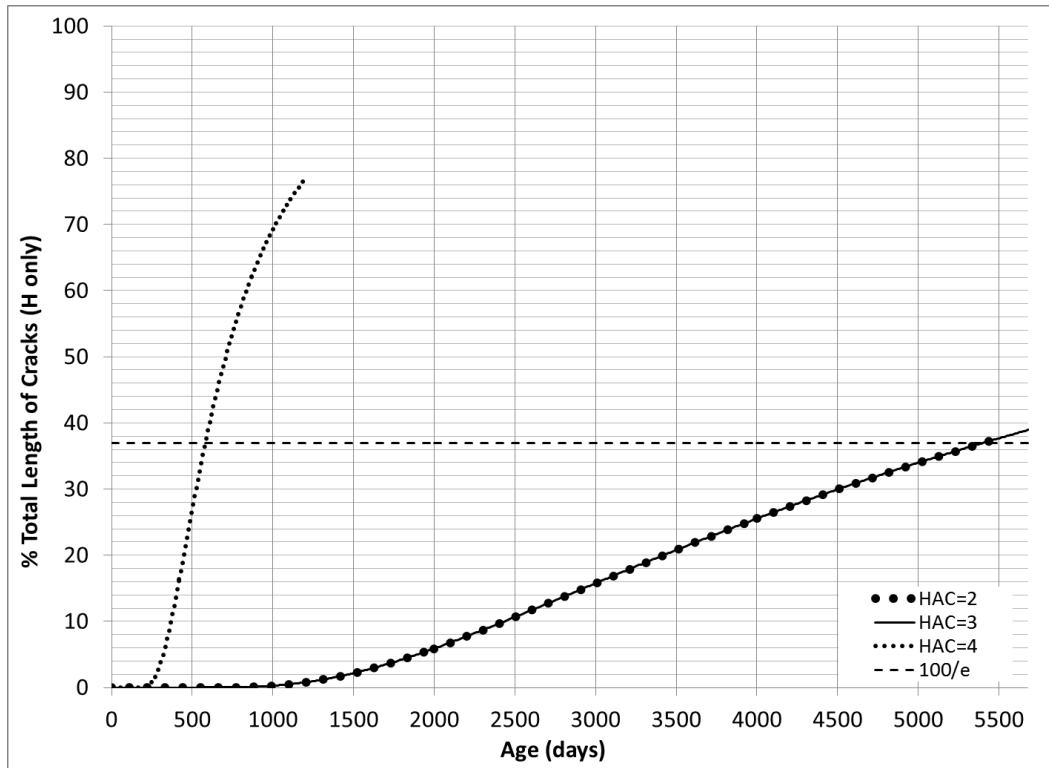


Figure 26. Influence of HMA overlay thickness on NCHRP 1-41 High (H) severity reflective cracking predictions

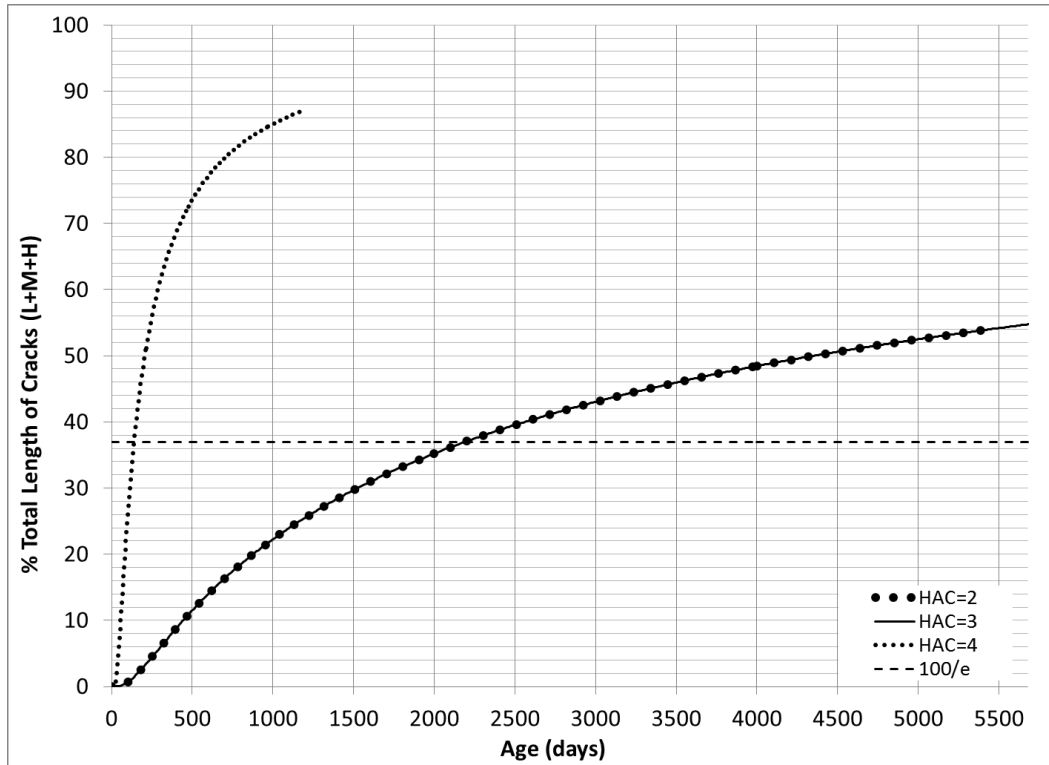


Figure 27. Influence of HMA overlay thickness on NCHRP 1-41 Low, Medium, and High (L+M+H) severity reflective cracking predictions

In Figure 26 and Figure 27, the curves for the reflective cracking at HMA overlay thicknesses of 3 inches and 4 inches are virtually indistinguishable, yet they are substantially different from the curve for reflective cracking associated with a 2-inch HMA overlay.

Figure 28 describes the influence of doweling on predicted performance in H and L+M+H reflective cracking for a sample project. In Figure 28, the inclusion of dowels corresponds to “High LTE,” and the exclusion of dowels corresponds to “Low LTE.”

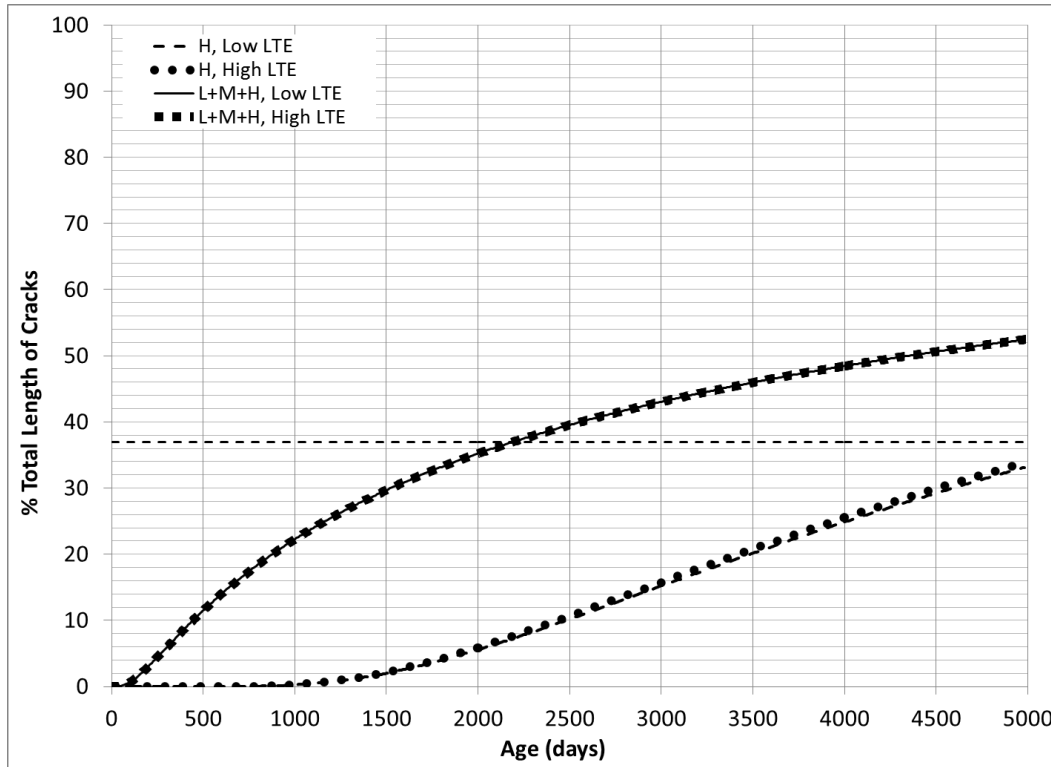


Figure 28. Influence of JPCP joint load transfer efficiency (LTE) on NCHRP 1-41 Low, Medium, and High (L+M+H) and High (H) severity reflective cracking performance predictions

Note that the curves for doweled and undoweled projects are indistinguishable for their corresponding severity level. Thus, while the 1-41 model accounts for load transfer, the implementation of the model in the software is entirely insensitive to LTE according to the analysis of Task 5.

As the previous examples show, the brief analysis of the NCHRP 1-41 software identified a number of issues with the predicted reflective cracking and with the NCHRP 1-41 procedure sensitivity to key structural parameters. Two possible explanations for the observed contradictory behavior in severity level prediction or model insensitivity to key parameters have been identified:

1. The default calibration coefficients have not been properly selected.
2. There is a bug in the NCHRP 1-41 software.

An attempt to resolve these issues by modifying the calibration coefficients has not been successful. Modifications of the calibration coefficients for the NCHRP 1-41 model did not lead to expected trends in results. This is illustrated in Figure 29, where, for all levels of cracking severity, calibration coefficients are assigned identical values.

Calibration Settings

Use default calibration parameter values and disregard the inputs
 Use input values as calibration parameters

Show Default Values

User Inputs

ρ LMH:	α_0	1000	α_1	-100	α_2	-100	α_3	15.0000000	α_4	5
ρ MH:	α_5	1000	α_6	-100	α_7	-100	α_8	15.0000000	α_9	5
ρ H:	α_{10}	1000	α_{11}	-100	α_{12}	-100	α_{13}	15.0000000	α_{14}	5
β LMH:	β_0	4.936424802	β_1	1.83213343	β_2	1.83213343	β_3	0.034968346	β_4	0.073071264
β MH:	β_5	4.936424802	β_6	1.83213343	β_7	1.83213343	β_8	0.034968346	β_9	0.073071264
β H:	β_{10}	4.936424802	β_{11}	1.83213343	β_{12}	1.83213343	β_{13}	0.034968346	β_{14}	0.073071264

OK Cancel

Figure 29. Calibration coefficients for 1-41 self-consistency validation cases

In this circumstance, one would expect that predicted cracking would be identical, yet this is clearly not the case in Figure 30, which illustrates the cracking curves for these three cases. They are not identical and in fact behave quite differently.

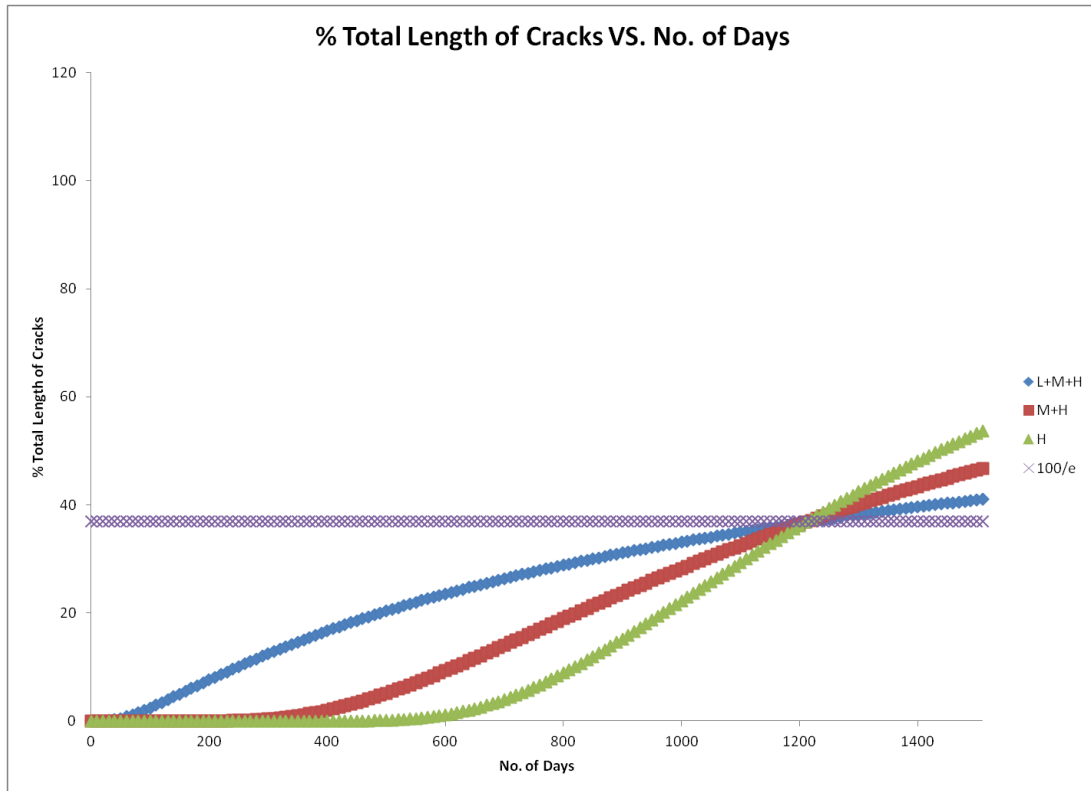


Figure 30. Results for 1-41 self-consistency validation

It should be noted that although the MEPDG/NCHRP 1-41 companion driver developed in Task 5 helped to create multiple project files used to identify the problems above, all results were later verified by manually creating NCHRP 1-41 project files from scratch. Thus, the issues observed were not caused by the use of the TPF-5(149) driver program.

In summary, although the NCHRP 1-41 model offers a potential improvement in reflective cracking prediction for the MEPDG, its current implementation in the NCHRP 1-41 software package is deficient. Thus the model cannot be immediately implemented without further software review and modification. However, after such modifications have occurred, the implementation of the NCHRP 1-41 procedure will be greatly accelerated by the use of the driver program developed for the work of Task 5.

3.3 CalME Reflective Cracking Model

The CalME model assumes that debonding occurs quickly after a HMA-PCC pavement is opened to traffic, and thus the HMA layer is effectively a flexural beam through the life of the HMA-PCC pavement. In this arrangement, the crack tip strain, ϵ , is the maximum bending strain at the bottom of the HMA layer. The CalME reflection cracking model is based on regression models for crack tip strains; these regression models are based on a large factorial of cases (i.e. pavement systems and applied traffic loads) solved using the finite element method (Wu 2005). Hence, the crack tip strain is a function of traffic and pavement structural properties and is defined as

$$\varepsilon = \alpha \times E_{an}^{\beta_1} \times E_{bn}^{\beta_2} \times (a_1 + b_1 \times \ln(LS_n)) \times \exp(b_2 \times H_{an}) \times (1 + b_3 \times H_{un}) \times (1 + b_4 \times E_{un}) \times \sigma_n \quad (3.6)$$

where

$$\begin{aligned} E_{an} &= E_a / E_s, E_{bn} = E_b / E_s, E_{un} = E_u / E_s, \sigma_n = \sigma_o / E_s, \\ LS_n &= LS / a, H_{an} = H_a / a, H_{un} = H_u / a \end{aligned} \quad (3.7)$$

and where E_a is the modulus of the HMA overlay; H_a is the thickness of the HMA overlay; E_u is the modulus of the PCC slab; H_u is the thickness of the PCC; E_b is the modulus of the base/sub-base; E_s is the modulus of the subgrade; LS is the crack spacing; σ_o is the tire pressure; and a is the radius of the loaded area for one wheel.

It is important to note that loading conditions considered do not include thermal loads – this is a modeling simplification specific to California, where pavements do not experience temperatures that are extremely low compared to construction temperatures. For these conditions, Caltrans is confident that thermal strains induced by temperature variation in the HMA layer are not significant and thus thermal loads are excluded from the CalME reflection cracking model.

To predict reflection cracking, the crack tip strain, ε , from Eq. 3.6 is used with the incremental damage model, which has the format

$$\log(E_{dam}) - \delta = \frac{\alpha(1 - \omega)}{1 + \exp(\beta + \gamma \log(tr))} \quad (3.8)$$

where tr is reduced time in seconds and δ , α , β , and γ are calibration constants. For this approach, which is similar to the fatigue damage discussion for rutting in Section 2.2.2, the damage, ω , is defined as

$$w = \left(\frac{MN_{tot}}{MN_p} \right)^\alpha \quad (3.9)$$

where MN_{tot} is the current number of load repetitions and the allowable number of load repetitions, MN_p , is defined as

$$MN_p = A \cdot \left(\frac{\mu\varepsilon}{\mu\varepsilon_{ref}} \right)^\beta * \left(\frac{E_{dam}}{E_{ref}} \right)^{\beta/2} = A' \cdot \left(\frac{SE}{SE_{ref}} \right)^{\beta/2} \quad (3.10)$$

and where E_{ref} is the reference asphalt modulus; $\mu\varepsilon_{ref}$ is the reference asphalt strain in microstrains; $\mu\varepsilon$ is the strain at the bottom of the asphalt layer; SE and SE_{ref} are strain energies; and A , A' , and β are calibration coefficients.

In addition to being an incremental damage approach, the CalME model benefits from its simplicity and ease of implementation. As noted earlier, it does not account for thermal loads, and it also does not account for load transfer at joints (i.e. doweling) or severity levels in cracking. Despite these drawbacks, there is much utility in the CalME approach. First, it benefits from having been validated using HVS data from the SHRP2 R21 project. In addition, it uses a framework that is similar to that of rutting (detailed in Section 2.2.2) and fatigue cracking.

3.4 TPF-5(149) Procedure for Predicting Reflective Cracking in TICP

3.4.1 NCHRP 1-41 Suitability for TPF-5(149) Procedure

The NCHRP 1-41 approach for reflective cracking was the early focus of the Task 5 research in reflective cracking. After evaluating both the model and program (Section 3.2), the research team was hesitant to incorporate the 1-41 approach without further understanding of the 1-41 model and program.

However, due to the focus of the TPF-5(149) technical advisory panel on the 1-41 model, the research team developed a framework that allows the 1-41 model to be more easily used alongside the MEPDG. This includes the driver program discussed in Section 3.2, which directly obtains climate information for the 1-41 model directly from the MEPDG climate files – doing so prevents the user from needing to manually enter this information into the 1-41 program.

While TPF-5(149) has developed a procedure that better fits the 1-41 model into the MEPDG framework, this procedure could not be calibrated and debugged due to previously discussed bugs in the 1-41 software and possible problems with the implementation of the 1-41 model itself. The research team has notified the 1-41 developers of the errors and bugs encountered in the 1-41 model and program.

Note that once these issues are resolved, TPF-5(149) is prepared to revisit and continue this work. The design and analysis of TICP would benefit from a reflective cracking model with the sophistication of the NCHRP 1-41 model. For this reason, the research team examined NCHRP 1-41 very closely given that future work may revisit that model. (As detailed above, in support of this examination the research team developed tools to assist the NCHRP 1-41 program to interface with the MEPDG during the work of Task 5.)

3.4.2 Modified CalME Reflection Cracking Model for TPF-5(149)

Due to difficulties with the NCHRP 1-41 model and program, the research team also developed a modified CalME reflection cracking model for a procedure similar to the rutting procedure developed for TPF-5(149) and described in Chapter 2. It should be noted that the observed problems with the NCHRP 1-41 model and program were not anticipated, thus the Task 5 work with the CalME reflection cracking model was unexpected and required an additional effort to complete.

For the TPF-5(149) procedure, CalME is once again combined with MEPDG to augment typical MEPDG results with more specific results concerning reflective cracking. In this case, the CalME model for reflection cracking has been slightly modified to account for:

- Thermal loading;
- Joint load transfer (i.e. dowels); and
- Two severity levels of cracking: Low + Medium + High (L+M+H) and Medium + High (M+H), where notation is borrowed from 1-41 conventions.

These modifications remedy the few issues the research team had in applying the HMA-PCC projects outside of the state of California. As noted in Section 3.3, the CalME reflective cracking model is very useful: it is both simple and direct, and it has been well documented. Thus its modification and incorporation into the TPF-5(149) approach is relatively straightforward.

To modify CalME, the research team consulted a methodology developed by Bennert (2011). The incremental damage approach for reflective cracking described in Section 3.3 is modified so that the calculated damage is a function of both thermal loads and axle loads. Two levels of total damage are considered for the two severity levels of cracking (L+M+H and M+H).

3.4.2.1 L+M+H Severity Reflective Cracking Model

To begin, Low, Medium, and High reflective cracking RC_{LMH} is defined similar to the CalME definition for reflective cracking, such that

$$RC_{LMH} = \frac{100}{1 + \left(a_1 \frac{DAM_{LMH}}{h_{HMA}} \right)^{b_1}} \quad (3.11)$$

where h_{HMA} is the HMA overlay thickness; a_1 and b_1 are calibration constants (determined to be 0.05 and -6, respectively); and DAM_{LMH} is the total damage leading to Low, Medium, and High severity cracking. DAM_{LMH} can be further defined as

$$DAM_{LMH} = \frac{DAM_{LMH}^{temp}}{DAM_0^{temp}} + \frac{DAM_{LMH}^{load}}{DAM_0^{load}} \quad (3.12)$$

where parameters corresponding to damage due to thermal effects have the superscript *temp*, parameters corresponding to damage due to axle loads have the superscript *load*, and the subscript 0 indicates a damage scaling parameter. Each of the parameters in Equation (3.12) is defined below in more detail.

The damage due to axle load repetitions is based on Equations (3.9) and (3.10) above and has the form

$$DAM_{LMH}^{load} = \omega \quad (3.13)$$

It should be noted that a determination of the allowable number of load repetitions using Equation (3.10) requires the use of critical strains from Equation (3.6). As Equation (3.6) was developed for undoweled HMA-PCC pavements, to account for the effect of reduction in the pavement deflections and corresponding reduction in asphalt strains, the following correction was introduced

$$\varepsilon_{doweled} = \psi \varepsilon_{undoweled} \quad (3.14)$$

where $\varepsilon_{undoweled}$ is the strain from Equation (3.6) and ψ is a correction factor (assumed to be equivalent to 0.8 for this study). To determine load-induced portion of the damage, Equation (3.6) was used to predict critical HMA strains. Equation (3.6) requires a single modulus of elasticity. The MEPDG input is the subgrade resilient modulus for the optimum moisture content, but the MEPDG later subdivides the subgrade in several sublayers and adjusts the moduli for each sublayer based on the sublayer moisture content for each month. It should be also noted that the MEPDG does not adjust the moduli for the stress level sensitivity which is built-in into the MEPDG E-to-k conversion for rigid pavements.

To provide an input into Equation (3.6), these moduli, preferably adjusted to the stress level, should be combined back into one composite modulus, which is not a trivial task. To address this issue, it was decided not use the elastic moduli of the individual sublayer, but rather composite k-values from the rigid part. These values were converted to composite E using the relationships between the backcalculated E and k-values established by Khazanovich et al. (2001), based on the several hundred LTPP test sections.

$$k = 0.296E_{subgr} \quad (3.15)$$

Furthermore, the damage load scaling factor, adopted from CalME initiation damage, is defined as

$$DAM_0^{load} = \frac{0.54}{1 + \left(1 + \frac{h_{HMA}}{10}\right)^{-0.9}} \quad (3.16)$$

The damage due to thermal effects has the form

$$DAM_{LMH}^{temp} = \sum \frac{n(\Delta T_i)}{N(\Delta T_i)} \quad (3.17)$$

where ΔT_i is the difference between the daily maximum and minimum temperatures at the top of the PCC layer, as predicted by EICM; $n(\Delta T_i)$ is the number of days ΔT_i occurs; and $N(\Delta T_i)$ is the allowable number of joint openings associated with change in PCC temperature ΔT_i . $N(\Delta T_i)$ is

adopted from Bennert (2011), German and Lytton (1979), and Zhou and Scullion (2005) and is defined as

$$N(\Delta T_i) = k_1 (\Delta T_i)^{k_2} (\Delta L_i)^{k_3} \quad (3.18)$$

where ΔL_i is the joint movement and k_1 , k_2 , and k_3 are material specific coefficients that are determined using the Texas Transportation Institute (TTI) overlay testing device. Bennert (2011) reported example values for these coefficients for several mixtures used in New Jersey HMA overlays of JPCP. This study adopted the respective values 2.10×10^{-7} , 1.3, and -2 for k_1 , k_2 , and k_3 .

Furthermore, the model adopts the relationship developed by Bennert (2011) between the joint movement, ΔL_i , and the change in temperature ΔT_i .

$$\Delta L_i = \beta \alpha_{PCC} L \Delta T_i \quad (3.19)$$

where α_{PCC} is the coefficient of thermal expansion of the PCC layer, L is the joint spacing, and β is the PCC-base friction coefficient (assumed to be 0.5 for this study, a value commonly assumed for granular bases). Finally, the damage scaling factor for temperature is assumed to be equivalent to 1.

3.4.2.2 M+H Severity Reflective Cracking Model

The use of the critical HMA strain, defined by Equation (3.6), to relate traffic loading and reflective cracking is reasonable to describe the stages of crack initiation and propagation (i.e. the development of Low severity cracking). However, after the crack has propagated, the strains disappear and, therefore, cannot be used to determine crack deterioration (i.e. the progression from Low to Medium and High severity).

In this study, a different mechanistic parameter was selected: differential energy of subgrade deformation, DE , which is used by the MEPDG to characterize the development of joint faulting. It was hypothesized that crack deterioration is caused by excessive vertical deflections of the crack edges, which in turn causes high shear stress at the HMA-PCC interface and high differential deflections of the crack edges. The use of DE addresses both of these mechanistic concerns as DE , for one load application, is defined as follows

$$DE = k \frac{\delta_l + \delta_u}{2} (\delta_l + \delta_u) \quad (3.20)$$

where δ_l is the deflection of the loaded-side of the joint (crack); δ_u is the deflection of the unloaded-side of the joint (crack); and k is the coefficient of subgrade reaction. The procedure for the adoption of DE is adopted from the MEPDG faulting model, modified for HMA-PCC pavements in the work of Task 5 as described in Chapter 5.

As only a portion of the total number of cracks can be both Medium and High severity, the following functional form is adopted for the expression for the Medium and High severity level reflective cracking

$$RC_{MH} = \frac{RC_{LMH}}{1 + (a_2 \sum DE)^{b_2}} \quad (3.21)$$

where a_2 and b_2 are calibration coefficients (determined for this study to be 8×10^{-6} and -0.34, respectively).

There are a number of advantages to the TPF-5(149) approach for reflective cracking. The first advantage is that the approach adopts the MEPDG sigmoidal model, detailed in Section 3.1. Furthermore, it generalizes the CalME model by accounting for the effect of temperature variations and load transfer efficiency, both of which were observed by Bennert (2011) important factors in the development of reflective cracking. Finally, it adopts mechanistic modeling of JPCP joint faulting to characterize deterioration of cracking from Medium to High severity.

3.4.3 Modification of TPF-5(149) Companion Program to the MEPDG

Note that the TPF-5(149) procedure works within the MEPDG framework. Hence, all inputs required for the TPF-5(149) procedure for reflective cracking are taken from MEPDG project inputs in a manner similar to that described in Section 2.3. Both the rutting and reflective cracking procedures are now part of the same companion program to the MEPDG. Thus, for any given TPCP project file, a MEPDG user can run the TPF-5(149) companion program to receive modified rutting and reflective cracking predictions according to the models described in this report.

3.5 Validation of TPF-5(149) Procedure for Reflection Cracking

To validate the developed procedure, the TPF-5(149) research team used readily available reflective cracking data to evaluate the fitness of the procedure. As the CalME model had been extensively calibrated and validated against HVS data, the validation of the TPF-5(149) procedure is limited to recent reflective cracking data from MnROAD.

Furthermore, given that the original MEPDG and NCHRP 1-41 procedures both use the same MEPDG project files required for the TPF-5(149) procedure (as all accommodate the MEPDG framework), the research team also ran the original MEPDG and the NCHRP 1-41 software for the project file describing MnROAD Cells 106 and 206. This validates the TPF-5(149) procedure against existing, well-known models for reflective cracking.

(It is important to note that this use of the NCHRP 1-41 software includes the Windows driver developed under TPF-5(149). Without this tool, the 1-41 program is not functional until the user manually creates inputs for the 1-41 model climate analysis. By using the driver, the NCHRP 1-41 climate input files are automatically generated from the MEPDG climate files.)

As noted in the validation of the TPF-5(149) procedure for rutting in Section 2.4.1, TICIP full-scale test sections were constructed at MnROAD Cells 106 and 206. These test sections have been described in earlier task reporting and are summarized in Table 5. Regular monitoring of Cells 106 and 206 has included surveys of reflective cracking according to crack length and severity level. Severity of cracking is denoted as Low (L), Medium (M), and High (H); these abbreviations may be adopted in the subsections to follow.

Figure 31 illustrates a comparison of collected MnROAD observed M+H reflective cracking with M+H reflective cracking predicted by the TPF-5(149) procedure using MPEDG project files describing Cells 106 and 206 (with a 20-year service life). Figure 31 also includes reflective cracking predictions for Cells 106 and 206 using the original MEPDG procedure for reflective cracking and the NCHRP 1-41 model for reflective cracking. Note that as the original MEPDG reflective cracking model does not consider joint load transfer, the predicted reflective cracking for these test sections is identical; the same is true of the 1-41 predicted cracking for Cells 106 and 206 given that the 1-41 procedure is currently insensitive to the presence of dowels. Furthermore, while the original MEPDG model does not specify the severity of cracking it predicts, based on the results for the project file, it is assumed it predicts M+H level severity cracking, and thus these results are included.

Given that reflective cracking data has only been collected for two years, a validation of the model for the first 24 months of the predicted performance is illustrated in Figure 32. Figure 32 also includes predicted reflective cracking according to the original MEPDG procedure.

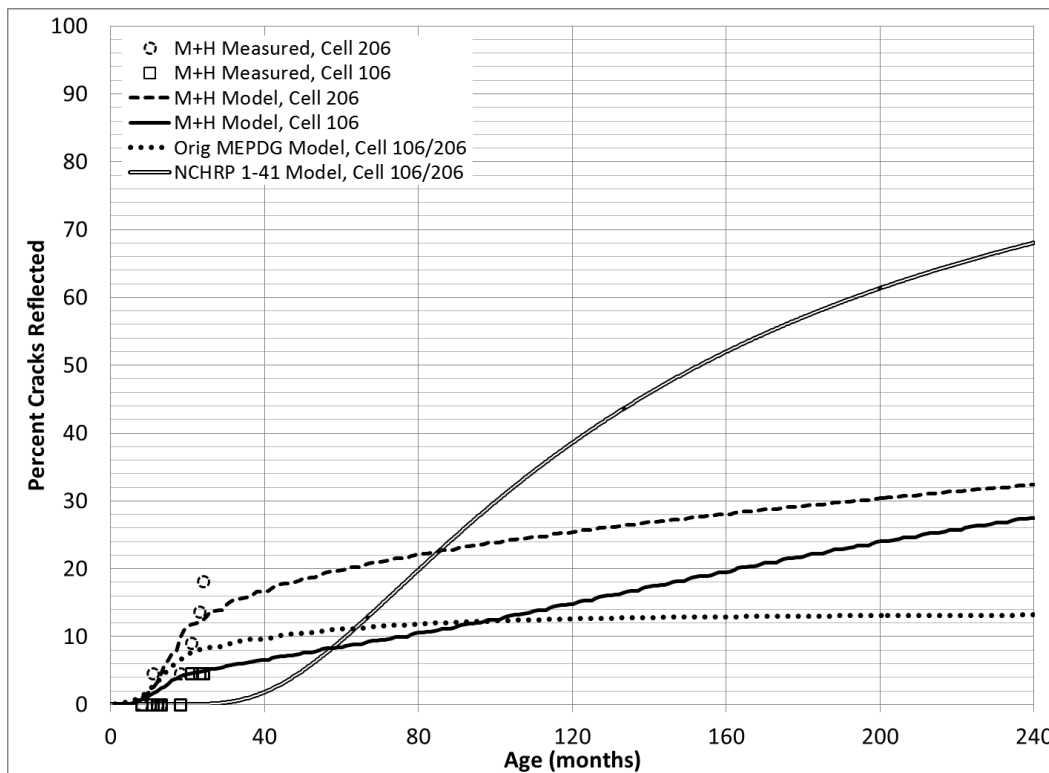


Figure 31. TPF-5(149) procedure predicted 20-year M+H severity reflective cracking performance for MnROAD Cells 106 and 206

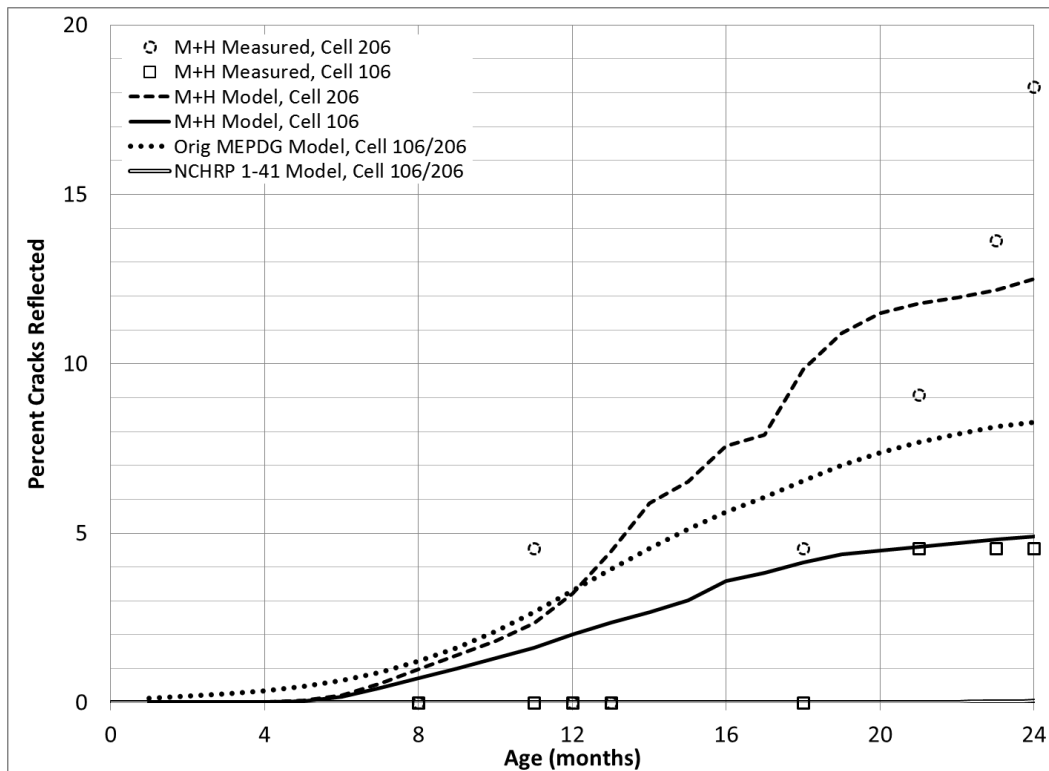


Figure 32. The first two years of MnROAD Medium and High (M+H) severity reflection cracking data versus TPF-5(149) modeled M+H performance and Original MEPDG modeled performance

For both projects (which differ only in the presence of doweling), the data appears to validate the TPF-5(149) procedure. In the model predictions and the observed M+H reflective cracking data, the effect of the 1-inch dowels in Cell 106 is apparent. This agrees with expectations: as noted earlier, one advantage of the TPF-5(149) procedure is that in addition to considering axle loads for M+H severity reflective cracking, it has modified the CalME procedure to include LTE in the model. This result confirms the influence of that new information in the model. In summary, the model properly describes the experimental data.

Furthermore, the TPF-5(149) model seems to reproduce the trend in the data of Figure 32 relative to the performance of other available reflective cracking models for the MEPDG. While the original MEPDG model seems to capture M+H cracking for MnROAD conditions, the NCHRP 1-41 does not perform as well. Although the 1-41 predicted M+H cracking appears unrealistic, as detailed earlier in the Chapter, this performance is most likely due to issues with the software and not the model itself.

Including Low severity cracking data, and corresponding predictions for L+M+H reflective cracking, results in much higher predicted and observed cracking in Cells 106 and 206, as illustrated in Figure 33. Note that Figure 33 also includes L+M+H cracking predictions according to the NCHRP 1-41 procedure as an additional means of validating the TPF-5(149) procedure. As was the case for M+H reflective cracking data, L+M+H data is available for the

first two years of Cells 106 and 206, hence a validation of the model for the first 24 months of the predicted L+M+H performance is illustrated in Figure 34.

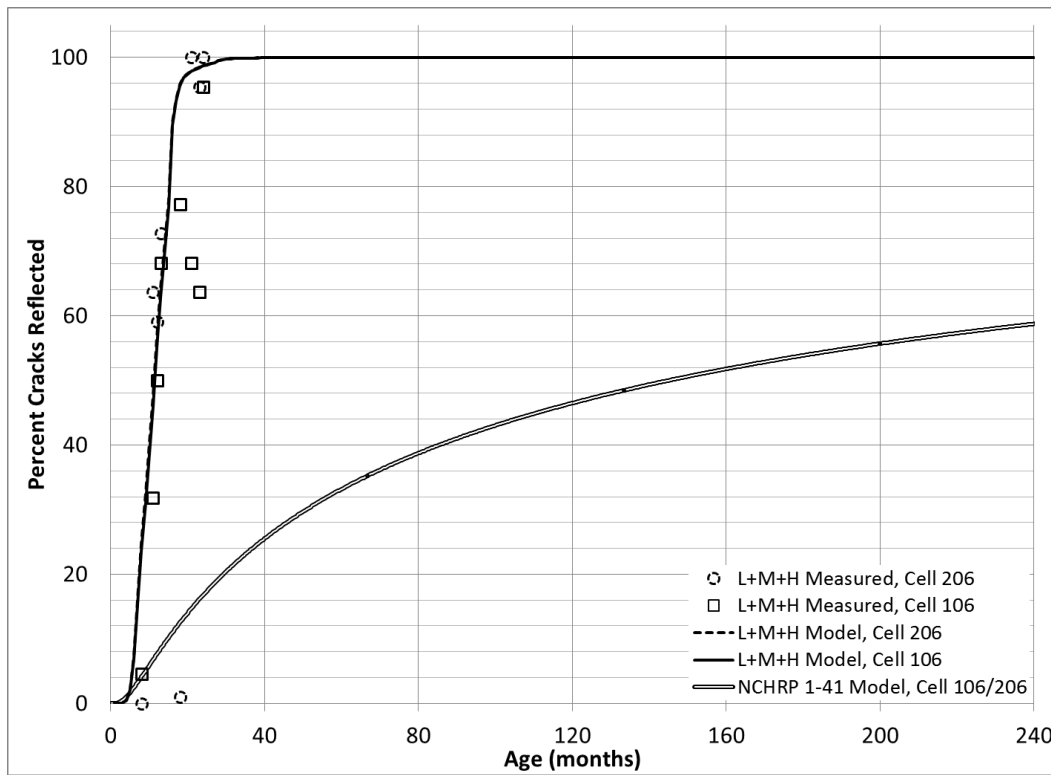


Figure 33. Predicted 20-year Low, Medium, and High (L+M+H) severity reflective cracking performance for MnROAD Cells 106 and 206 according to TPF-5(149) procedure

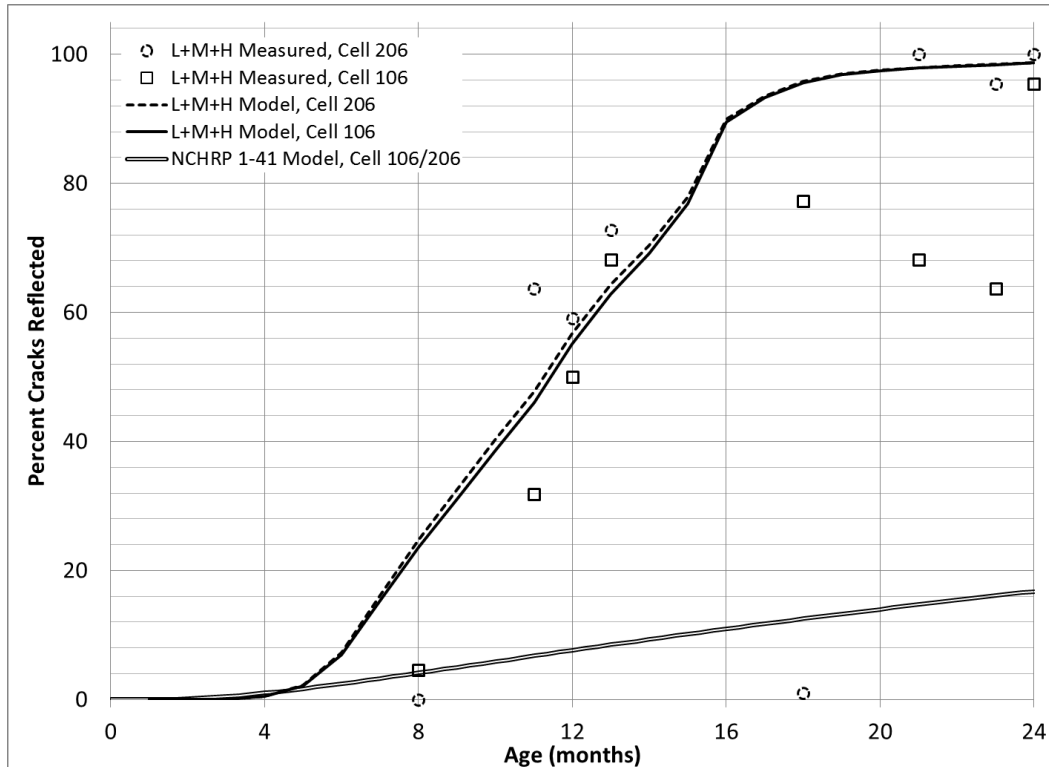


Figure 34. First two years of MnROAD Low, Medium, and High (L+M+H) severity reflection cracking data versus TPF-5(149) modeled L+M+H performance

As the L+M+H model considers thermal effects, we anticipate that model predictions would far exceed those of the M+H case over the service life of the projects. This expectation is upheld in a comparison of Figure 31 and Figure 33. Furthermore, in Figure 33 (and Figure 34) the presence of doweling does not appear to mitigate overall cracking; the model prediction in this regard is upheld by observed reflective cracking for the first 24 months of Cells 106 and 206. As noted above, the TPF-5(149) model of L+M+H reflective cracking includes thermal effects, and thus for these severity levels the Low cracking due to thermal effects predominate. Again, this model prediction appears to be validated by the available MnROAD data.

Both the model and the MnROAD field data show that Low severity cracking can be expected within a few years after opening to traffic. Therefore, saw-and-sealing should be recommended to eliminate this distress.

Overall, the TPF-5(149) procedure clearly represents an improvement on the existing MEPDG and NCHRP 1-41 procedures. Furthermore, given these results and its accommodation of the MEPDG, it is a possible candidate for incorporation into the new AASHTO DARWin-ME program. However, for the TPF-5(149) procedure to be considered as a serious model for reflective cracking, more work needs to be done in terms of calibration, validation, and sensitivity analysis. The following section describes a brief sensitivity analysis conducted during Task 5 to address this concern.

3.6 Sensitivity Analysis of TPF-5(149) Procedure for Reflection Cracking

As was the case for the sensitivity analysis of the rutting procedure of Section 3.5, both the MEPDG and CalME rutting model have been subjected to extensive review and sensitivity analysis. However a difference in the reflective cracking case is that the CalME model has been modified to account for thermal effects, LTE, and two levels of cracking severity.

The research team undertook a brief analysis of rutting performance sensitivity to two important parameters: HMA thickness and climate. Other than these two parameters, the sensitivity study assumed a HMA-PCC pavement with a 2-inch HMA overlay of a 7-inch JPCP. Furthermore, the analysis assumed MEPDG defaults for material properties (Level 3 inputs) for all projects. All projects are assumed to be doweled unless otherwise indicated. Assumed traffic was 2000 AADTT.

3.6.1 Climate

Figure 35 and Figure 36 illustrate the sensitivity of reflective predictions to climate for 5 locations in M+H severity and L+M+H severity. Each of these locations corresponds to EICM climate files (*.icm) for Seattle, WA; Pullman, WA; Sacramento, CA; San Francisco, CA; and Minneapolis-Saint Paul, MN.

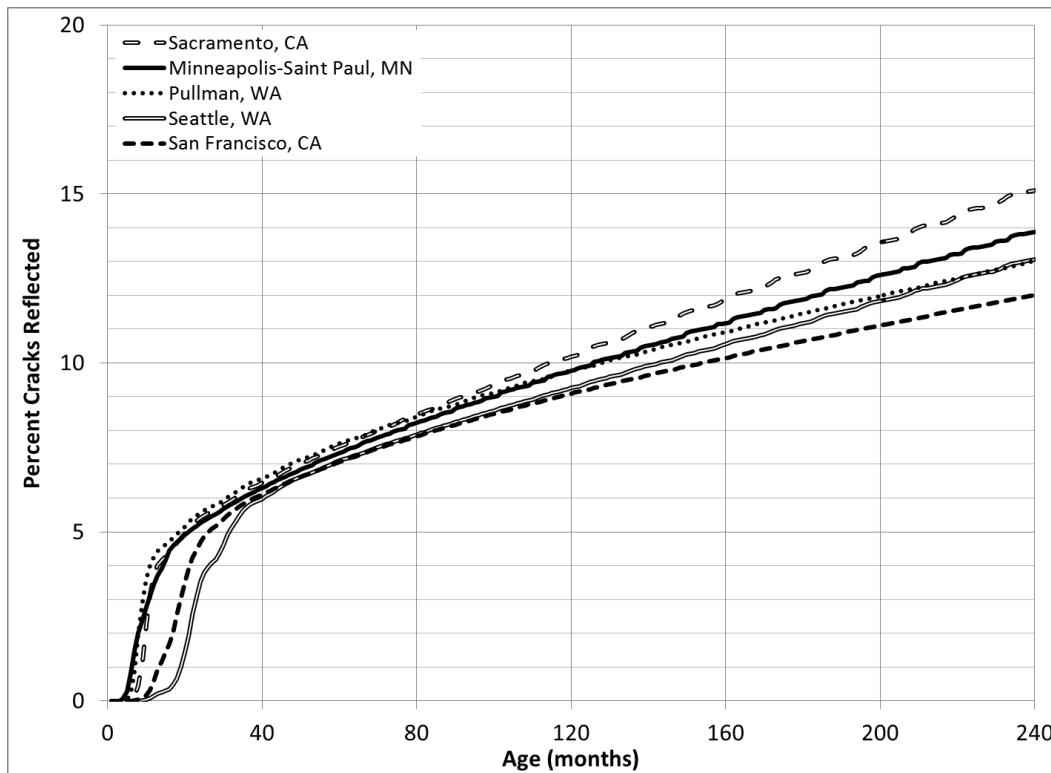


Figure 35. Influence of climate file on TPF-5(149) procedure for M+H reflective cracking

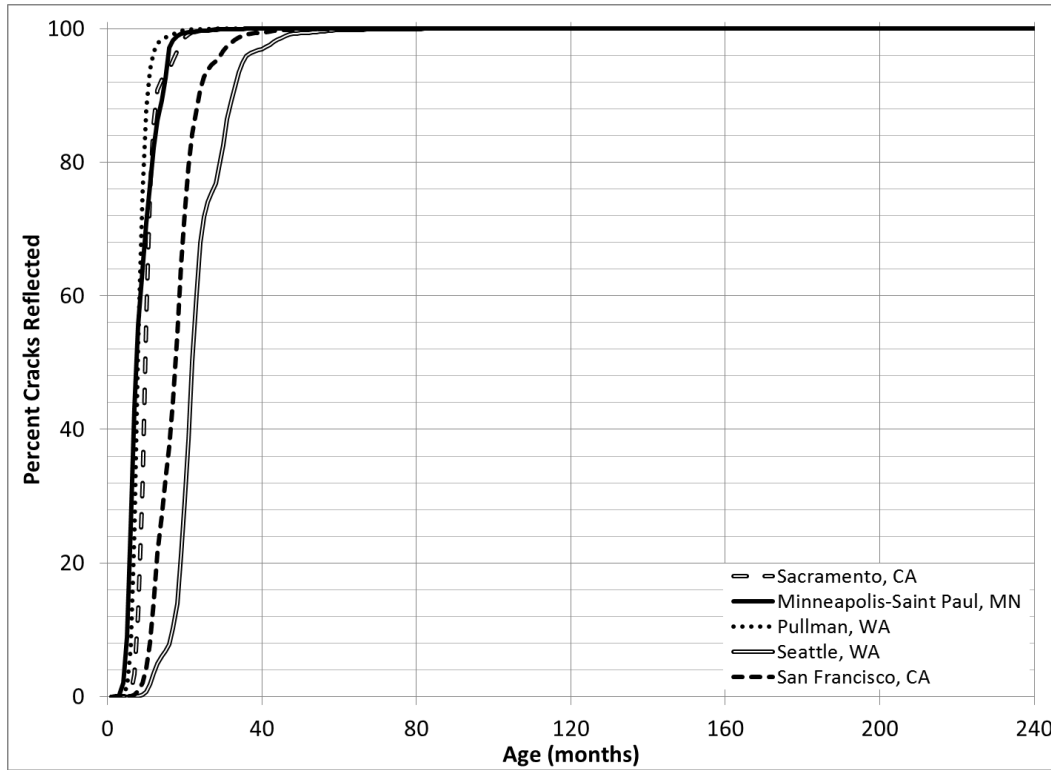


Figure 36. Influence of climate file on TPF-5(149) procedure for L+M+H severity reflective cracking

A comparison of Figure 35 and Figure 36 immediately describes the sensitivity of Low severity cracking to climate and, by extension, the inclusion of thermal effects in the Low severity reflective cracking model. The sensitivity of the model is more easily identified in Figure 37.

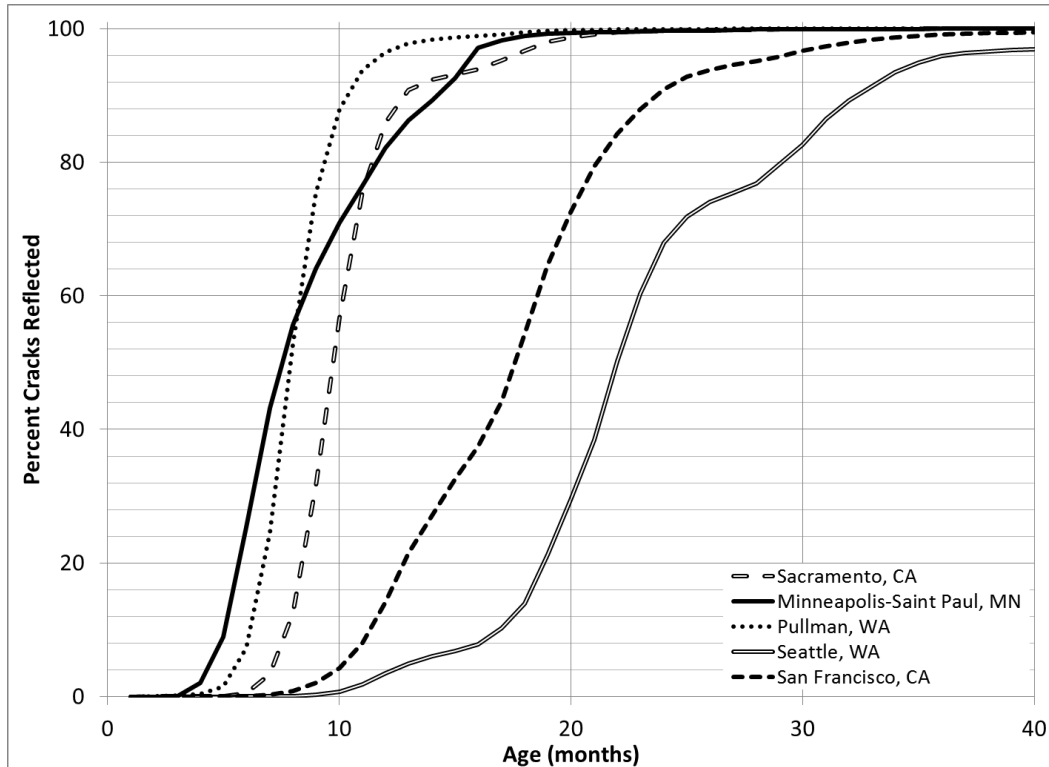


Figure 37. First 40 months of predicted L+M+H severity reflective cracking by TPF-5(149) procedure for five climate files

It can be seen in Figure 37 that the onset of 20% L+M+H cracking is predicted to occur 13 months later in Seattle than it is in Minneapolis. Furthermore, the percent L+M+H cracking associated with pavements of 10 months of age for different climates ranges from 1% (for Seattle) to 88% (for Pullman). Thus, whereas M+H cracking (whose model does not include thermal effects) occurs for all climates at the same percentage of incidence within a few months, for L+M+H cracking the onset and extent of cracking can differ by over a year for different climates. This observation not only confirms that the TPF-5(149) procedure is sensitive to climate, it also validates the inclusion of thermal effects in the L+M+H reflective cracking model developed under TPF-5(149).

3.6.2 Pavement thickness

Figure 38 and Figure 39 illustrates the sensitivity of TPF-5(149) procedure predictions for M+H and L+M+H reflective cracking to three levels of HMA thickness. These projects were developed for an EICM climate file developed from weather data for Minneapolis-Saint Paul International Airport (MSP) in Minneapolis, MN. For projects examining sensitivity to HMA thickness, PCC thickness was held at a constant 7 inches (175 mm).

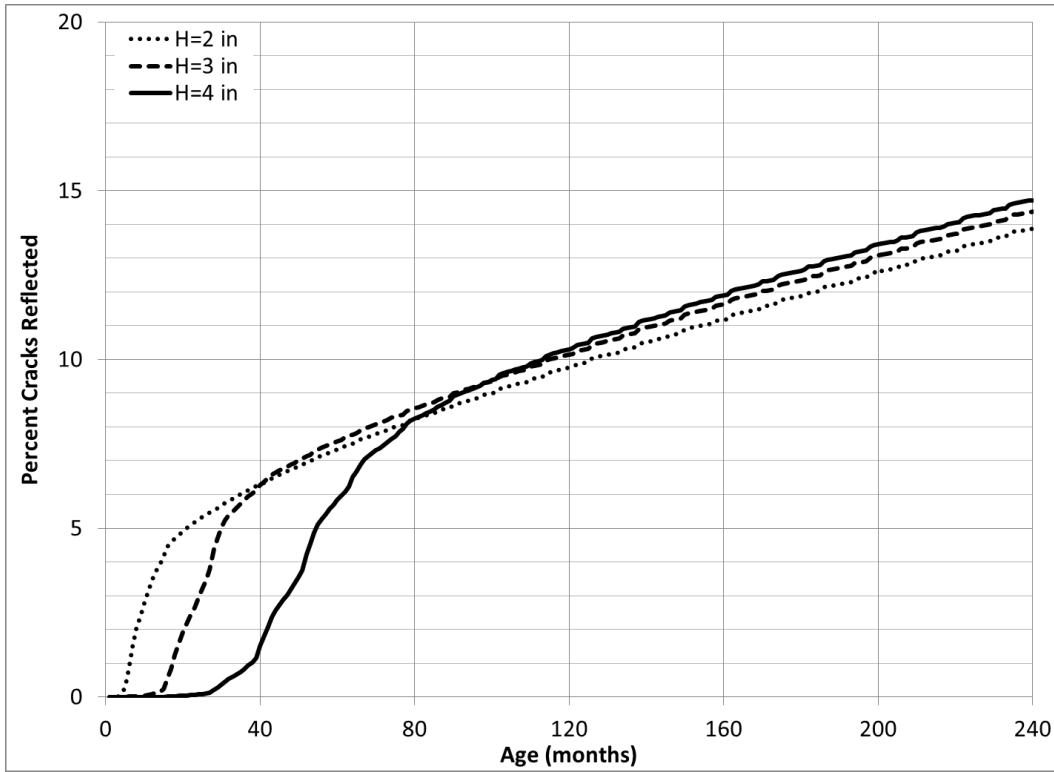


Figure 38. Influence of HMA overlay thickness on TPF-5(149) procedure for M+H severity reflective cracking

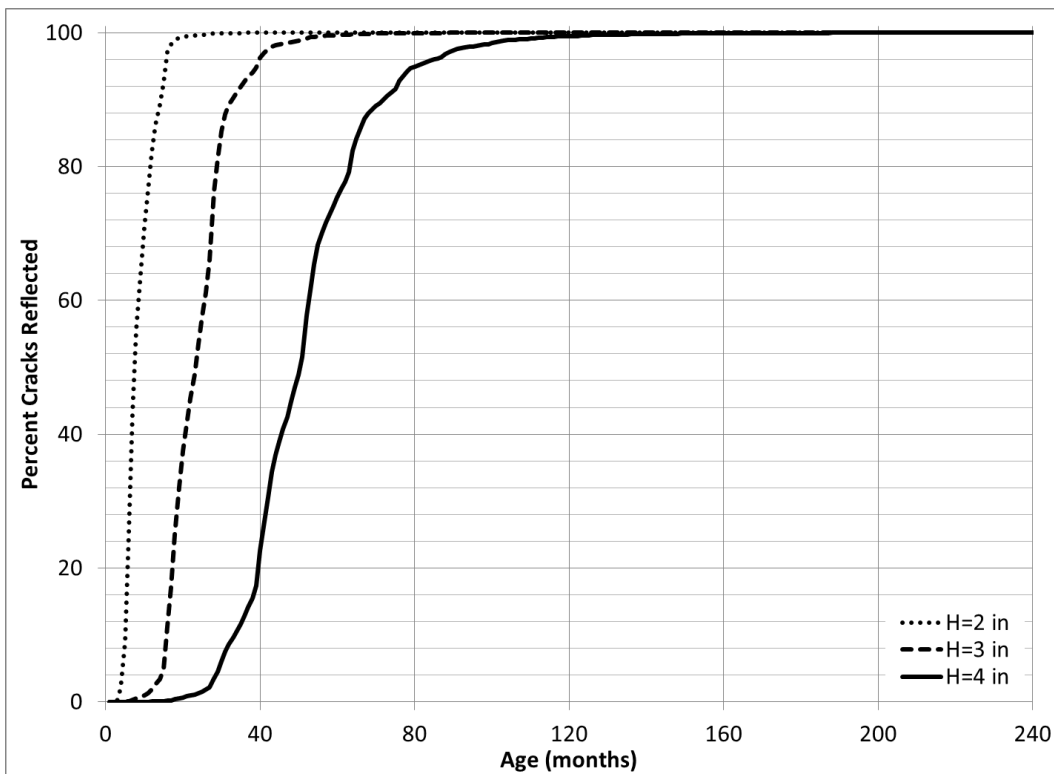


Figure 39. Influence of HMA overlay thickness on TPF-5(149) procedure for L+M+H severity reflective cracking

The sensitivity of both the M+H and L+M+H models to HMA overlay thickness prompts two key observations. First, total reflective cracking over the service life of the pavement will not be reduced significantly by increased overlay thickness. However, an increase in overlay thickness does significantly mitigate (by nearly 1/6th of the pavement service life in the example above) the predicted onset of initial reflective cracking. The sensitivity of the model in this regard is supported by other models and observations of in-field reflective cracking, which have been used to support regular maintenance and renewal of HMA-PCC systems.

3.6.3 Joint load transfer

It should be noted that the study of Cells 106 and 206 in Section 3.5 is itself a sensitivity study of the model to the presence of doweling. As noted earlier, for M+H cases in Figure 31, the model is sensitive to the presence of dowels while being insensitive to LTE in L+M+H cases, represented by Figure 33. Note again that Cell 106 has 1-inch dowel at transverse joints, and Cell 206 is undoweled. The sections are otherwise identical.

However, it may be so that for less severe climates, there is some sensitivity in the L+M+H reflective cracking model. To test this, given the results of the sensitivity analysis for climate, the Seattle climate file was used for a brief study of sensitivity to joint load transfer (or simply LTE). Predicted M+H and L+M+H severity cracking by the TPF-5(149) procedure for projects in Seattle with and without 1-inch dowels are presented in Figure 40 and Figure 41, respectively.

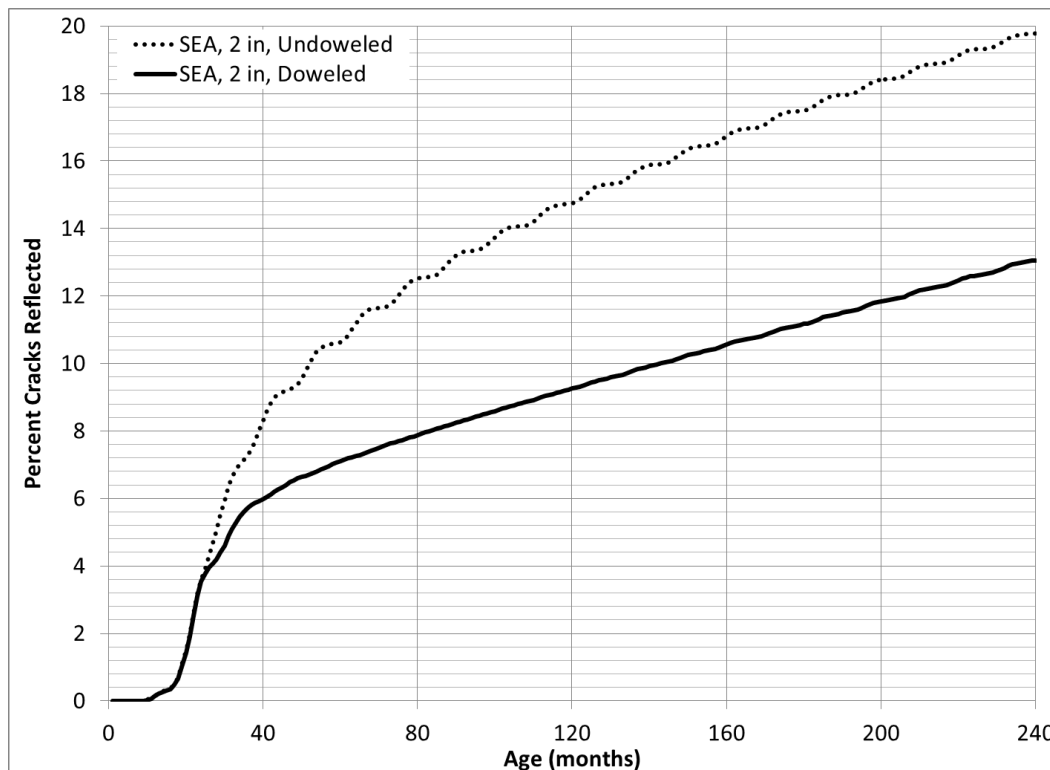


Figure 40. Influence of dowels on TPF-5(149) procedure for M+H severity reflective cracking for project using Seattle, WA, climate file

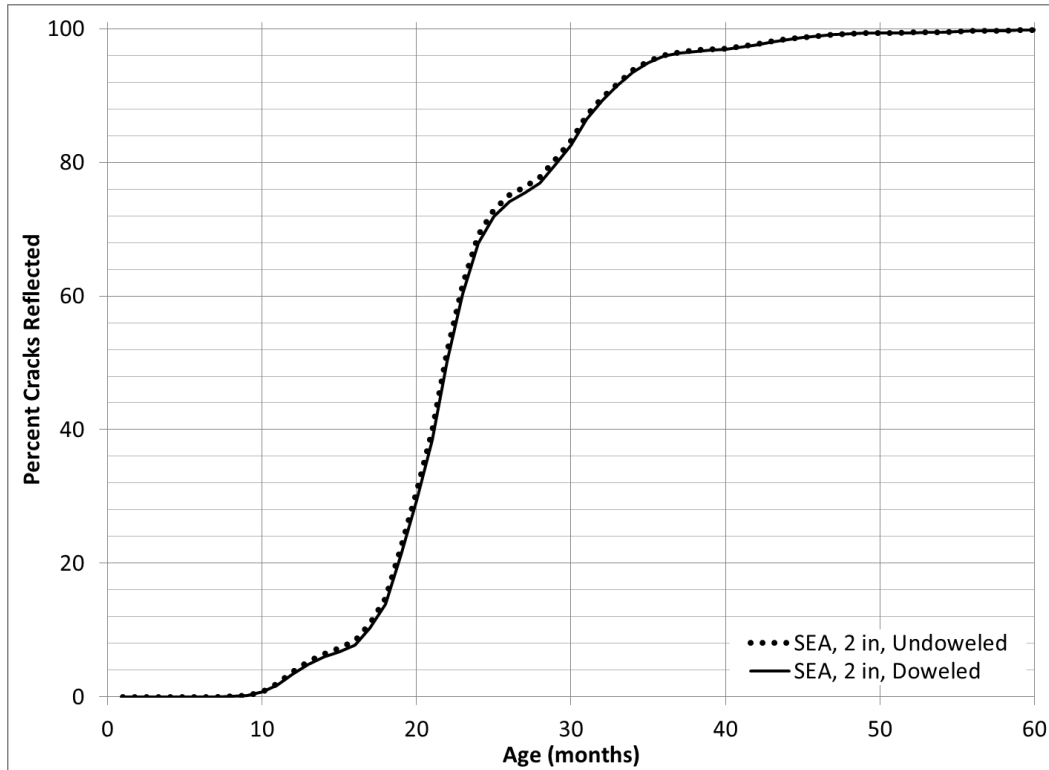


Figure 41. Influence of dowels on TPF-5(149) procedure for L+M+H severity reflective cracking for project using Seattle, WA, climate file

As in the case with the MnROAD results, Figure 40 confirms the sensitivity of the M+H cracking model to LTE, which is to be expected given that the M+H model considers only axle loads. Figure 41 shows that even for projects with less severe climatic conditions than those of MnROAD, L+M+H predictions remain fairly insensitive to LTE. While this is to be expected given the predominance of Low severity cracking, it illustrates that even for less severe climates, thermal effects will contribute to damage far more than axle loads in the L+M+H model.

4. JPCP Cracking Models for HMA-PCC

Many HMA overlays fail prematurely due to transverse cracking in the PCC layer reflecting through the asphalt. The MEPDG identifies transverse cracking in the PCC layer as a major distress that is important to control. The MEPDG assumes that a transverse crack developed in the PCC layer will eventually propagate through the HMA layer over time and traffic. Figure 42 illustrates the propagation of a fatigue crack in the PCC layer to the top of the HMA layer.

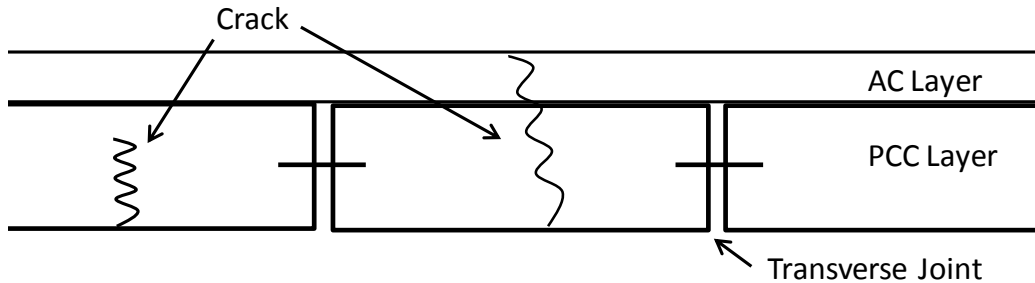


Figure 42. Propagation of fatigue cracking in a composite pavement

For HMA-PCC projects, the MEPDG uses a separate distress model to compute reflective cracking, as detailed in Chapter 3. However, the MEPDG currently uses only the existing model for JPCP in determining the extent of transverse cracking in the PCC layer. Although the JPCP cracking model is quite robust and comprehensive, there is a concern that the HMA characterization used in the model may be inadequate.

The work of Task 5 included a review of the existing JPCP transverse cracking model and a modification of this model for HMA-PCC projects. Task 5 also included a brief validation and sensitivity analysis. These efforts are detailed in the following subsections.

4.1 MEPDG Transverse Cracking Model for JPCP

The MEPDG distress model for predicting transverse cracking in JPCP has the form

$$TCRACK = (CRK_{Bottom-up} + CRK_{Top-down} - CRK_{Bottom-up} \cdot CRK_{Top-down}) \cdot 100\% \quad (4.1)$$

$$CRK = \frac{100}{1 + FD^{-1.68}} \quad (4.2)$$

$$FD = \sum \frac{n_{t,j,k,l,m,p}}{N_{t,j,k,l,m,p}} \quad (4.3)$$

$$\log(N_{t,j,k,l,m,p}) = C_1 \left(\frac{MR}{\sigma_{t,j,k,l,m,p}} \right)^{C_2} \quad (4.4)$$

where $TCRACK$ is the total transverse cracking (percent; all severities); CRK is the percentage of bottom-up or top-down PCC cracking; FD is the fatigue damage; n is the applied number of load applications at conditions t, j, k, l, m , and p ; N is the allowable number of load applications at conditions t, j, k, l, m, p ; t, j, k, l, m , and p are conditions relating to the age, month, axle type, load level, temperature difference, and traffic path, respectively; MR is the modulus of rupture of PCC; σ is the applied stress at conditions t, j, k, l, m , and p ; and C_1 and C_2 are calibration constants ($C_1 = 2.0$; $C_2 = 1.22$).

4.2 Modifications to JPCP Transverse Cracking Model for HMA-PCC Projects and Incorporation into the MEPDG

Equation (4.4) implies that cracking in the PCC layer is a function of the “applied stress” and thus depends on the various factors related to traffic loads and temperature gradients. Accurate computation of the stress at the critical location in the PCC layer is an important step in the calculation of fatigue cracking.

To compute structural responses such as stresses, strains, and displacements, constitutive relationships for each layer in the structural model should be provided. Asphalt is a viscoelastic material; its structural responses depend not only on the magnitude of the applied load but on the load duration as well. However, conducting a viscoelastic analysis for each combination of site and loading conditions required by the MEPDG damage computation process would be computationally prohibitive. In order to simplify the structural analysis, the MEPDG treats asphalt layers as elastic, but to account for the viscoelastic behavior of the asphalt layer, the MEPDG assumes that the asphalt modulus of elasticity is equal to the load duration-dependent dynamic (complex) modulus.

The loading duration for traffic loads depends on the vehicle speed. If vehicle speed is approximately 60 mph, then the loading duration ranges between 0.01 sec and 0.05 seconds. However, the duration of temperature loading is significantly longer. The MEPDG analysis of flexible pavements ignores temperature-induced asphalt stresses and strains for all the distress models except the low-temperature cracking model. In the low-temperature cracking model, the temperature-induced stresses are accounted for but asphalt material is characterized differently and the axle load-induced stresses are ignored. Therefore, the MEPDG framework used to account for the viscoelastic behavior of asphalt layers in the design of flexible pavements can be considered reasonable.

The situation is quite different in the case of asphalt overlays of concrete pavements because the MEPDG implicitly accounts for both traffic and temperature induced stresses and strains in the asphalt layer. The MEPDG recognizes that there is an interaction between temperature curling and deformations due to traffic loading for the JPCP and HMA overlays of JPCP. Moreover, the loading durations of temperature gradients and fast moving traffic loads are significantly different. Therefore, for the case of asphalt overlays of JPCP in the MEPDG framework, the characterization of the HMA layer using a single dynamic modulus may be an oversimplification.

The MEPDG distress model for predicting transverse cracking in the PCC layer of an HMA overlaid JPCP was adopted directly from the fatigue cracking model of a new JPCP detailed in Section 4.1. Under Task 4 of TPF-5(149), an approximate two-moduli analysis for the prediction of the critical concrete stresses was developed. However, a direct implementation of that method was not feasible due to a need to re-train a portion of the MEPDG neural networks and replace the current temperature distribution linearization procedure. These activities will be a subject of future research. A simplified procedure for TPF-5(149) was instead adopted.

For each combination of traffic loading and temperature distribution throughout the composite pavement system, three stresses were computed using the MEPDG.

1. The first stress, $\sigma(E_{red}, \Delta T)$, was computed using the current MEPDG HMA complex modulus and zero temperature gradient;
2. the second, $\sigma(E_{red}, 0)$, was calculated using the reduced HMA modulus to account for longer duration of curling process and the actual temperature gradient;
3. and the third and final stress, $\sigma(E^*, 0)$, was calculated using the reduced HMA modulus and zero temperature gradient.

These stresses were combined for the subsequent fatigue analysis according to

$$\sigma_{comb} = \sigma(E_{red}, \Delta T) - \sigma(E_{red}, 0) + \sigma(E^*, 0) \quad (4.5)$$

where E^* is the MEPDG HMA complex modulus currently used HMA overlay cracking analysis and E_{red} is the reduced modulus. Currently, the reduced modulus is assumed to be 50% of the complex modulus.

4.3 Sensitivity Analysis of Modified MEPDG JPCP Transverse Cracking Model

The research team undertook a brief sensitivity analysis of the modified transverse cracking performance relative to two important parameters: HMA overlay thickness and climate. Other than these two parameters, the sensitivity study assumed a HMA-PCC pavement with 2 inches (50 mm) HMA over 7 inches (175 mm) JPCP. Furthermore, the analysis assumed MEPDG defaults for material properties (Level 3 inputs) for all projects. Assumed traffic was 2000 AADTT.

To begin, a number of JPCP projects were created to assess the effect of the HMA overlay on overall PCC transverse cracking performance. These JPCP projects (for a 7-inch, 8-inch, and 9-inch slab) were run using the original MEPDG. The HMA-PCC project was run using both the original MEPDG procedure and the TPF-5(149) procedure for PCC transverse cracking developed in Task 5. Figure 43 and Figure 44 present the predicted PCC transverse cracking for these cases.

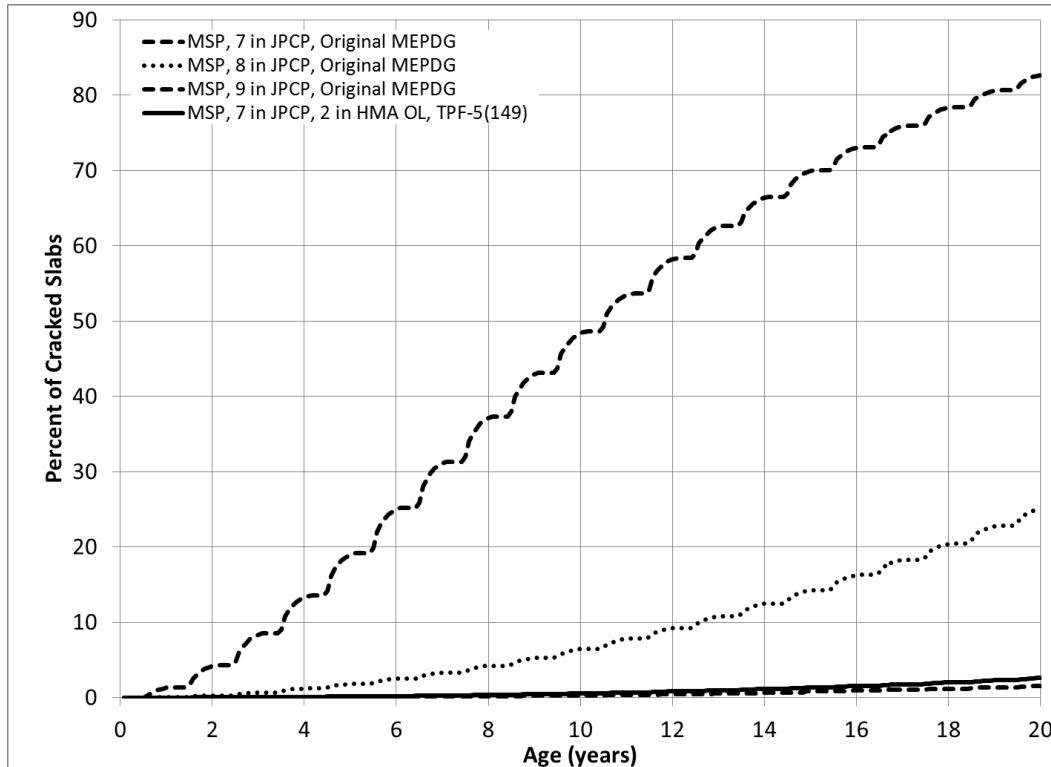


Figure 43. Predicted JPCP transverse performance for three JPCP projects (according to original MEPDG) and a HMA-PCC project (according to TPF-5(149) procedure)

As expected, a presence of an overlay reduces PCC cracking. Figure 43 shows, however, that this effect can be very pronounced. The MEPDG predicts that after 10 years a 7-in thick JPCP would exhibit 50 percent of cracked slabs while a TPCP would have almost negligible amount of cracking. An 8-in JPCP would also exhibit higher cracking than the composite pavement and only 9-in JPCP would have lower cracking. This behavior can be explained by the fact that presence of a HMA overlay significantly reduces temperature gradients in the PCC layer (i.e. it is “thermally insulated”) thus reducing fatigue damage. It should be noted that a similar trend produced by the original MEPDG cracking model for HMA overlays.

Furthermore, Figure 44 shows that the original MEPDG model predicts even lower cracking in the composite pavements compared to a 9-in JPCP under the same site conditions.

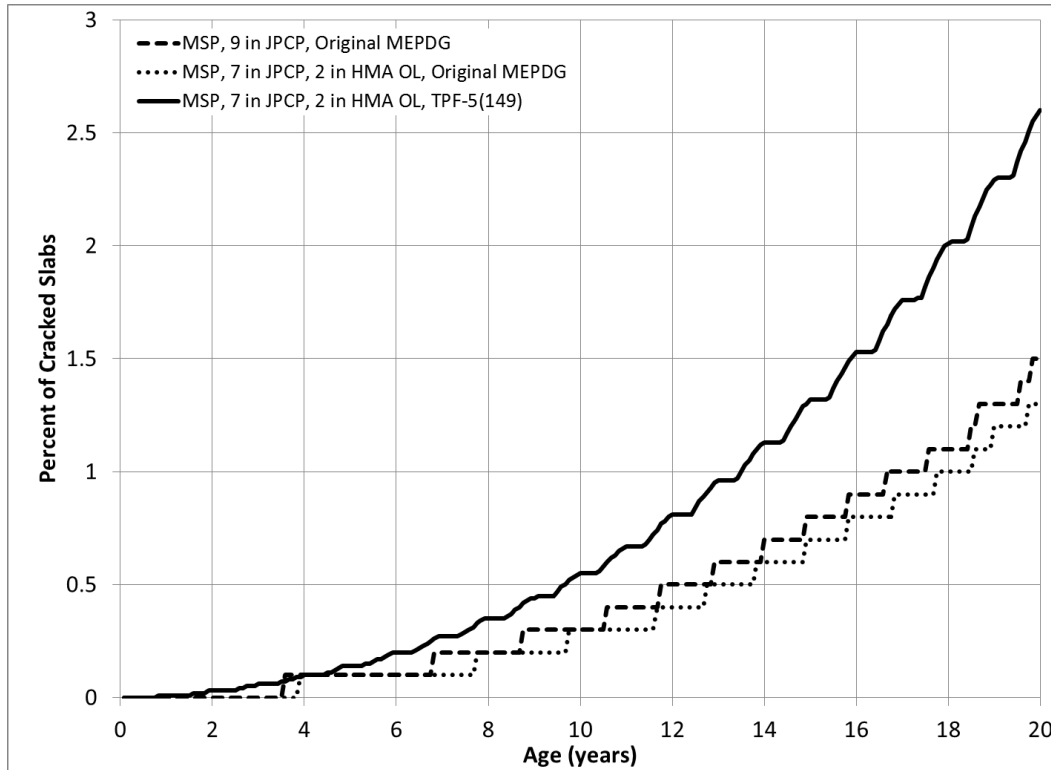


Figure 44. Comparison of 9-inch JPCP project and model predictions for PCC transverse cracking according to original MEPDG and TPF-5(149) procedures

Figure 45 illustrates the sensitivity of transverse cracking predictions for the PCC layer to climate for 3 levels of HMA overlay thickness (and in turn composite pavement thickness). For each of these cases, the PCC thickness is a constant 7 inches.

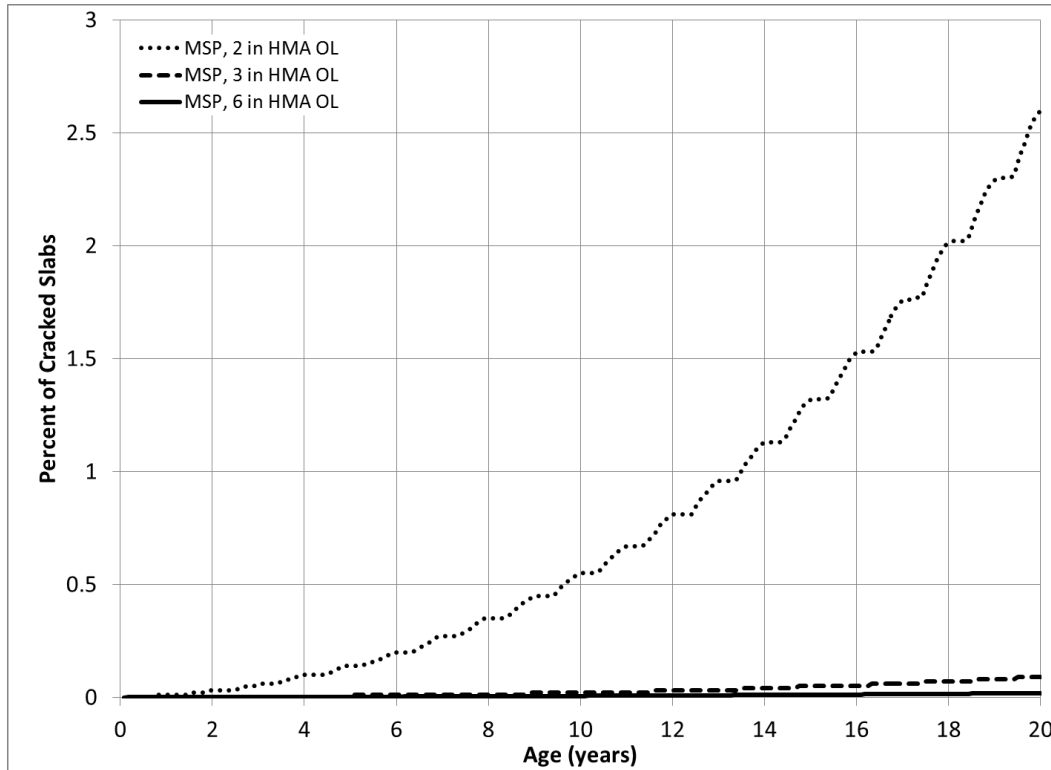


Figure 45. Influence of HMA overlay thickness on predicted JPCP transverse cracking for a HMA-PCC project

As expected, an increase in HMA overlay thickness decreases cracking. It should be noted that this trend (a decrease in PCC cracking with an increase in HMA thickness) was experimentally confirmed at HVS testing conducted under the SHRP2 R21 project. It is also worth considering, however, that both HVS testing and the analysis from this study concluded that an increase in HMA thickness increases HMA rutting

Figure 46 illustrates the sensitivity of transverse cracking predictions for the PCC layer to climate for 4 locations. Each of these locations corresponds to EICM climate files (*.icm) for Seattle, WA; Pullman, WA; San Francisco, CA; and Minneapolis-Saint Paul, MN.

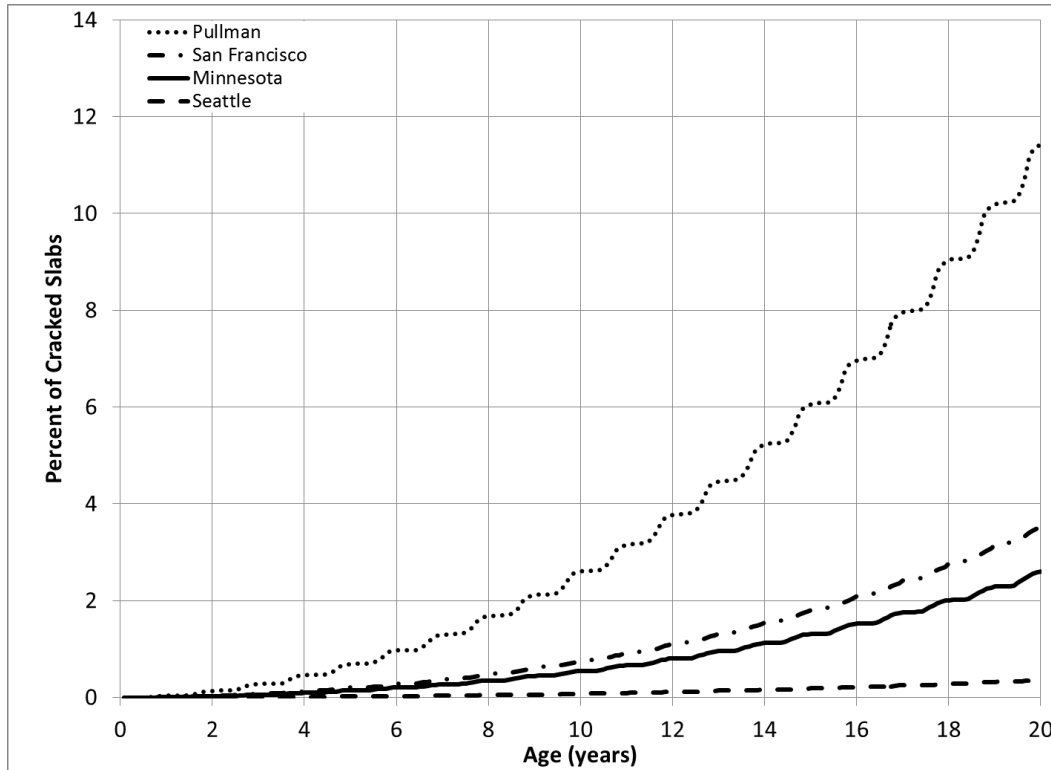


Figure 46. Influence of climate on JPCP transverse cracking for a HMA-PCC project

It can be observed that the cracking prediction is sensitive to the climate data, as it was discussed in the previous task reports.

4.4 Confirmation of TPF-5(149) Modifications to MEPDG JPCP Transverse Cracking Model for HMA-PCC Projects

Figure 47 illustrates a comparison of predicted JPCP transverse cracking for HMA-PCC projects in Minneapolis, MN, and Pullman, WA using the original MEPDG and the modified MEPDG that utilizes the JPCP transverse cracking revised during the work of Task 5. These projects assume a cross-section of a 2-inch HMA overlay of 7-inch JPCP with Level 3 inputs.

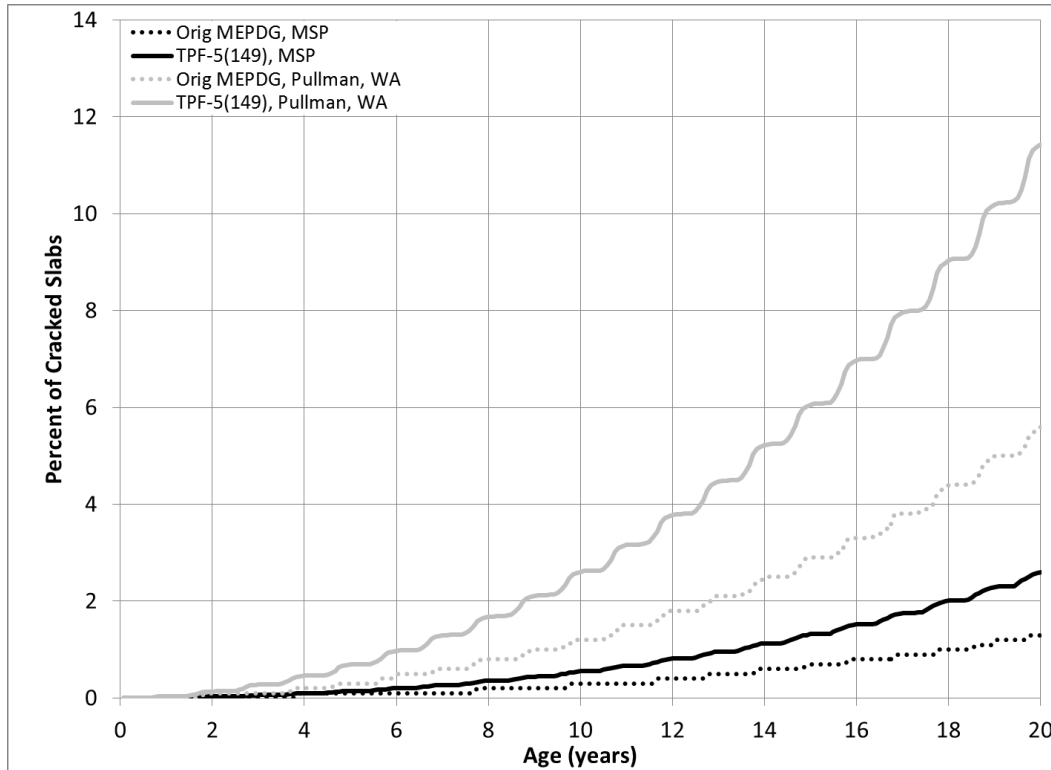


Figure 47. Predicted JPCP transverse cracking in HMA-PCC projects for Minneapolis, MN, and Pullman, WA, according to the original and TPF-5(149) modified MEDPG

Both models produce the same trends. It is possible that the developed TPF-5(149) procedure may not be conservative enough. At the same time, as it was observed from the analysis of MnROAD Cells 106 and 206, the original MEDPG model may produce higher cracking than the TPF-5(149) model. More comparison with field performance data is needed to establish what model is better. Meanwhile, it is recommended to run both models and use a more conservative prediction.

Figure 48 compares transverse cracking prediction for Cells 106 and 206 using the original MEDPG procedure and the TPF-5(149) model.

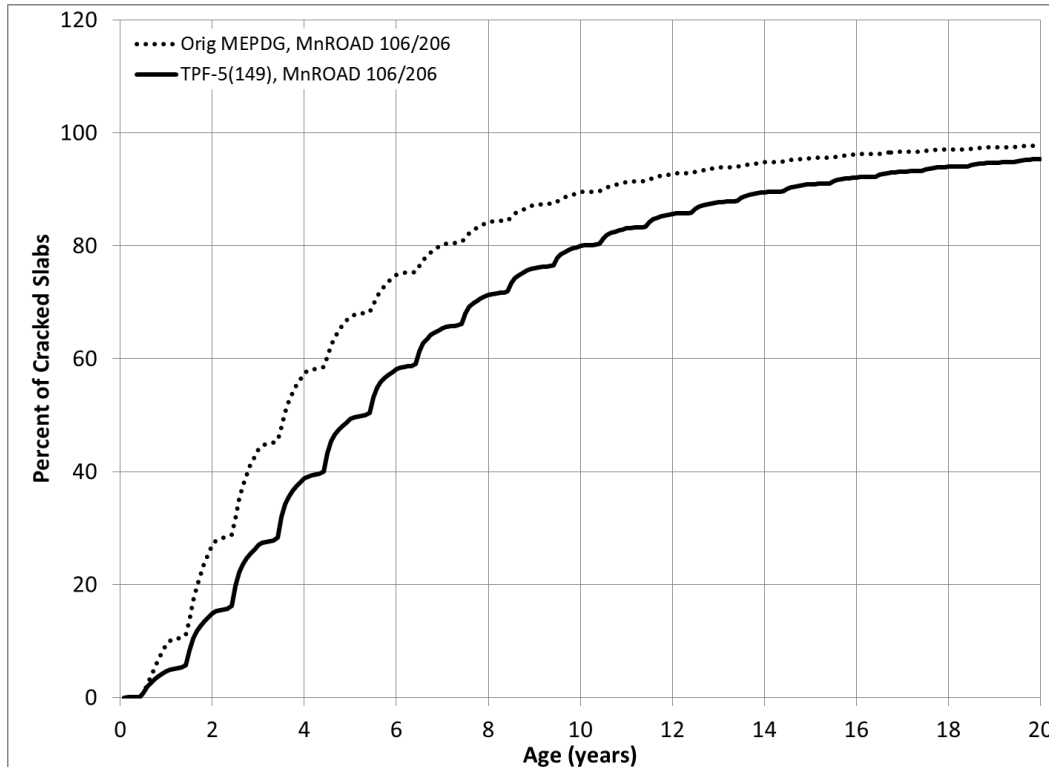


Figure 48. Predicted transverse cracking in MnROAD Cells 106 and 206 according to the original MEPDG and TPF-5(149) procedures

As shown in Figure 48, both models predict a high percentage of cracking two years after construction. This somewhat agrees with field observations, as structural performance of both cells was reported by MnROAD to be poor and they were reconstructed after three years of service.

At the same time, the main structural distress in the PCC layer was longitudinal and not transverse cracking. Currently, the MEPDG does not have a model for the prediction of longitudinal cracking in JPCP and HMA-PCC. However, a predicted high transverse cracking fatigue damage can be used as an indirect estimate of the longitudinal cracking damage. Since both models predict high fatigue damage, one can conclude that both models predicted poor performance for both Cells 106 and 206.

5. JPCP Faulting Models for HMA-PCC

The faulting model in the current MEPDG is for newly constructed JPCP pavements only; thus, a faulting model has not been implemented for HMA-PCC projects. One of the reasons for this is that for conventional HMA-PCC pavements, faulting does not develop until reflective cracks propagate, which then complicates observation of cracking that can be directly attributed to faulting. Furthermore, faulting data is typically not collected for HMA-PCC.

Nevertheless, given the popularity of saw-and-seal techniques for HMA-PCC and the recommendation of saw-and-seal for HMA-PCC by the SHRP2 R21 project, there is a need to quantify the benefits of the use of dowels in terms of design and analysis. As noted earlier, the MEPDG does not provide this, and therefore the work of Task 5 included the modification of the MEPDG faulting model for HMA-PCC and the incorporation of this modified model into the existing MEPDG framework for HMA-PCC projects.

5.1 MEPDG JPCP Faulting Model

The mean transverse joint faulting is predicted using incremental approach as illustrated in Figure 3. A faulting increment is determined each month and the current faulting level affects the magnitude of increment. The faulting at each month is determined as a sum of faulting increments from all previous months in the pavement life since the traffic opening using the following model:

$$Fault_m = \sum_{i=1}^m \Delta Fault_i \quad (5.1)$$

$$\Delta Fault_i = C_{34} * (FAULTMAX_{i-1} - Fault_{i-1})^2 * DE_i \quad (5.2)$$

$$FAULTMAX_i = FAULTMAX_0 + C_7 * \sum_{j=1}^m DE_j * \text{Log}(1 + C_5 * 5.0^{EROD})^{C_6} \quad (5.3)$$

$$FAULTMAX_0 = C_{12} * \delta_{curling} * \left[\text{Log}(1 + C_5 * 5.0^{EROD}) * \text{Log}\left(\frac{P_{200} * \text{WetDays}}{P_s}\right) \right]^{C_6} \quad (5.4)$$

where C_{12} , C_{34} , C_5 , C_6 , and C_7 are calibration constants and

$Fault_m$	= Mean joint faulting at the end of month m , inches
$\Delta Fault_i$	= Incremental change (monthly) in mean transverse joint faulting during month i , inches
$FAULTMAX_i$	= Maximum mean transverse joint faulting for month i , inches
$FAULTMAX_0$	= Initial maximum mean transverse joint faulting, inches
$EROD$	= Base/subbase erodibility factor
DE_i	= Differential deformation energy accumulated during month i
$\delta_{curling}$	= Maximum mean monthly slab corner upward deflection PCC due to temperature curling and moisture warping
PS	= Overburden on subgrade, pounds
$P200$	= Percent subgrade material passing #200 sieve

WetDays = Average annual number of wet days (greater than 0.1 inch rainfall)
FR = Base freezing index, defined as the percentage of time the top base temperature is below freezing (32 °F) temperature.

Khazanovich et al (2004) and AASHTO (2008) further describe the differential energy concept used to define parameter DE_i (which accounts for joint load-transfer efficiency, aggregate interlock, and the presence and type of joint dowels). Furthermore, calibration coefficients C_{12} and C_{34} are related to the base freezing index, FR , as follows

$$C_{12} = C_1 + C_2 * FR^{0.25} \quad (5.5)$$

$$C_{34} = C_3 + C_4 * FR^{0.25} \quad (5.6)$$

where C_1 through C_4 are calibration constants and the base freezing index, FR , is defined as the percentage of time the top base temperature is below freezing (32 °F) temperature.

The functional form of the model reflects the hypothesis that faulting potential for a given pavement structure depends on the extent of slab curling, the erodibility of the base material, and the presence of fines and free water in the subgrade. Faulting potential decreases with an increase of overburden pressure on the subgrade. The rate of faulting development depends on the current faulting level, and that rate decreases as faulting increases. Eventually the faulting stabilizes at a certain level.

5.2 Modifications of MEPDG Faulting Model for HMA-PCC and Incorporation into the MEPDG Procedure

Two major modifications of the MEPDG faulting model were implemented during the work of Task 5.

- The composite HMA-PCC structure was replaced by an equivalent single layer system.
- The load transfer efficiency characterization was modified.

5.2.1 Equivalent single-layer pavement

For a fully bonded PCC-base system, the neutral axis of the bonded system, assuming the origin is at the top of the PCC layer, is given as follows:

$$x = \frac{\int_0^h E(z)zdz}{\int_0^h E(z)dz} = \frac{E_{PCC}h_{PCC}\left(\frac{h_{PCC}}{2}\right) + E_{Base}h_{Base}\left(h_{PCC} + \frac{h_{Base}}{2}\right)}{E_{PCC}h_{PCC} + E_{Base}h_{Base}} \quad (5.7)$$

where x is the location of the neutral axis from the top of PCC layer. The thickness and modulus of the equivalent single-layer slab can be established in terms of the thicknesses and moduli of the corresponding multi-layered slab as follows:

$$E_{eff} h_{eff}^3 = E_{PCC} h_{PCC}^3 + E_{base} h_{base}^3 + 12 \left[E_{PCC} h_{PCC} \left(\frac{h_{PCC}}{2} - x \right)^2 + E_{Base} h_{Base} \left(h_{PCC} + \frac{h_{Base}}{2} - x \right)^2 \right] \quad (5.8)$$

For a fully bonded HMA-PCC-base system, the neutral axis x is located as follows, assuming the origin is located at the surface of the HMA overlay:

$$x = \frac{\frac{E_{HMA}}{E_{PCC}} \frac{h_{HMA}^2}{2} + h_{PCC} \left(h_{HMA} + \frac{h_{PCC}}{2} \right) + \frac{E_{Base}}{E_{PCC}} h_{Base} \left(h_{HMA} + h_{PCC} + \frac{h_{Base}}{2} \right)}{\frac{E_{HMA}}{E_{PCC}} h_{HMA} + h_{PCC} + \frac{E_{Base}}{E_{PCC}} h_{Base}} \quad (5.9)$$

where E_{eff} , E_{HMA} , E_{PCC} , and E_{Base} are the Young's moduli of the effective composite system, HMA overlay, PCC layer, and base layers, respectively, and h_{eq} , h_{HMA} , h_{PCC} , and h_{Base} are the thicknesses of the effective composite slab, HMA overlay, PCC layer, and base layers, respectively.

One check of the solution for the neutral axis in the three-layer PCC system is to consider that if $E_{HMA} = E_{PCC}$, equation (5.9) will reduce to equation (5.7), which represents the location of the neutral axis in a single-layer PCC over base layer system. The thickness and modulus of the equivalent single-layer slab for the three-layer system can be established as in equation (5.8), where

$$E_{eff} h_{eff}^3 = E_{HMA} h_{HMA}^3 + E_{PCC} h_{PCC}^3 + E_{Base} h_{Base}^3 + 12 \left[E_{HMA} h_{HMA} \left(x - \frac{h_{HMA}}{2} \right)^2 + E_{PCC} h_{PCC} \left(h_{HMA} + \frac{h_{PCC}}{2} - x \right)^2 + E_{Base} h_{Base} \left(h_{HMA} + h_{PCC} + \frac{h_{Base}}{2} - x \right)^2 \right] \quad (5.10)$$

All variables in equation (5.10) are defined above for equation (5.9).

5.2.2 Load transfer in a HMA-PCC system

For transverse joints, the total deflection LTE includes the contribution of three major mechanisms of load transfer:

- load transfer by PCC aggregates;
- load transfer by joint dowels (if applicable); and
- joint transfer by the base/subgrade.

In the MEPDG, the combined LTE for a JPCP project is defined as

$$LTE_{joint} = 100 \left(1 - (1 - LTE_{dowel} / 100)(1 - LTE_{agg} / 100)(1 - LTE_{base} / 100) \right) \quad (5.11)$$

where LTE_{joint} is the percentage of total joint LTE; LTE_{dowel} is the percentage of joint LTE if dowels are the only mechanism of load transfer; LTE_{base} is the percentage of joint LTE if the

base is the only mechanism of load transfer; and LTE_{agg} is the percentage of joint LTE if aggregate interlock is the only mechanism of load transfer.

For composite pavements, it is the HMA overlay also provides load transfer until the reflective crack propagates to the surface. To account for this effect, equation (5.11) has been modified to become

$$LTE_{joint} = 100 \left(1 - \left(1 - \frac{LTE_{dowel}}{100} \right) \left(1 - \frac{LTE_{agg}}{100} \right) \left(1 - \frac{LTE_{base}}{100} \right) \frac{RC_{LMH}}{100} \right) \quad (5.12)$$

where RC_{LMH} is the total reflective cracking, defined in Equation (3.11). Equation (5.12) – i.e. the modification of Equation (5.11) – states that the HMA overlay:

1. dominates the joint load transfer until the cracks propagate and
2. does not directly contribute to the load transfer after all reflective cracks (100 percent) propagate to the surface

5.3 Validation and Sensitivity Analysis of Modified MEPDG Faulting Model for HMA-PCC

Faulting data are not routinely collected for composite pavements. To validate the model, the predictions were compared with the predictions of the field-calibrated faulting model for new JPCP pavements as well as through the analysis of sensitivity of the predictions to the input parameters. Since the faulting prediction is especially important for saw-and-seal pavements, this type of joint is considered below.

Figure 49 presents a comparison of the predicted faulting a 2-inch HMA overlay of 7-inch undoweled JPCP with the predicted faulting for 8-inch and 9-inch thick new undoweled JPCP projects.

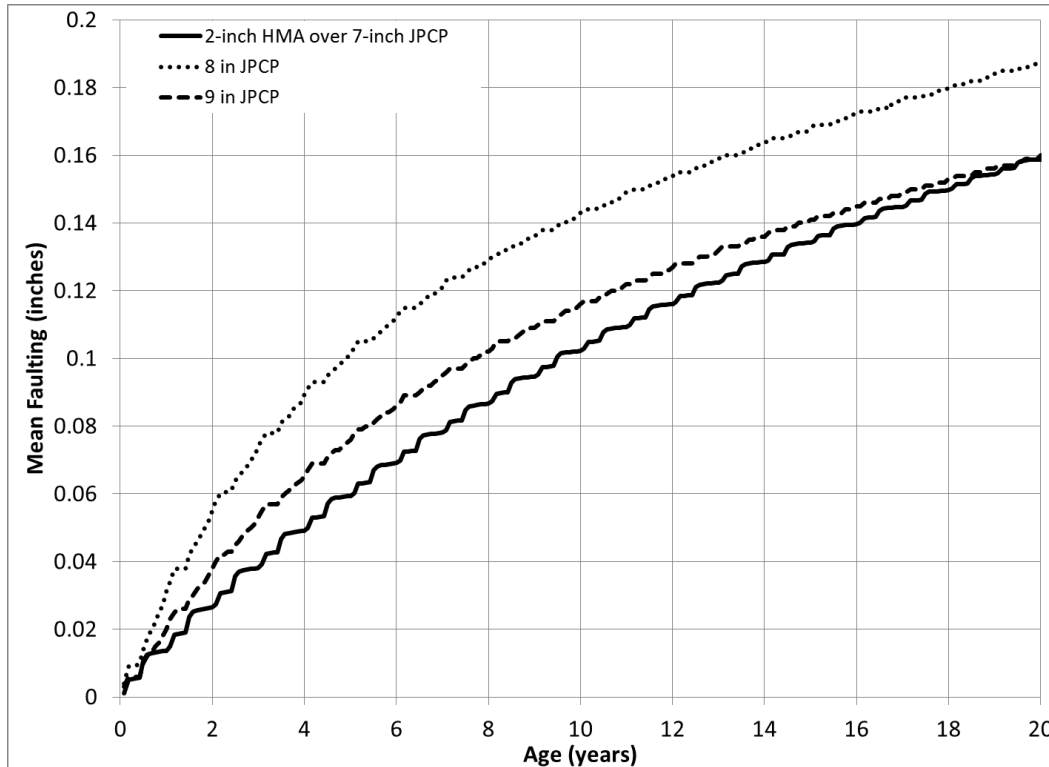


Figure 49. Comparison of predicted faulting for HMA-PCC and JPCP projects using MEPDG modified according to TPF-5(149)

One can observe in Figure 49 that the predicted faulting for the HMA-PCC project is lower than for the 8-inch JPCP and is comparable with the predicted faulting for the 9-in JPCP. Such behavior might be expected, because although the replacement of the top two inches of PCC with HMA increases the flexibility of the pavement, the presence of an HMA layer decreases temperature gradients throughout the PCC slab thickness. Also, the HMA layer seals off the PCC surface thus reducing the PCC shrinkage. It should be also noted that the PCC cracking models for the same site conditions also predicted similar cracking for the HMA-PCC and 9-inch thick JPCP.

Figure 50 compares the predicted faulting for HMA-PCC projects in Minneapolis, MN, and Pullman, WA, whose cross-section is a 2-inch HMA overlay of 7-inch JPCP with Level 3 inputs assumed otherwise.

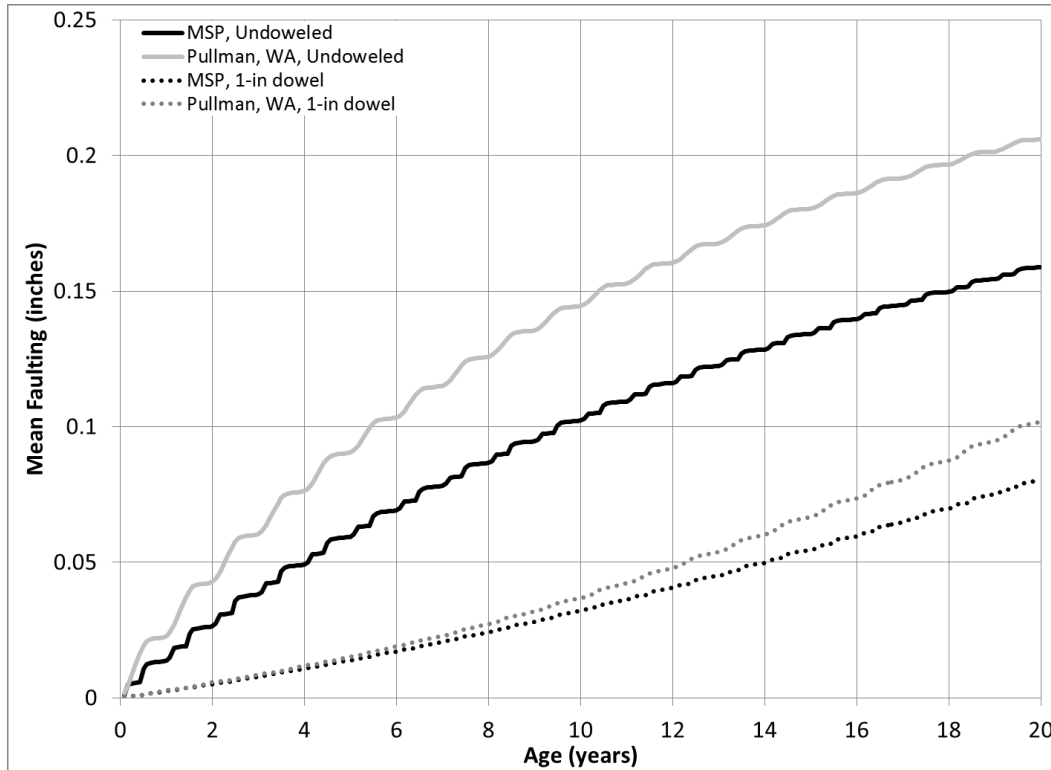


Figure 50. Effect of 1-inch dowels in HMA-PCC projects for Minneapolis, MN, and Pullman, WA

The presence of doweling for these projects mitigates predicted faulting by nearly one-third for these cases. For both locations, the presence of dowels significantly reduces the predicted faulting. This trend was expected, as the presence of dowels significantly improves the load transfer efficiency of the PCC joint.

Figure 51 and Figure 52 demonstrate the effect of climate on faulting prediction for doweled and undoweled HMA-PCC pavements, respectively. Here the projects assume a cross-section that is 2-inch HMA overlay of 7-inch JPCP, and MEPDG Level 3 default parameters are otherwise assumed. The projects are associated with four EICM climate files: Minneapolis, MN; Seattle, WA; Pullman, WA; and San Francisco, CA.

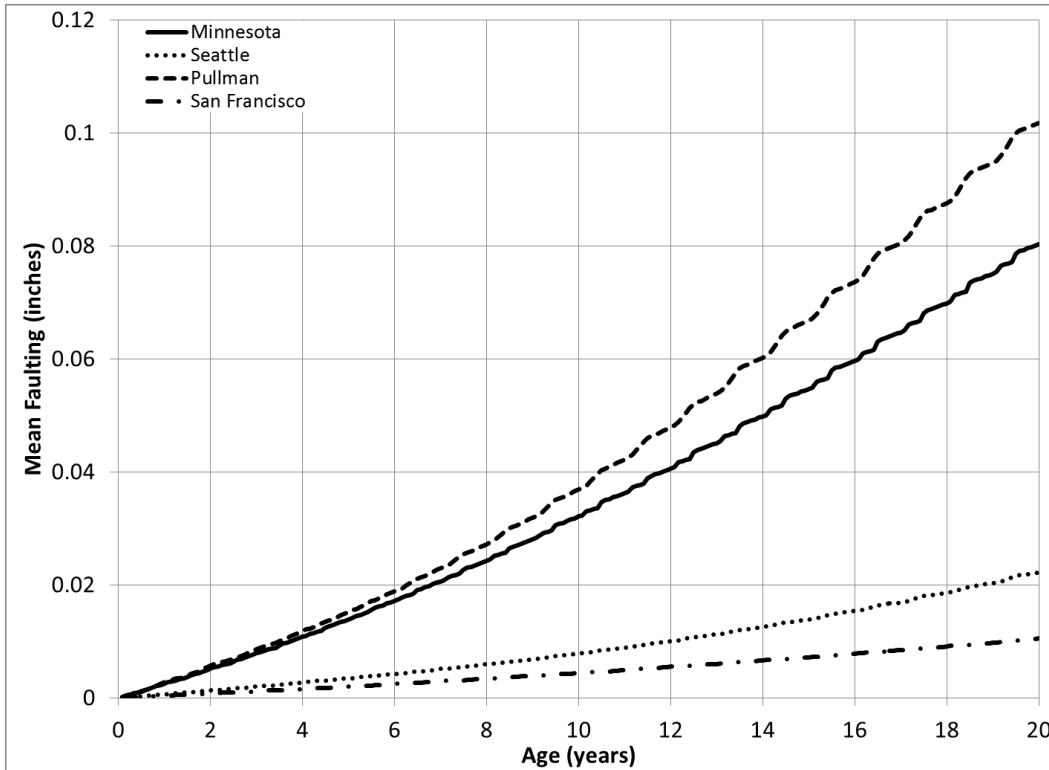


Figure 51. Influence of climate on predicted faulting in HMA-PCC using TPF-5(149) modified MEPDG for HMA-PCC project with 1-inch dowels

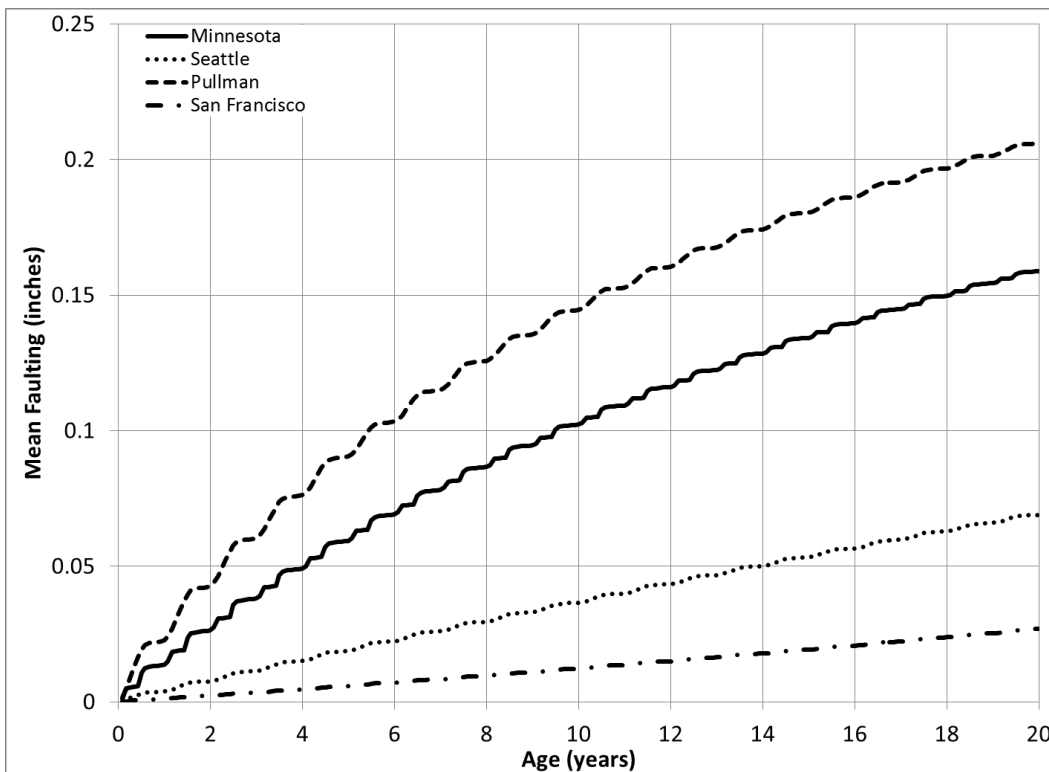


Figure 52. Influence of climate on predicted faulting in HMA-PCC using TPF-5(149) modified MEPDG for HMA-PCC project without dowels

As expected, the predicted faulting is lower in a milder climate, provided that other design features and site conditions remain fixed from project to project. This is true for both doweled and undoweled composite pavements. It should be noted, however, that Figure 51 and Figure 52 illustrate only the effect of climate *and not* location. The subgrade properties for these locations can be different and this may significantly affect the relative magnitude of faulting for the same design features and traffic.

Finally, Figure 53 and Figure 54 describe the influence of HMA overlay thickness on faulting predictions for doweled and undoweled projects, respectively. For these projects, we assume a cross-section that is 2-inch HMA overlay of 7-inch JPCP, and MEPDG Level 3 default parameters are otherwise assumed. The projects are associated with an EICM climate file for Minneapolis, MN.

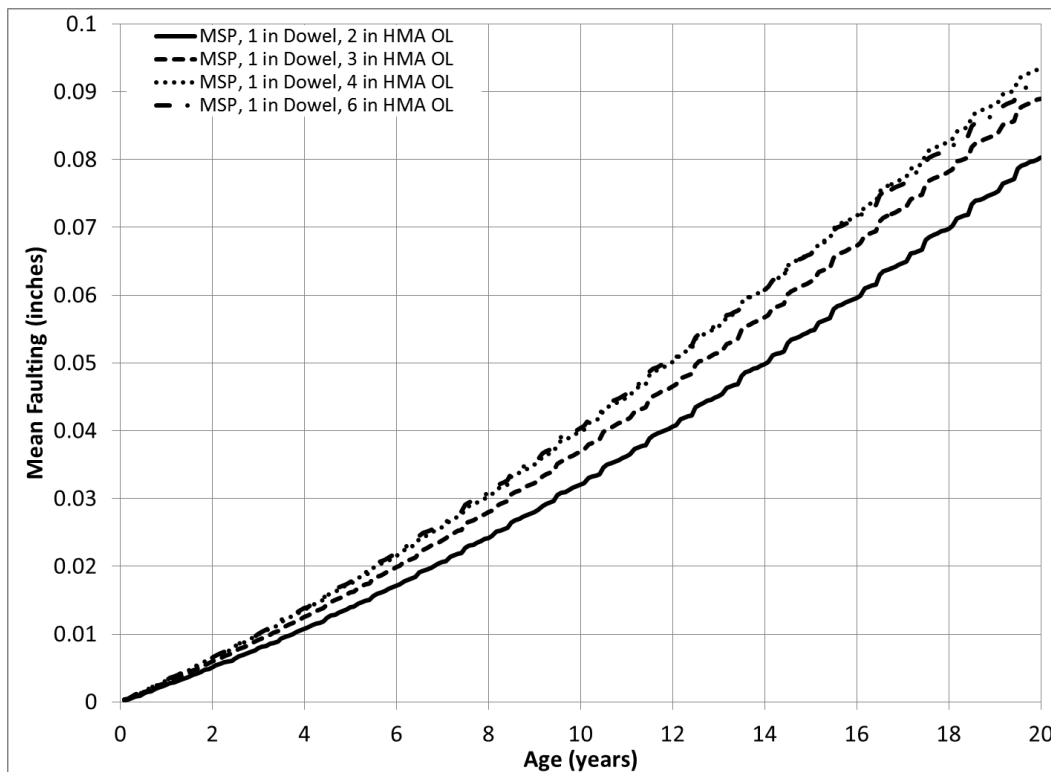


Figure 53. Influence of HMA overlay thickness on predicted faulting in HMA-PCC using TPF-5(149) modified MEPDG for HMA-PCC project with 1-inch dowels

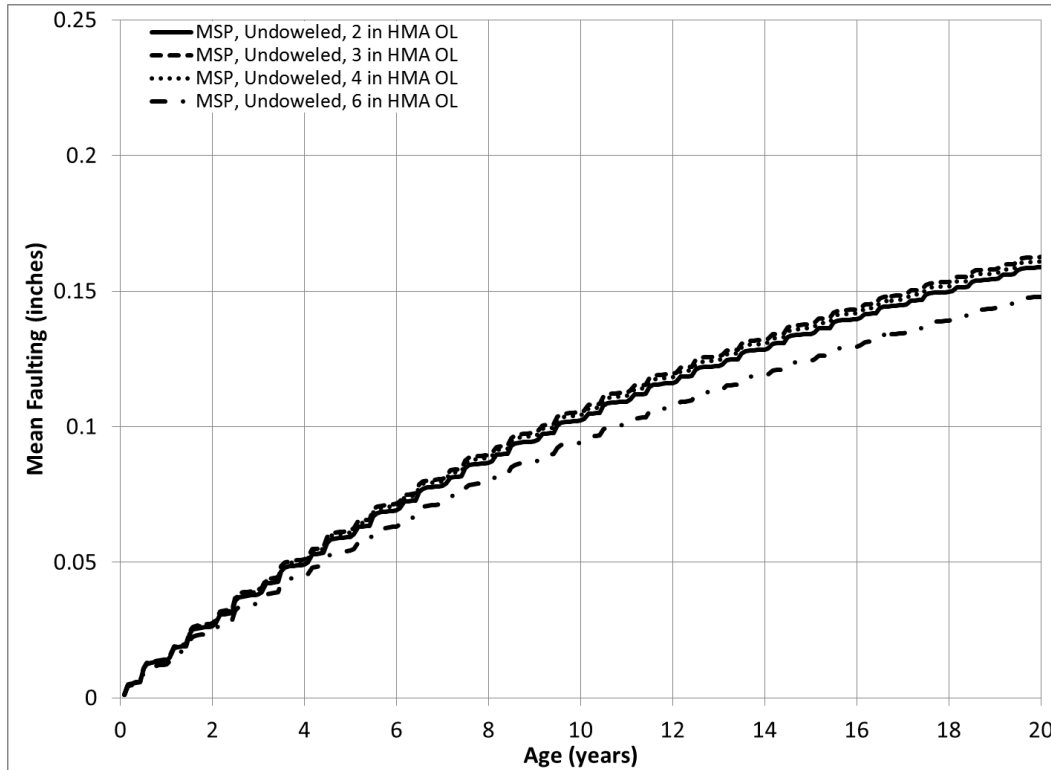


Figure 54. Influence of HMA overlay thickness on predicted faulting in HMA-PCC using TPF-5(149) modified MEPDG for HMA-PCC project without dowels

One can observe in Figure 53 and Figure 54 that an increase in the HMA overlay thickness over two inches does not appreciably reduce faulting. The HMA overlay is less stiff than concrete and its relative contribution to slab rigidity is not very significant. At the same time, the HMA layer has a high coefficient of thermal expansion. Making the HMA layer thicker increases the “thermal moment” on the PCC slab; under certain conditions it may even increase faulting.

In summary, the analysis presented above demonstrates robustness of the faulting model. However, to fully validate the model, field performance data should be collected to enable comparison with the model predictions.

6. Guidelines to TPF-5(149) Procedure for Design and Analysis of TICP

The work of Task 5 developed four separate programs that allow an MEPDG user to interface with the MEPDG project and intermediate files for a TICP project to develop revised rutting, reflective cracking, faulting, and transverse cracking predictions to use in design and analysis. The following outline describes the steps a general user would take in creating an MEPDG project creation and running the TPF-5(149) programs to obtain modified performance results according to the TPF-5(149) procedure.

6.1 Creating MEPDG Project File

The first step is the basic creation of an MEPDG project.

1. Design Type: Select “Overlay.” (Although TICP is a newly constructed composite pavement and not an overlay of an existing JPCP, this is the proper Design Type to select until the MEPDG is modified by AASHTO to include newly constructed HMA-PCC projects.)
2. Pavement Type: Select “HMA/JPCP” for AC/JPC
3. Design Life: Select desired life of pavement.

Once a project file has been initiated, the user must select all design inputs for a trial design. The unique inputs for a TICP composite pavement are as follows.

4. Design reliability and performance for composite pavements:
 - a. Design reliability should be based on traffic level of the highway. Higher traffic levels warrant higher reliability levels (95% to 99%).
 - b. Structural fatigue cracking should range between 5% and 15% JPCP transverse fatigue cracking
 - c. Smoothness (Terminal IRI) should be based on traffic level of the highway. Higher traffic levels warrant lower terminal smoothness levels (~150 in/mile).
 - d. Permanent deformation (rutting of HMA only which is total also) should be ~0.50-in mean wheel path
 - e. Joint faulting for “bare” JPCP comparisons: 0.15 to 0.20 in.
 - f. Initial IRI: The initial IRI for HMA/PCC composite pavements can be very low due to the multiple layering of the pavement. Initial IRI values as low as 35 in/mile have been achieved, with routine values from 40 to 50 in/mile.
 - g. Type and thickness of HMA surface layer. The type depends on the design objectives. If reducing noise levels to a minimum are required, then some type of porous asphalt surface can be used. Thickness should be the minimum possible to provide durability and surface characteristics desired for a given truck traffic and climate. In warmer weather locations, a thinner surfacing is feasible, such as 1 in, but for colder weather and heavier traffic, up to 3 in total may be required.
5. Type (JPCP) and thickness of the PCC layer. This is the load carrying capacity layer for the composite pavement. The trial design should start with a typical thickness used for

bare pavement. Depending on the thickness of the HMA surface, the slab thickness may be reduced by 1 to 3 inches of concrete.

6. Joint design. Joint design includes joint spacing and joint load transfer.
 - a. Joint load transfer requirement is similar to bare JPCP design in that dowels of sufficient size are required to prevent erosion and faulting for any significant level of truck traffic. The greater the dowel diameter the higher the joint LTE and the more truck loadings the pavement can carry to the terminal level of faulting.
 - b. Simplified dowel design: the dowel diameter should be at least 1/8 the slab thickness
 - c. Low volume roadways where dowels would not normally be used for bare JPCP do not require dowels for composite pavement. This is true for residential or farm to market streets where JPC or RCC is used as the lower layer. When dowels are not used, it is highly recommended to reduce the joint spacing to 10 ft to reduce reflection cracking severity and increase joint LTE.
7. Concrete slab recommendations:
 - a. Typical concrete used in bare JPCP can be used for TICP with no changes. There are no special requirements different than that for bare pavement.
 - b. Lower cost concrete based on local aggregates or recycled concrete. The strength, modulus of elasticity, CTE, and drying shrinkage of the concrete can be varied as inputs.
 - c. The SHRP2 R21 MnROAD test sections showed that recycled concrete from a local roadway or local aggregates can be used for the lower layer. Both of these alternatives provided sustainability advantages and cost savings.
 - d. Base layer and other sublayers should be selected similar to bare JPCP or CRCP designs based on minimizing erosion, construction ease, and cost effectiveness. No attempts should be made to reduce the friction between the slab and the base because as friction helps control erosion and pumping and reduces stress in the slab.

At this point, the user should have a full project file created.

6.2 Execute MEPDG analysis for TICP project

In the second step, the user runs the MEPDG program for the created TICP project file (or more generally, an HMA-over-JPCP project file). The MEPDG software performs traffic and EICM (climatic) analysis and creates intermediate project files, which later will be used in the TPF-5(149) analysis.

6.3 Execute TPF 5(149) analysis for TICP project

In the third step, the user will implement the TPF-5(149) procedure to revise MEPDG predicted performance for the HMA-PCC distresses discussed earlier in this report. The designer may choose to execute any or all of the following models:

- TPF-5(149) rutting model
- TPF-5(149) JPCP cracking model

- TPF-5(149) faulting model
- TPF-5(149) reflective cracking model (if the saw-and-seal option is not selected)

Each model will predict the corresponding distress for every month of the pavement design life.

6.4 Interpret design outputs

After the TPF-5(149) analysis is complete, the designer should compare the predicted level of distresses with distresses with the specified performance threshold values. The designer can use either MEPDG or the TPF-5(149) procedure. The following basic checks will assist the user in determining an adequate structural design for a given TICP project:

1. Transverse fatigue cracking, IRI, and HMA rutting must all meet the design reliability requirements for a trial design to be feasible.
2. If any of these do not “Pass” at the reliability level, a modification in the design is required. Some guidelines are as follows for making modifications:
3. For excess transverse cracking of JPCP, increase slab thickness, shorten joint spacing, add a tied PCC shoulder or 1-ft widened slab, use a stabilized base course, increase PCC strength (with appropriate change in the modulus of elasticity), or use different aggregate source (one with lower CTE).
4. For excess rutting of HMA surface, modify binder grade, modify mixture parameters such as as-built air voids and binder content, and reduce layer thickness. If these changes are not effective or acceptable, program a surface removal and replacement at the point of predicted rutting reaching the critical level.
5. For excess IRI, reduce JPCP and HMA rutting, or require a smoother initial pavement.
6. For excess Medium and High severity reflective cracking, select saw-and-seal, use dowels, increase HMA thickness, or modify mixture parameters.

7. Task Discussion and Conclusions

As detailed in the report, the work of Task 5 was a challenging research objective for the TPF-5(149) project, and its completion and the results produced are potentially very useful to the design and analysis of HMA-PCC pavement, in particular TICP. Where other research projects have assessed the fitness of certain models or design procedures for HMA-PCC (let alone TICP), few of them have both 1) modified existing models or developed new models for HMA-PCC and 2) tailored those efforts to accommodate the MEPDG framework (i.e. project creation and structural/material inputs). In this way, the TPF-5(149) project is not only singular for advancing the design and analysis of HMA-PCC, it is especially valuable in having done so for the MEPDG, the most popular and readily available M-E design tool for pavement engineers.

The work of Task 5 can be summarized in terms of the models and procedures that were modified for the sake of TPF-5(149):

1. The CalME rutting procedure was reviewed and modified slightly. This procedure was then incorporated into the MEPDG framework using an accessible, “one button” program for general MEPDG users.
2. The NCHRP 1-41 model for reflective cracking and its accompanying software were evaluated, and a driver program was developed under Task 5 so that the NCHRP 1-41 program could easily interface with the MEPDG for continued evaluation and, perhaps, future implementation for TPF-5(149).
3. The CalME model for reflective cracking was reviewed, and a TPF-5(149) model for reflective cracking was developed based on this review of the CalME procedure. This model is also incorporated into an user-friendly program that interfaces with the MEPDG in a manner similar to that of the CalME rutting procedure.
4. The MEPDG model for JPCP transverse cracking was reviewed and modified so that HMA-PCC projects run in the MEPDG accommodate for transverse fatigue cracking in the PCC layer. As with earlier models, a user-friendly program was developed to interface with an existing MEPDG project file for a TICP project (or general HMA-PCC project).
5. The MEPDG model for JPCP joint faulting was reviewed and modified so that HMA-PCC projects run in the MEPDG account for joint faulting. As with earlier modifications, this model is associated with a user-friendly program to interface with the MEPDG.

There are a number of benefits to this comprehensive review and modification of models associated with key distresses in HMA-PCC pavements.

- The proposed models utilize the MEPDG framework, but also incorporate the results of research conducted outside of the MEPDG development.
- The designer is given a choice of performance models, and this choice comes with the convenience of not requiring different input parameters per choice. At the same time, the modified models enable the designer to incorporate the results of different material characterization procedures (such as the CalME rutting test protocol and the TTI overlay tester) in the design process.

- The proposed models enable the designer to quantify the effect of dowels on the long-term performance of composite pavements, which cannot be done with the current MEPDG models.

Finally, the work of Task 5 has further supported HMA-PCC design concepts using M-E modeling. As illustrated in the report, increasing HMA overlay thickness reduces JPCP cracking, delays the onset of reflective cracking, and slows the rate of progression of reflective cracking, and reduces faulting. However, as shown by the TPF-5(149) procedure and supporting SHRP2 R21 data, increasing HMA overlay thickness also increases rutting. Furthermore, the M-E models developed in TPF-5(149) allow for recommendations on the use dowels in HMA-PCC. The study found that joint load transfer in the PCC layer delays the onset of reflective cracking; slows the rate of reflective cracking; and reduces faulting.

References

- AASHTO (2008). *Mechanistic-Empirical Pavement Design Guide: A Manual of Practice*. American Association of State Highway and Transportation Officials, Washington, D.C.
- Bennert, T.A. (2011). A rational approach to the prediction of reflective cracking in bituminous overlays for concrete pavements. Doctoral thesis. Rutgers University, New Brunswick, New Jersey.
- Deacon, J.A, Harvey, J.T., Guada, I., Popescu, L., and C.L. Monismith (2002). *Analytically based approach to rutting prediction*. Transportation Research Record: Journal of the Transportation Research Board 1806:1, pp. Transportation Research Board of the National Academies, Washington D.C.
- Jayawickrama, P.W. and R.L. Lytton (1987). Methodology for predicting asphalt concrete overlay life against reflection cracking. *Proceedings of the 6th International Conference on the Structural Design of Asphalt Pavements, Vol. I*, University of Michigan, July 13-17, 1987, Ann Arbor, Michigan.
- Khazanovich, L., Darter, M., and T. Yu (2004). *Mechanistic-Empirical Model for Transverse Joint Faulting Prediction*. Transportation Research Record: Journal of the Transportation Research Board 1896, pp. 34-45. Transportation Research Board of the National Academies, Washington D.C..
- Khazanovich, L., Tayabji, S., and M. Darter (2001). *Backcalculation of Layer Parameters for Long Term Pavement Performance (LTPP) Test Sections, Volume I: Slab on Elastic Solid and Slab on Dense-Liquid Foundation Analysis of Rigid Pavements*. Report FHWA-RD-00-086, Federal Highway Administration, Washington, DC.
- Kohale, V. and Lytton, R.L. (2000). *Design of Asphalt Concrete Overlay to Mitigate Reflective Cracking*. Report, Project No. 7256, Florida Department of Transportation, Tallahassee, Florida.
- Larson, G., and B. J. Dempsey (1997). Enhanced Integrated Climatic Model. Version 2.0. Final report. Department of Civil Engineering, University of Illinois at Urbana-Champaign.
- National Cooperative Highway Research Program (2010). *Models for Predicting Reflection Cracking of Hot-Mix Asphalt Overlays*. NCHRP Report 669, Transportation Research Board of the National Academies, Washington D.C.
- Scarpas, A., Blaauwendraad, J., De Bondt, A. H., and A.A.A. Molenaar (1993). CAPA: A Modern Tool for the Analysis and Design of Pavements. *Proceedings of 2nd International RILEM Conference, Reflective Cracking in Pavements: State of the Art and Design Recommendations*, p. 121-128. Belgian Research Centre for Plastics and Rubber Materials, March 10-12, 1993, Liege, Belgium.

Strategic Highway Research Program (2012). *SHRP2 R21 Composite Pavements Final Report*. In Press. Transportation Research Board of the National Academies, Washington D.C..

Ullidtz, P., Harvey, JT, Tsai, BW, and C.L. Monismith (2006). *Calibration of Incremental-Recursive Flexible Damage Models in CalME Using HVS Experiments*. Report UCPRC-RR-2005-06. University of California, Pavement Research Center. California Department of Transportation, Sacramento, CA.

Ullidtz, P., Harvey, J.T., Tsai, BW, and C.L. Monismith (2008). *Calibration of Mechanistic-Empirical Models for Flexible Pavements Using California Heavy Vehicle Simulators*. Transportation Research Record: Journal of the Transportation Research Board 2087:1, pp. 20-28. Transportation Research Board of the National Academies, Washington D.C.